12-2013

# A study about aqueous reversible air electrode- Catalyst, Electrolyte and Structure

Ming Qi
*University of Tennessee - Knoxville*, mqi@utk.edu

To the Graduate Council:

I am submitting herewith a dissertation written by Ming Qi entitled "A study about aqueous reversible air electrode- Catalyst, Electrolyte and Structure." I have examined the final electronic copy of this dissertation for form and content and recommend that it be accepted in partial fulfillment of the requirements for the degree of Doctor of Philosophy, with a major in Chemical Engineering.

Thomas A. Zawodzinski, Major Professor

We have read this dissertation and recommend its acceptance:

Alexander B. Papandrew, Robert M. Counce, Matthew M. Mench

Accepted for the Council:

Carolyn R. Hodges

Vice Provost and Dean of the Graduate School

(Original signatures are on file with official student records.)

# A study about aqueous reversible air electrode

# Catalyst, Electrolyte and Structure

A Dissertation presented for the

Doctor of Philosophy

Degree

The University of Tennessee, Knoxville

Ming Qi

December 2013

# Acknowledgements

There are many people that I need to appreciate for their help during my graduate school. First, I need to thank my supervisor, Dr. Thomas Zawodzinski, for giving me this opportunity to do this research and a wonderful experience of working in his lab. I also need to thank him for being very patient with my continuous new ideas about my research and always encourage me to explore new things. I also need to thank my committee members, Dr. Mench and Dr. Papandrew, for giving me advice on catalyst preparation and structure design. I also need to thank Dr.Counce for many suggestions about discussion and writing in this thesis. I also need to thank two senior researchers in our group, Dr Gabriel Goenaga and Dr. Shane Foister, for many suggestions to my research. And other graduate students also offer many help, especially Rob Atkinson helped me with XRD and Luke Servedio helped me with my organic electrochemistry. Dr. Jagjit Nanda and Dr. Gabriel Veith also helped me in the aspect of understanding lithium ion battery.

For my personal life, I must thank my girlfriend, Yang Li, for being such a good accompany in my life. My life is more colorful because of you. I also need to thank many of my friends here for making my life full of fun.

At last, I need to thank TN-Score program for the funding support to make this work possible.

# Abstract

Developing a better high energy density rechargeable battery has becoming critically important for several industries. For building such kind of battery, reversible air electrode has been widely accepted as one of the key components. One of the major challenges for reversible air electrode is finding a good bifunctional catalyst to greatly reduce the recharge overpotential and increase the system efficiency. To achieve this goal, a new air battery chemistry based on cobalt salen modified Au catalyst is proposed in this dissertation as a very promising solution. The unique catalytic activity of this catalyst is found to be a two electron reversible ORR in alkaline electrolyte, which is the most reversible air electrode chemistry system known to date. The reaction mechanism of this catalyst is explained by the surface double layer theory. Cobalt salen is believed to locate in the outer Helmholtz layer, inducing Au surface reconstruction and promoting oxygen chemisorption. Temperature and pH are found to be important environmental conditions for controlling the catalyst ORR reversibility. Electropolymerization is found to be a effective method to stabilize the surface modification without jeopardizing catalytic activity. The nano size Au particles are found to be harmful for ORR reversibility because of the stronger peroxide reduction ability. EDTA, as peroxide stabilizer, is found to be an excellent additive to the electrolyte environment. Three new electrochemical systems are proposed according to the catalyst structure on peroxide production and battery application. An energy storage method and flowing cell structure are discussed in detail for applying this catalyst. The influence of the cation to the ORR catalytic activity on noble metal catalyst is also

explained by surface double layer structure, for which the cation proved to have significant influence on the chemisorptions of oxygen containing species.

# Table of Contents

# List of Figures

# Chapter 1

# Introduction

## 1. 1 Energy challenge

Solutions to energy problems are of major concern to humans in their outlook on the future. Ever since the industrial revolution, an increase in food production, clothing and housing has resulted in unprecedented population growth. This has also greatly increased fuel consumption as a result. This population explosion will drain fossil resources like gasoline and coal because these energy resources are not renewable. Identifying and developing inexhaustible alternative and renewable energy sources are critical to our society. We must find an alternative to replace fossil energy. Several different renewable energy resources have been developed gradually over the years to try to answer this question:

- Wind Power
- Hydropower
- Solar energy
- Biomass
- Geothermal energy
- Nuclear Power

In order to determine which of these renewable energy resources is most realistic and reliable, one should consider not only the capacity of this energy source, but also the

effectiveness and efficiency of using this renewable fuel. By analyzing these renewable energy sources from the perspective of how to use them, we can also divide them into two kinds of energy sources. The first category contains resources that are portable—the consumer can carry this resource and use it wherever it is needed. The other kind requires that the energy resource be transformed into electrical energy and then transferred to the places where energy is needed. Due to the limitations caused by the way the energy is created, the most widely used type of energy source is the latter: transporting previously generated electrical energy. Electrical energy can be created by many routes, such as nuclear energy, solar energy and so on. After it has been transported, it can be stored as heat with thermal storage, or as chemical energy in batteries and capacitors for transportation use.

Nowadays, in the automobile industry, scientists are also seeking possibilities to replace the combustion engine with clean technology that will reduce the pollution caused by burning gasoline. Two of the leading solutions proposed by scientists to achieve this goal correspond to two different kinds of electrochemical devices, fuel cells and batteries. A fuel cell is a class of device that converts the chemical energy from a fuel into electricity through an electrochemical reaction with oxygen. A fuel cell powered vehicle would replace the internal combustion engine of today's automobile with a fuel cell stack and an environmentally friendly fuel would be substituted for the traditionally used gasoline. The fuel cell converts the fuel's chemical energy into electrical energy and uses it to power the car. The most popular and widely used fuel cell for the automobile industry is the proton exchange membrane (PEM) fuel cell, which uses hydrogen as a fuel and oxygen as an oxidant. As its name implies, a proton exchange membrane is used as the electrolyte. Direct

methanol fuel cells (DMFC) have also been considered as an alternative power sources for portable electronic device use. These fuel cell technologies have been greatly developed in recent years by both the academic and industrial fields. Several automobile companies have already released their commercialized versions of a fuel cell car and they have proven that the traditional automobile can be easily outfitted with a fuel cell stack to alternatively power the vehicle in place of the internal combustion engine. However, the real obstacle to widely apply these technologies comes from the difficulty of inexpensively producing the fuel source and building a new fuel supply system. Some popular fuels like hydrogen are not naturally occurring and the technology related to reforming another fuel into hydrogen still face significant challenges. Unfortunately this approach is not mature enough for massive, cost-effective production. In addition, fuel storage materials and the technology that makes fuel easy and safe to transport also needs to be further developed. Aside from all of these problems, the investment required to establish a new method of fuel production, storage and the requisite transport system across an entire nation seems to be a project too daunting for any country. Due to the complex reasons mentioned above, the interest in fuel cells by industry leaders has declined recently despite its potential as a very active research direction for future clean energy application. In this background, an alternative solution for transportation applications will be discussed which utilizes a battery and a super capacitor system that has been proposed by many companies and scientists in recent years.

Batteries and super capacitors are devices that transfer and store electrical energy into chemical energy and electric field energy. Although battery and super capacitor systems cannot continuously provide electrical energy like fuel cells, and the battery recharge time

is a much longer process than a fuel cell refill process, the established grid system makes applying this technology a viable option. In addition to the logistical problems associated with creating an efficient network to support widespread fuel cell use, the fuel cell has other technical challenges with production, transport and storage of hydrogen. On the other hand, the challenges facing the battery and super capacitor all lie within the device itself. Therefore, if the scientific problems of battery or super capacitor can be solved, this could be an easier way for the automobile industry to adopt a clean energy technology. There are still significant scientific challenges that remain for battery and super capacitor technology. Nowadays, the lithium-ion battery is the most developed and widely used battery system available and has already been used in the automotive industry in the form of hybrid cars and short-range electrical cars. Compared to batteries, capacitor technology is generally considered to feature faster charging speed but lower capacity. The super capacitor has been studied in an effort to provide greater capacity than a normal capacitor, yet it is still far away from the desired energy density level. Super capacitor technology has only been applied in niche transportation applications so far. One example of this limited use is in buses that are able to charge very often but require the charge speed to be very fast. In order to achieve the goal of building an electrochemical system that can match the internal combustible engine's performance, the super capacitor system and battery system will need to improve in many ways. This system will need to have an energy density three times that of today's lithium ion battery, ability to fully recharge within several minutes, guarantee safe operation and at least a 30% reduction in cost compared to the current lithium ion battery. The existing battery or super capacitor technology cannot be the final solution for the above requirements. A new electrochemical system must be established.

## 1. 2 Battery basics

A battery is a device that can store electrical energy into chemical oxidation-reduction energy and convert this chemical energy into electrical energy when it is in use. Chemical energy is stored in the negative electrode's active materials. When discharging, electrons travel from negative to the positive electrode through an external circuit to power the load and complete the discharge reaction at the same time as the ions that flow directly from negative side to positive side through the electrolyte. The primary functions of the three key components are as follows:

1. Negative electrode (anode) gives up electrons and undergoes oxidation reaction during discharge
2. Positive electrode (Cathode) accepts electrons and undergoes reduction reaction during discharge
3. Electrolyte facilitates the flow of ions between the two electrodes and also acts as a separator to keep the electrodes electronically isolated.

In a rechargeable battery, the electrons and ions travel in opposite direction during recharge. (Fig 1.1)

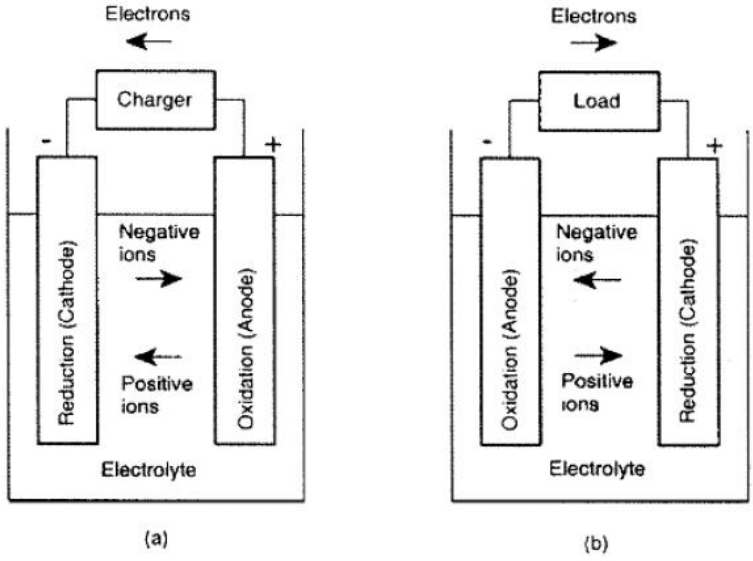


Figure 1.1 Electrochemical operation of battery while charging (a) and discharging (b).

The theoretical voltage of a battery is determined by the difference between the Gibbs free energy of reactants and products of the redox reaction of the battery.

$$\Delta G^{o}_{reaction} = \sum \Delta G^{o}_{f(products)} - \sum \Delta G^{o}_{f(reactants)} \qquad (1.1)$$

$$\Delta G^{o} = nFE \qquad (1.2)$$

In equation 1.2, E is the cell voltage, n is the number of electrons consumed in the reaction, and F is the Faraday's constant, the charge of one mole of electrons. The potential of hydrogen reduction has been set as 0 V. The voltage difference from standard hydrogen reduction is set as its standard potential for the material. Table1.1 shows standard redox potentials for various redox couples versus a standard hydrogen electrode.

Table 1.1 Standard electrode potentials in aqueous solutions at 25°C in V vs. SHE.

| Electrode reaction | E° /V | Electrode reaction | E° /V |
|---|---|---|---|
| $Li^+ + e- \rightarrow Li$ | − 3.045 | $AgI + e^- \rightarrow Ag + I^-$ | − 0.152 |
| $K^+ + e- \rightarrow K$ | − 2.925 | $Sn^{2+} + 2e^- \rightarrow Sn$ | − 0.136 |
| $Ca^{2+} + 2e^- \rightarrow Ca$ | − 2.84 | $Pb^{2+} + 2e^- \rightarrow Pb$ | − 0.125 |
| $Na^+ + e^- \rightarrow Na$ | − 2.714 | $2H^+ + 2e^- \rightarrow H_2$ | 0 exactly |
| $Mg^{2+} + 2e^- \rightarrow Mg$ | − 2.56 | $Sn^{4+} + 2e^- \rightarrow Sn^{2+}$ | 0.15 |
| $Sc^{3+} + 3e- \rightarrow Sc$ | − 2.03 | $AgCl + e^- \rightarrow Ag + Cl-$ | 0.2223 |
| $Be^{2+} + 2e- \rightarrow Be$ | − 1.97 | $½O_2 + H_2O + 2e^- \rightarrow 2OH^-$ | 0.40 |
| $Al^{3+} + 3e- \rightarrow Al$ | − 1.67 | $Cu^+ + e^- \rightarrow Cu$ | 0.520 |
| $Ti^{2+} + 2e^- \rightarrow Ti$ | − 1.63 | $Fe^{3+} + e^- \rightarrow Fe^{2+}$ | 0.771 |
| $Mn^{2+} + 2e^- \rightarrow Mn$ | − 1.18 | $Ag^+ + e^- \rightarrow Ag$ | 0.799 |
| $Zn^{2+} + 2e^- \rightarrow Zn$ | − 0.763 | $Pd^{2+} + 2e^- \rightarrow Pd$ | 0.915 |
| $Fe^{2+} + 2e^- \rightarrow Fe$ | − 0.44 | $O_2 + 4H^+ + 4e^- \rightarrow 2H_2O$ | 1.229 |

The gravimetric capacity of a cell is the total quantity of charge involved in the reaction, usually defined as coulombs or ampere-hours, normalized by the mass of the material, usually presented in units of milliampere-hours per gram (mAh/g). The volumetric capacity is normalized by the volume of material and is usually in units of milliampere-hours per liter (mAh/L). Except for capacity, the specific energy $S_E$ is used to express the whole energy of the system and is calculated by multiplying the specific capacity and the theoretical voltage of the system.

$$S_{E(specific\ Energy)} = Voltage\ (E) \times amperehour(Ah) \qquad (1.3)$$

Battery power is a function of current measured in C rates. The 1C rate is defined as the amount of current needed to fully discharge the battery in one hour.

As can be seen from table 1.1, lithium has high voltage and high capacity, making it an ideal anode material for batteries.

## 1. 3 Lithium-ion battery

Lithium anodes are quite safe for primary cells; however safety becomes more of a concern when it is used in a secondary, rechargeable, battery. During a recharge process in a secondary lithium battery, metallic lithium is electroplated onto the anode surface forming a porous deposit with a larger surface area than the original metallic electrode. As the surface area increases with repeated charging and discharging of the battery, the metallic lithium anode becomes less stable. This usually needs further treatment on the surface of lithium metal and careful operation within the undercharge range, which will be further discussed later. The utilization of lithium metal anodes is rising again with lithium air battery use and a significant amount of research has been conducted to ensure safety with many cycles of fast charge and discharge. Lithium ion electrodes seem to be a solution to safety and stability issues. In the anode of a Li-ion battery, carbon-based materials stabilize the electrode/electrolyte interface and can operate at voltages beyond lithium metal. Typical cathode intercalation compounds are transition metal oxides ($LiCoO_2$, $LiMn_2O_4$ and $LiFePO_4$) which incorporate lithium in their lattices and undergo oxidation to higher valences when Li is removed during charge and discharge. Figure 1.2 shows a schematic of a rechargeable Li-ion battery.[1]

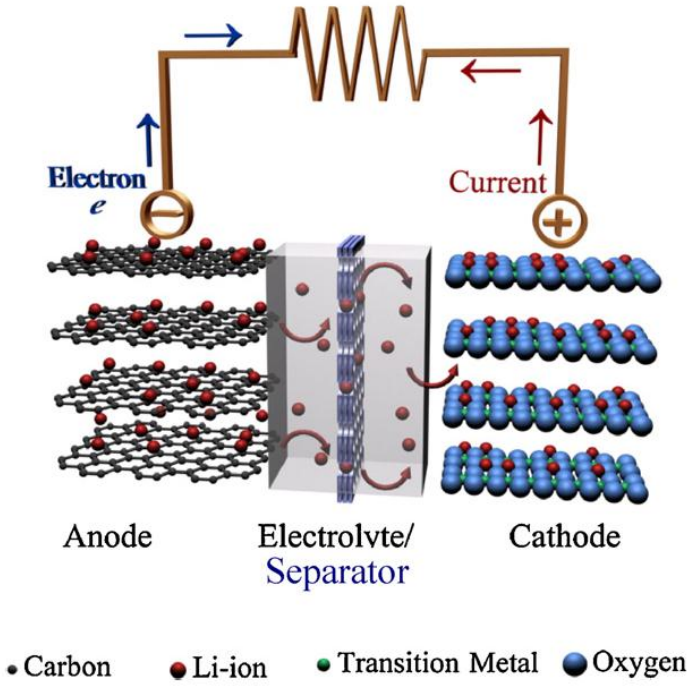


Figure 1.2 Schematic illustration of a typical Lithium-ion battery[1].

Cathode intercalation electrode materials contain transition metals (M) such as (Co, Mn, Ni, Fe) and the prominent examples include $LiCoO_2$, $LiNiO_2$ and $LiMn_2O_4$, which are the state of the art. At full charge, graphite can only incorporate one Lithium per hexagon ($LiC_6$). As a result, the anode capacity drops from 3861 Ah/g for the case of metal Li to 372 mAh/g for graphite—almost a 90% decrease.[2] This is a very limited number if considering storage energy for automobile usage. With respect to cost for the cells, cathodes make up about 50% of the cost for the whole cell.

## 1. 4 Alkaline fuel cell

Alkaline fuel cells (AFC) were the first working fuel cells in history due to the pioneering work of Bacon.[3] AFCs can realize a high overall electrical efficiency greater than most

other fuel cell types.[4] The AFC was generally developed and studied extensively from the 1960s to the 1980s, prior to the emergence of the proton exchange membrane (PEM) fuel cell. Since then, most of the attention paid to fuel cells has been attracted by the PEM fuel cell. However, because of cost and durability issues of the PEM fuel cell, the AFC has recently attracted some interest from developers and several companies have devoted efforts to developing a low cost AFC system. The overall electrochemical reaction for an AFC is the same as a PEM fuel cell.

$$H_2 + ½\, O_2 \rightarrow H_2O$$

However, the difference in electrolyte environment makes the anodic and cathodic reaction different from a PEM fuel cell.

Anode: $H_2 + 2OH^- \rightarrow 2H_2O + 2e^-$

Cathode: $H_2O + ½\, O_2 + 2e^- \rightarrow 2OH^-$

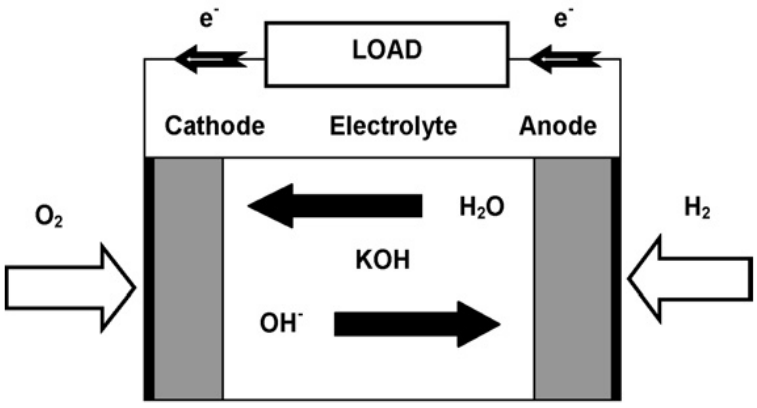


Figure 1.3 Diagram showing the fundamentals of an alkaline fuel cell[5].

An alkaline fuel cell working diagram is shown in Fig 1.3. Generally, the cathode of the AFC generates $OH^-$, and $OH^-$ travels though the electrolyte in the middle to the anode. The anode produces $H^+$ ions and electrons. The electrons travel through the external circuit to the cathode. Four different types of fuel cells have been developed and a description of each has been given by Gulzow.[6] These can be summarized as follows: (1) cells with free liquid electrolyte, (2) cells with liquid electrolyte in pore-system, (3) matrix cells where the electrolyte is fixed in the electrode, (4) falling film cells. The one common aspect of these cells is that they all use porous electrode architectures which are similar to the electrode used in metal air batteries.[7] The main problem within AFC in early years was the formation of carbonate salt from the reaction of electrolyte and $CO_2$ in the air that tremendously decreased the conductivity of electrolyte and decreased the performance of the cell. The solution for this problem lies in using a $CO_2$ scrubbing system[8] and the structure of circulating electrolyte.[8,9,10,11] The fifth type that recently has been rapidly developed is the alkaline membrane fuel cell. The alkaline membrane fuel cell has three advantages over conventional alkaline fuel cell: no precipitated carbonate, no electrolyte weeping and potentially reduced corrosion. However, these advantages require an anion exchange membrane with good conductivity; such a membrane is currently under development. Compared with PEM fuel cells, alkaline fuel cells have several advantages based on state of the art research:

- Non precious metal catalyst can have very good performance at low cost.
- Normal electrolyte (KOH) is much cheaper than a proton conduction membrane.
- Circulating electrolyte structures can enhance water and thermal management.
- Freezing condition startup is not a problem in circulating electrolyte situation.

## 1. 5 Oxygen reduction reaction in alkaline solution

The study of oxygen reduction reaction (ORR) is an older research topic that has been widely studied with various catalysts and electrolyte situations combined with various electrochemical systems. Because of the general global research interest in PEM fuel cells in the last two decades, the most studied specific application of the ORR is platinum on carbon catalysis in acidic solution, which has been proven as one of the best solutions to reduce oxygen efficiently and is still being widely used in industry today. Generally, in this process, oxygen goes through a four-electron transfer reaction with four proton ions and generates water as a product.

$O_2 + 4e^- + 4H^+ \rightarrow 2H_2O$

The ORR in alkaline solution has recently attracted more attention due to the emerging interest in metal-air batteries and alkaline fuel cells. One difference between acid and alkaline solution is in the different concentrations of proton and hydroxide ions, so the charge and charge density on the surface of an electrode within two layers of the Helmholtz layer is very different. Therefore, different reaction mechanisms occur as previously shown. Except for the direct electrocatalytic effect that results from the different $H^+$ and $OH^-$ concentrations in the electrolytes, indirect effects on the working potential are also very important. For electrochemical processes occurring in aqueous media, an electrochemical window limits the working potential range. According to the Nernst equation, this range shifts by -59mV for every increase of 1 pH unit, the standard hydrogen electrode (SHE) potential shifts by -0.83V as a result of the change from a 1 molar solution of acid to a 1

molar solution of base. Such a shift can change the local electric field and Helmholz layer (HL) of the interface, leading to changes in adsorption strengths even for neutral species.

The ORR in alkaline solutions is generally easier than in acid solutions and is not as dependent on a catalyst. Many kinds of catalysts, including non-precious metal catalysts, have good performance for ORR in alkaline solution, while developers are still searching for the non-precious metal catalyst that could replace Pt in acid systems. Depending on the specific catalyst and electrolyte environment, the ORR follows a different mechanism in the alkaline solution. Several species like $O_2^-$ and $HO_2^-$ have been proposed as possible intermediates in this multistep reaction. Two reaction pathways have been suggested as the most likely mechanisms. The first pathway, or direct pathway, is a direct reaction with 4 electrons producing $OH^-$. The other pathway is a two-step pathway involving $HO_2^-$ as a reaction intermediate, which is subsequently reduced to $OH^-$ as the final product. The difference between these two mechanisms lies into the different rate for each step. No matter which pathway, it is widely accepted that proton transfer to $O_2$ producing adsorbed $HO_2$ or $HO_2^-$, occurs prior to cleavage of the O-O bond during the ORR on Pt-group metals. Formation of an intermediate adsorbed $HO_2$ species is likely in both pathways. Comparing the difference of ORR in acid and alkaline conditions, the much lower working potential of an ORR electrode would facilitate desorption of $HO_2$ and $HO_2^-$ ions in the alkaline environment, while the higher working potentials in acidic media would tend prevent $HO_2$ desorption, so that further protonation would be required in order for peroxide desorption to occur. Therefore, the total four electron reduction is usually called a direct pathway in acid electrolyte environment and a series pathway in alkaline environment.

On the other hand, the different working potentials of the acid and alkaline electrolyte environments can also influence the two electron ORR mechanism. Two electron ORR is specifically useful for the electrochemical production hydrogen peroxide. And the critical point for a two electron ORR to happen instead of four electron ORR is the stability of $HO_2^*$. A comparison of four electron ORR series reaction pathway and the two electron ORR series reaction pathway is listed below:

Four electron ORR:

$$O_2(g) + H^+ + e^- \rightarrow OOH^*$$

$$OOH^* + H^+ + e^- \rightarrow O^* + H_2O(l)$$

$$O^* + H_2O(l) + H^+ + e^- \rightarrow OH^* + H_2O(l)$$

$$OH^* + H_2O(l) + H^+ + e^- \rightarrow 2H_2O(l)$$

Two electron ORR:

$$O_2(g) + H^+ + e^- \rightarrow OOH^*$$

$$OOH^* + H^+ + e^- \rightarrow H_2O_2(l)$$

As can be seen from the comparison, the four electron ORR needs to have very stable $HO_2$* intermediate for the further protonation and O-O bond breakage to happen. Therefore, the lower working potential of ORR electrode in alkaline which can facilitate desorption of $HO_2$* can also execute the two electron ORR electrode with better selectivity.

The rate limiting step for a two electron ORR or a four electron ORR is also related with other reaction intermediates including, OH*,O*. People also found that there exists a scaling relationships between these oxygen intermediates; the activity is govern by a single parameter and can be plotted as a function of OH* bonding energy.[12–14] The different

intermediates bonding energy also results in a different catalyst activity volcano plot, as shown in Fig 1.4.[15]

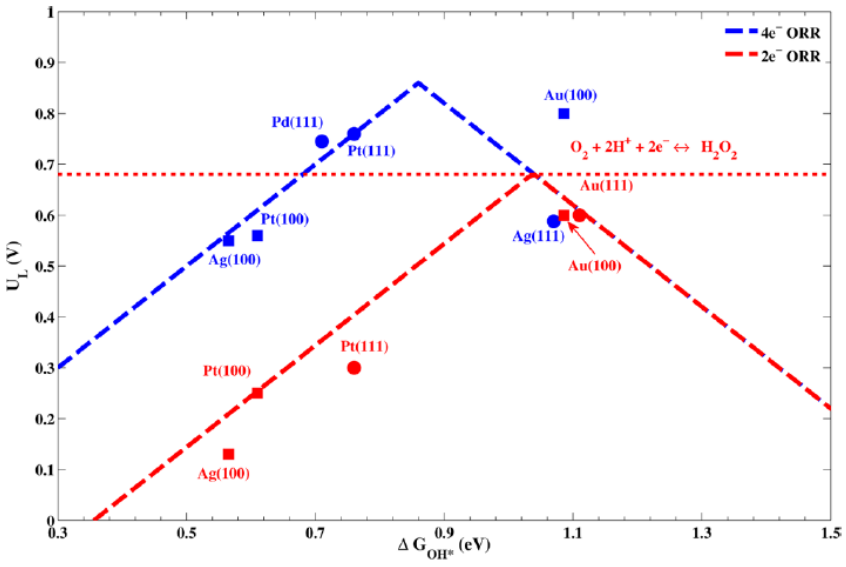


Figure 1.4 Activity volcanoes for the 2e- and 4e- reduction of oxygen are shown in red and blue respectively.[15]

As shown in Fig 1.4, different metal surfaces fall in different places in the two volcanoes because of different bonding energy with oxygen containing intermediates.

Excerpt for this significant difference in the working potential, the difference in the electrode surface double layer between acid and alkaline electrolyte environment also can greatly influence the catalytic activity. The first feature of double layer structure that changed with pH is the chemisorbed spectator species on the IHL and the other species that interact with each other in the OHL. Having these changes in the double layer, some mechanisms proposed that the interaction between the oxygen and electrode is changed, while, others proposed that the electron transfer mechanism is changed. Nagappan and

Mukerjee from Northeastern University proposed a mechanism in which the adsorbed hydroxyl species on Pt catalyst surface will not only inhibit direct molecular adsorption of oxygen but also promotes a two electron reduction of $O_2$ to $HO_2^-$ by an outer-sphere electron transfer mechanism.[16] The interpretation for this is possible hydrogen bonding formation between solvated oxygen clusters and specifically adsorbed surface hydroxyl group. The influence of the electrode surface double layer on the ORR catalytic activity is also related with other spectator species within the double layer. Different anion and cation and even neutral species are also shown to be capable of changing the ORR catalytic activity, and this thesis will focus on the influence of cation and neutral species.

## 1. 6 Lithium-air battery

With a similar structure to other battery systems, the Lithium air battery consists of a lithium metal anode, an air cathode and electrolyte in the middle to separate the two electrodes. When discharging, lithium metal anodes release lithium ions and an electron. The electron goes through an external circuit and lithium ions travel through the electrolyte to the cathode. Oxygen combines with electrons and lithium ions to complete the reaction and produce lithium oxide or lithium peroxide (lithium hydroxide or lithium salt in aqueous solution). When charging, lithium oxide or lithium peroxide decomposes to produce oxygen and lithium ions travel back to the anode and are reduced to lithium metal again. Due to a large theoretical energy density, the Li-air battery has been proposed as one of the most promising battery systems to replace the Li-ion battery. Much research effort all over the world has been devoted to the development of the Li-air battery. Depending on the type of electrolyte,[17] four different types of Li-air battery have been proposed. (Fig 1.5)

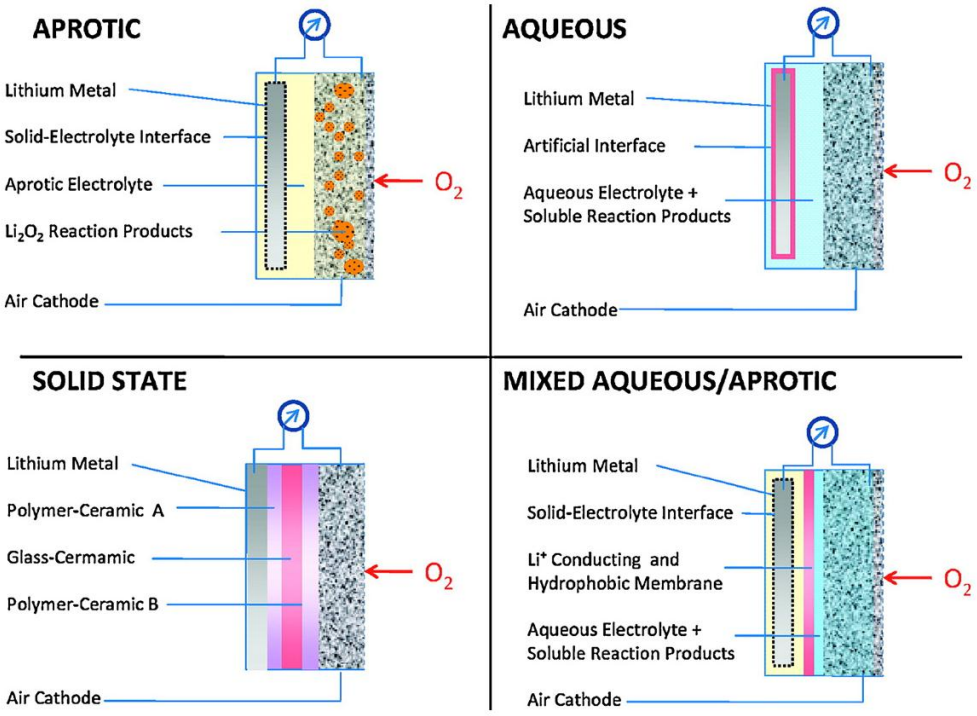


Figure 1.5 Four different configurations of Li-air batteries based on the type of electrolytes[17].

Each type of Li-air battery has different features in the aspect of cell performance. By choosing a different electrolyte and different battery structure, you are also choosing different tradeoffs between different properties. Recent research on the different types of lithium air batteries is discussed in the following sections.

### 1.6.1 Aprotic lithium-air battery

The Aprotic Li-air battery is the most studied system of all of the Li-air structures and was first reported by Abraham and Yang et al in 1996.[18] This very first Li-air battery was actually discovered accidentally rather than invented on purpose. Researchers discovered after some oxygen accidently entered a Li/graphite cell they were testing that it resulted in a higher current than they were expecting. Further thought eventually led to the idea of the

Li-air battery. There are many choices of aprotic electrolytes but the most commonly used ones include organic carbonates (ethylene carbonate, propylene carbonate, dimethyl carbonate) or other ethers, which can solvate lithium salts such as $LiPF_6$, $LiAsF_6$ or $LiN(SO_2CF_3)$.[19] In a non-aqueous (aprotic) electrolyte, the oxygen electrode reactions can be described as follows:

$$2Li + O_2 \underset{\text{Charge}}{\overset{\text{Discharge}}{\rightleftharpoons}} Li_2O_2 \quad E^\circ = 2.96\,V \qquad 4Li + O_2 \underset{\text{Charge}}{\overset{\text{Discharge}}{\rightleftharpoons}} 2Li_2O \quad E^\circ = 2.91\,V$$

Although large amounts of effort have been devoted to studying aprotic Li-air batteries by industry and academia, great challenges still remain. According to the problems different groups are trying to address, the research has focused on the chemical stability of materials in a new chemistry system, air cathode structure and material that can help the transport of oxygen within the cell, ORR and OER reaction mechanisms and new catalysts that perform better in specific environments.

- Catalyst and Reaction mechanism

One problem with the aprotic Li-air battery is that the overpotential to drive the product back to oxygen and Lithium metal is too large—usually over 1.5V. Utilizing a bifunctional catalyst that promotes ORR and OER at the same time is crucial to the system efficiency. It is also very important to understand the mechanism of the formation of lithium peroxide and lithium oxide, which will help improve the deep discharge of the battery.

Cormac O' Laoire et al. have investigated the mechanism of ORR in the aprotic electrolyte by RDE experiments with different electrolytes. They found that the electrolyte

environment with larger size cations and the same anion assists the reversible ORR reaction mechanism to happen.[20] Later, they demonstrated the production of $Li_2O_2$ and $Li_2O$ in the electrolyte environment of TEFDME-$LiPF_4$ with only carbon as catalyst. However, the ability to recharge the cell is limited, and they attributed this to the high impedance they measured along with cycling associated with $Li_2O_2$ deposition.[21] Yi-Chun Lu et al. investigated the intrinsic ORR activity of glassy carbon, gold and platinum catalysts. They found that gold is the most active catalyst towards ORR.[22] Later, they found that Pt has a better catalytic effect on OER. Thus, a mixed catalyst of Au and Pt is suggested to have a good energy efficiency.[23] V. Giordani et al. studied the relationship between the $H_2O_2$ decomposition rate and the Li-$O_2$ battery recharge voltage and the results indicate that $H_2O_2$ decomposition can be a good screening tool for investigating the Li-$O_2$ charging mechanism.[24] J. Read observed that quaternary ammonium salts can act as a "phase transfer catalyst" to facilitate the further reduction of lithium peroxide into lithium oxide in low concentrations. This additive not only reduces the polarization of lithium peroxide, but also increases the overall discharge capacity.[25]

- Chemical stability

The main reason why the aprotic electrolyte is the most widely studied electrolyte in lithium air battery structures is that this battery structure is so similar to the lithium ion battery. However, oxygen reduction and evolution in organic electrolytes is a much more complicated process than in the widely studied aqueous solution. The desired reaction product, lithium peroxide, has a very strong attacking nature. Many materials used in Li-

ion batteries are not applicable to Li-air batteries. Therefore, the most important research thrusts for aprotic Li-air batteries in the initial stages should be chemical stability.

Gabriel M. Veith pointed out that, when using Nickel as a current collector, degradation of the electrolyte contributes to the current measured. [26] Since this discovery, some recent research has reverted back to more basic chemistry on some electrolytes that were previously used in experiments and were later believed to be unstable. In addition to some of the current collectors reacting with the electrolyte, carbon as the most popular catalyst support or product container has been proven to react with lithium peroxide and produce carbon dioxide. B.D. McCloskey and his colleague from IBM points out that chemical and electrochemical electrolyte stability in the presence of lithium peroxide is of critical importance. Also, for properly characterizing the rechargeability of the Li-$O_2$ battery, it's necessary to couple using coulometry and quantitative gas consumption and evolution data. After analyzing the source of carbon dioxide from the lithium air cell, they found that both the electrolyte (ether) and carbon can react with lithium peroxide to produce carbon dioxide.[27] Later, together with scientists from the Volkswagen group (US), they found that the catalyst only influences the oxidation of the solvent, not the oxidation of $Li_2O_2$. While they proved that the recharge current is due to the $Li_2O_2$ oxidation process, the overpotential of Li-$O_2$ battery did not improve after changing the catalyst.[28] Peter G. Bruce et al. observed that carbonate is also not an ideal solvent for aprotic Li-$O_2$ battery. In the discharging process, $Li_2CO_3$, $CH_3CO_2Li$, $CO_2$ and $H_2O$ etc. is formed, and there is no evidence of reversible oxygen reduction to $Li_2O_2$. [29] The group of Ji-Guang Zhang reached the same conclusion. They investigated the discharge products of a lithium-$O_2$ battery with alkyl-carbonate electrolytes and KB-carbon-based air electrodes, and only a small amount of

$Li_2O_2$ was found. They explained that the formation of $Li_2CO_3$ and $LiRCO_3$ is caused by the nucleophilic attack of $Li_2O$ on the alkylcarbonate solvent. [30] Peter G. Bruce's group first published the experimental proof that a possible clean charge and discharge cycle is possible for an aprotic Li-air battery; FTIR and SERS has been used to confirm the formation of Lithium peroxide.[31] However, in this experiment, only gold has been used as an electrode material as carbon has been proven to be a cause of instability. A realistic battery composition with adequate stability is yet to be found.

- Air electrode optimization and capacity improvement

One of the major problems in an aprotic Li-air cell is that the product is not soluble in the electrolyte. This result a serious clogging problems that prevents oxygen from diffusing in and causes electrical insulation, which will further influence battery capacity. Another problem is that the aprotic electrolyte should not interact with water and $CO_2$; when it operates at ambient condition, there needs to be a membrane that can keep water and $CO_2$ out of the cell while allowing oxygen to efficiently diffuse into the cell. J.Read et al. test the oxygen transport properties of several aprotic electrolytes through measurements of oxygen solubility and calculated electrolyte diffusion coefficients using the Stokes-Einstein relation.[32] They later proposed that using partially fluorinated solvents can enhance the dissolution kinetics and solubility of oxygen and further enhance the discharge performance of the cell, although the ionic conductivity of the electrolyte is decreased.[33] R.E. Williford et al. use a modeling method to propose an interconnected dual pore system to improve oxygen transport for long term applications. [34] S.D. Beattie and et al. use a Swagelok cell structure to build up a Li-air battery.[35] Jeffrey Read et al. propose a two-

phase reaction zone for the aprotic Li-air battery. Apart from the fuel cell's classic three-phase reaction zone, the cathode structure here emphasizes large porous space to prevent any blockage of transport oxygen to the catalyst. However, the reaction rate is still limited by the low diffusion rate of oxygen in the electrolyte, as shown in Fig 1.6.[36]

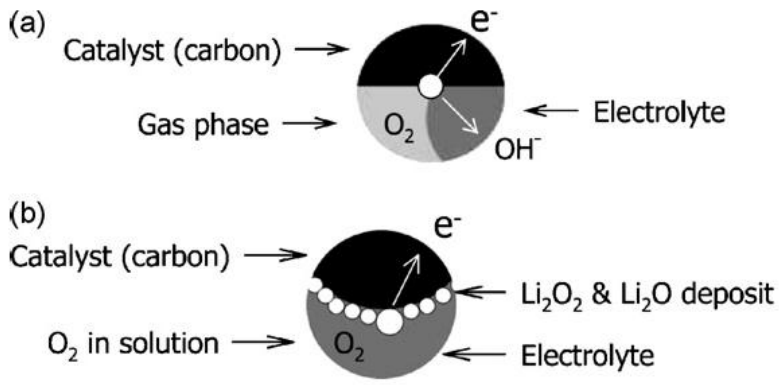


Figure 1.6 The difference between three phase oxygen reduction and two phase oxygen reduction[36]

Wu Xu et al. investigate the effects of non-aqueous electrolytes on the performance of aprotic Li-air cell. As opposed to previous research[36], they point out that open channel for oxygen can increase the power performance and let oxygen diffuse into electrolyte. This leads to the design for a three phase zone in the aprotic electrolyte. Thus, electrolyte polarity is a important factor to consider for electrolyte. Tris(pentafluorophenyl)borane as a functional additive to the electrolyte is also discovered to help dissolve $Li_2O$ and $Li_2O_2$ formed on the surface of catalyst, which can increase the discharge capacity in some extent.[37] C.K.Park et al. did a set of experiments to study the difference of different carbon supports; they found carbon material with large surface area and pore volume is good for cell capacity. However, all experiments conducted with a Nickel current collector decrease the accuracy of the results.[38] G.Q. Zhang et al. tried to use single wall nanotubes and carbon

nanofibers with no binder as cathodes. Results shows that the capacity of the cell decreases along with the increase of cathode thickness, indicating that the capacity of cell depends on structure of cathode, capacity can dramatically decrease because reaction product clogging and blocking on the side of the air cathode structure results long distance of oxygen diffusion length.[39]An air hydration membrane is studied by Jian Zhang et al. Silicalite zeolite and PTFE were used as inorganic and polymeric hydrophobic-type material to repel the $H_2O$. The results show that completely selective permeation of $O_2$ over $H_2O$ is very difficult. The cell with a certain level of relative humidity performs much worse than the cell that operates in dry conditions. [40] They later tried loading $O_2$-selective silicone oil of high viscosity which shows better cell performance, as shown in Fig 1.7.[41]

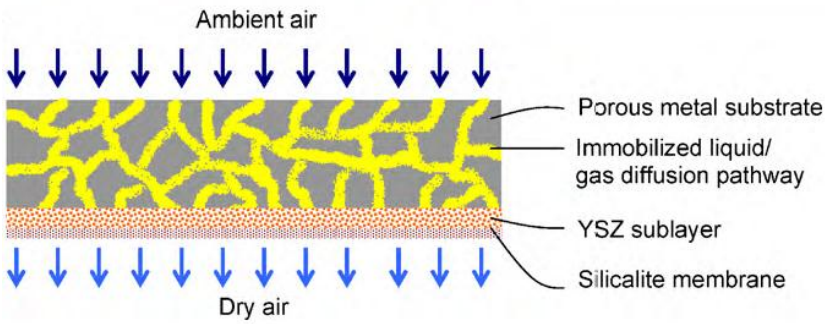


Figure 1.7 Schematic of Liquid immobilized in silicate membrane-coated porous metal substrate[41]

Since the material parameter of carbon pore size and oxygen partial pressure can greatly influence the performance of Li-air battery, P. Andrej proposed a physics-based model to simulate the battery system and suggest some ways to enhance the system.[42] Chris Tran and his colleagues emphasize the concept of tri-phase structure in the non-aqueous Li-air

cathode structure and create a linear relationship between the gas diffusion electrode capacity and average pore size of the carbon nano-material.[43]

After more and more people start to work on aprotic lithium air battery, many researchers found that issues of this structure discussed previously seems specially hard to improve. Some people are starting to believe that the mixed electrolyte lithium air battery structure has a bigger chance to become a successful battery structure.

### 1.6.2 Aqueous and mixed electrolyte lithium-air battery

Although aqueous air batteries have been studied and used for a long time, the aqueous lithium air battery is a relatively new research area. The reason is very simple: lithium metal is extremely reactive and is not stable with water. It will react and release hydrogen when contacts water. Therefore, research on aqueous lithium air battery has been limited until the concept of a protected lithium metal electrode was put forth. S.J. Visco and L.De Jonghe et al. are the first group to promote the idea of a protected lithium electrode.[44] They first presented this concept in the 12$^{th}$ International Meeting on Lithium Batteries at Nara of Japan, 2004. They later formed a company, called Polyplus, which has been doing R&D on lithium-sulfur, lithium-air and lithium water batteries using their protected lithium metal electrode. The initial protected lithium electrode consists of two layer of lithium conducting solid electrolyte. The layer in contact with lithium metal is made with $Cu_3N$ and $Li_3N$, which is stable against lithium metal. The second layer is what normally called “Lisicon” plate, which is lithium ion conducting solid electrolyte but also water stable, as shown in Fig 1.8. The tradeoff in using this protected structure is the performance sacrifice due to

the low conductivity of these solid electrolyte. The other issue comes from the chemical stability when contacting the corrosive strong acid or alkaline. As lithium metal battery is becoming more and more important, many groups are trying to development better solid electrolytes with higher conductivity and also water and chemical stability.[45–48]

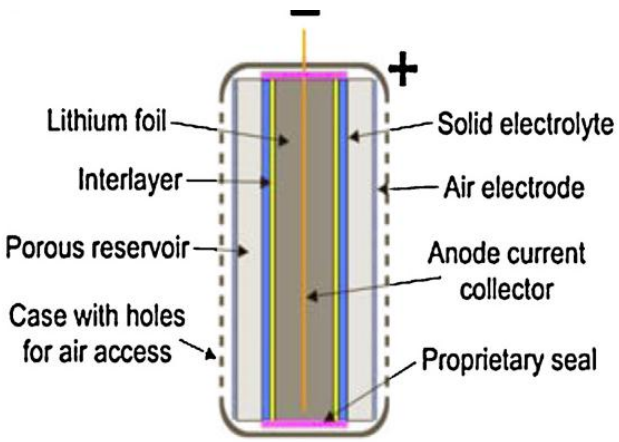


Figure 1.8 Schematic diagram of aqueous lithium-air battery developed by Polyplus[44]

Another structure, which is called “mixed electrolyte” structure, is actually similar to the aqueous lithium air battery structure. Compared with the previous structure, there is also a layer of organic electrolyte between the lithium metal and solid electrolyte. And this can benefit the system for the higher conductivity of organic electrolyte and better chemical stability of organic electrolyte versus lithium metal. Because this kind of battery has two kinds of liquid electrolyte on the two sides of the solid electrolyte, people call it a “mixed electrolyte” lithium air structure in some articles. Due to the fact that the “mixed electrolyte” battery structure is easier to construct, many labs without capability for making different solid electrolyte adapt this structure for concept demonstration. [49–54]

As discussed earlier, the low conductivity of the solid electrolyte and its poor stability in the aqueous solution causes a large performance loss and degradation of the cell. This drives many people to use the protected lithium anode with aqueous air electrode since the aqueous air electrode has many important advantages over an aprotic air electrode. The catalytic nature of aqueous air electrode is very different from aprotic air electrode. The aqueous air electrode is a three-phase reaction electrode. In discharging, the gas phase reactant oxygen diffuses to the solid phase catalyst, then produces water or hydroxide dissolved in the liquid phase. An aprotic air electrode is a two phase reaction electrode. In discharging, gas phase oxygen diffuse through the aprotic electrolyte, then reacts at the solid phase catalyst to produce a solid phase product. In charging, both processes will reverse. The solid phase product for the aprotic air electrode will cause great difficulty in both charging and discharging. In discharging, the solid phase product will block the oxygen diffusion and block catalyst surface. In recharging, the solid reactant peroxide is very hard to move to the catalyst surface, especially when the cell is constructed to have very large energy density. The aqueous air electrode has a great advantage for high power density because the discharge product can dissolve in the liquid phase. The study of the aqueous air electrode has a long history. Many technical problems, including catalyst composition, hydrophobic gas diffusion micro channel, diffusion media design, are very well optimized from fuel cell and air battery research. However, the aqueous air electrode also has several big unsolved challenges.

The conventional aqueous air electrode chemistry proceeds by a four electron oxygen reduction and oxygen evolution. This reaction is famous for high overpotential. A robust bifunctional catalyst which can promote both ORR and OER is very hard to develop.[55–64]

High overpotential causes problems for the bifunctional catalyst in the OER side and the ORR. Several research groups also tried a three electrode structure with two separate electrodes for oxygen reduction and oxygen evolution. [65] For lithium air battery structure, people usually use a two electrode structure for concept demonstration.

### 1.6.3 Ionic liquid and solid state lithium-air battery

Since aprotic Li-$O_2$ battery and aqueous Li-$O_2$ all have big challenges to solve, people are seeking other possible air battery structures for better performance. Several ionic liquids have the same electrochemical window as aprotic electrolytes and the hydrophobic property that certain ionic liquid process is also very attractive for ambient operation. For a high energy density cell, solid-state batteries always have an advantage with safety considerations. Especially, when using lithium metal as negative electrode, there can never be too much consideration for safety. For these two air battery structures, several groups around the world are producing some initial research results.

Scientists from Toshiba first tried to use ionic liquids at room temperature, they manage to make a high capacity cell but with very low power output.[66] Z.H.Cui et al. built a lithium air cell using (PP13TFSI) ionic liquid and $LiClO_4$ as electrolyte, vertically aligned carbon nanotube (VACNT) as air cathodes. The discharge capacity and cycle life of the cell is found to be greatly dependent on the current density and depth of the discharge. The impedance of the cell is found to be greatly increased along with cycling; a partial reason of this is the aggregation of Li carbonates.[67]

The idea of using solid state electrolytes comes from lithium ion batteries first. People tried to use inorganic solid electrolytes to replace conventional organic electrolyte to overcome the safety hazard issues of the conventional lithium ion battery.[68] Because aprotic lithium air battery also have serious safety problems, it is very reasonable to build an all solid state battery when using lithium metal anode. Binod Kumar et al. demonstrated an all solid state lithium-$O_2$ cell using glass-ceramic and polymer-ceramic materials. The cell also exhibited excellent thermal stability and rechargeability in the 30-105$^{o}$C temperature range.[69]

## 1. 7 Cobalt based catalyst

When the polymer electrolyte fuel cell (PEFC) started to draw attention, research about how to make the cost of the cell less expensive has also increased. One of the most important research directions is how to use non-precious metal catalyst (NPMC) to replace platinum (Pt). Over the decades, Pt is the best oxygen reduction catalyst and the best choice to use in both anode and cathode of the PEFC. It proceeds with a four electron oxygen reduction with high reduction potential in both acidic and alkaline environment, and has a very robust performance. However, as Pt is one of the rarest metals on earth. Finding a replacement catalyst is necessary. All kinds of transition metal catalyst have been proposed by labs all over the world. Cobalt based catalyst is one of the main replacement catalyst people are working on. Besides being used as an oxygen reduction catalyst, cobalt based catalysts are also seen as a possible oxygen evolution catalyst (OER) to be used in electrolyzer or air batteries.

Cobalt based catalyst are of many different types. Cobalt oxide based catalysts has been widely studied as OER catalyst. Both $Co_3O_4$ and $M_xCo_3$-$xO_4$ shows good activity, Boon

Siang Yeo and Alexis T.Bell looked at how the composition and structure of cobalt or its oxide electrode changes as a function of applied potential and the influence of these changes applies to the OER rates in alkaline environment. [70] Results shows that $Co_3O_4$ is oxidized to CoO(OH) as potential increases and $Co^{IV}$ seems essential for the OER to proceed efficiently. An Au electrode as a substrate on which cobalt oxide is deposited shows the best performance compared with Pt, Cu. Ibrahim M. Sadiek and his colleague also found that Cobalt oxide nanoparticles performance is PH and loading dependent.[71] S. Palmas and his colleagues confirmed that $Co^{IV}$ containing species is the key element of the oxygen evolution reaction for cobalt based catalysts, EIS measurement also indicates that OH- diffusion in pore solution is slower than the quasi-reversible electron transfer process and is the limiting step of the whole process.[72] C. Bocca et al. compared $Co_3O_4$ and lithium doped $Co_3O_4$ on chemically pickled nickel electrode. They showed that different method of preparation also greatly influence the performance of the catalyst.[73]

Besides cobalt oxide catalyst, several cobalt complexes also have interesting properties to be a potential OER, OER or bifunctional (both OER and ORR) catalyst. Cobalt chelate structures based on a $Co\text{-}N_4$ or $Co\text{-}N_2O_2$ center structure shows good catalytic activity in this aspect. Tatsuhiro Okada and his colleagues tried to use polymerization and heat-treatment to immobilize several cobalt chelate compounds on the high-density pyrolytic graphite (BHPG) disk electrode. Cyclic voltammograms and XPS were used to characterize these complexes. Results show that those complexes have better ORR activities after heat-treated at 600$^{o}$C and, electropolymerized catalysts also impart a high level of oxygen reduction ability; the author proposed that it is due to the improved molecular orientation for oxygen coordination and formation of good chelating sites on the

graphite surface.[74] Richard P. Kingsborough also studies the cobalt salen containing polymer, a polythiophene-cobalt salen hybrid polymer, as an ORR catalyst. They suggest that the improved performance of the catalyst is because of the highly electronic conductive nature of this polymer. The peroxide as a side product of the oxygen reduction is trapped by this polymer structure, based on the different peroxide oxidation results from cyclic voltammetary and RRDE experiment.[75]

## 1. 8 The goal and scope of this dissertation

Due to the various challenges mentioned previously for different air battery systems, current directions for building better air batteries do not seem to have potential to reach the requirements of next generation high energy density batteries. A desired air battery system needs to overcome the low system efficiency and low recharge rate limitations. To achieve that, an innovative catalyst which can tune the ORR and OER to meet these standards is needed. Currently, there are two fundamentally approaches to the development of such materials: (i) tuning the electronic properties of metal surface atoms and (ii) systematic arranging of the components and structure of the electrochemical double layer by using a special electrolyte environment or using a special modified surface layer. The first method has been used extensively in the catalyst development for PEMFC in several different ways including, alloying platinum with transition metals or de-alloying some alloys of platinum or platinum core shall structure.[76–82] The second approach emphasizes how non-covalent interactions of the molecules from electrolyte environment located within the outer Helmholtz plane influence the catalyst surface and species chemisorbed on the catalyst surface.[16,83–90] The molecules can be cations, which are very important in the alkaline

electrolyte environment, or they can also be special molecules put on purpose into the electrolyte environment to make the catalyst behave differently from its original reactivity. By understanding the mechanism of how these interactions happen and what kind of influence they have, we can design the catalyst for special purposes by creating a special surface double layer structure or making a special modified catalyst. This dissertation is a deep exploration of trying to find a suitable bifunctional catalyst for the next generation air battery using the second approach.

Chapter 3 focuses on the reaction mechanism of an innovative bifunctional air electrode catalyst, which is composed by cobalt salen and Au. Though a series of analytical electrochemistry experiments, the reaction mechanism is determined to be a two-electron reversible oxygen reduction reaction with peroxide self-decomposition as follow-up reaction. The reversible nature of the catalyst is discussed with two possible reasons. Further experiment results suggest that cobalt salen physisorption induced Au surface reconstruction is the most probable interpretation, which explaining the fact why no further peroxide reduction happens. The kinetic improvement after the modification is explained via surface double layer theory. Two hypotheses are proposed with the difference of two catalytic active centers.

Further characterization of the catalyst is discussed in chapter 4. The influence of temperature and pH on the reaction reversibility is discussed. Low temperature and pH above 12 are proved to be the preferred operation condition. The peroxide oxidation catalytic activity is also tested directly. This chapter discusses three important aspects for applying this catalyst composition into a catalyst layer in electrochemical systems. They

are (1) catalyst stabilization, (2) the effect of nano size Au particles on catalytic activity and (3) peroxide stabilization. Cobalt salen electropolymerized on an Au surface is proposed to be a very effective way to stabilize the catalyst composition. The influence of nano sized Au particle on the reaction reversibility is also tested. The cobalt salen modified nano size Au catalyst is proved to have poor reversibility because of the better peroxide reduction activity on nano size Au particles on bulk gold. Another important aspect is how to preserve peroxide after it is produced in the electrochemical cell, which is very important for battery recharge. Our experiment result shows that EDTA, the peroxide stabilizer, is a very good additive to the electrolyte and does not jeopardize the catalyst performance.

Chapter 5 is focused on the influence of cation related non-covalent interaction to the ORR catalytic activity in alkaline electrolytes. Two nanometer Pt and Au particles are chosen to be the catalyst because Pt and Au are the most well studied ORR catalyst and the non-covalent interaction effect on nano-size noble catalyst has not been addressed yet. The catalyst surface double layer structure is again used to explain this influence. RDE experiment results and tafel slope calculations are used to make the comparison.

Three applications are proposed for the cobalt salen modified Au catalyst in chapter 6. When used as an ORR catalyst, it seems to be efficient for electrochemical production of hydrogen peroxide. As a bifunctional air electrode catalyst, two battery structures are proposed for use with two kinds of metal anode. A flowing electrolyte air electrode structure is proposed for use with a lithium metal anode to solve the dilemma of preserving discharge product and jeopardizing discharge performance. However, for the lithium peroxide preservation, no good discharge product separation strategy is found that is able

to benefit energy density at the same time. The other battery application is a hydrogen peroxide preserving zinc air battery. An alkaline membrane is used in the middle to separate the zincate formed in the anode department and transfer the hydroxide ions formed in the cathode department. A hydrogen peroxide solution is proposed to be generated in the cathode when discharging, and preserving peroxide is critical for the battery operation. And a zinc air battery using this peroxide preserving concept will retain the energy density level compare with the conventional alkaline zinc air battery.

# Chapter 2

# Experimental Methods

## Electrode preparation

Three disk electrodes are used in this work: polycrystalline gold, polycrystalline platinum and glassy carbon disk electrode. They were all 5 mm in diameter, and were purchased from Pine Research Instrumentation. The glassy carbon disk electrode (AFE2A050GC) is for room temperature use. The polycrystalline platinum disk electrode (AFE5T050PTHT) we used is also for high temperature measurements. Two kinds of Polycrystalline gold are used for measurements: one for room temperature (AFE2A050AU); one for high temperature measurement (AFE5T050AUHT). The polycrystalline Au and Pt electrodes are first been mechanically cleaned and then electrochemically cleaned. The mechanical cleaning is done by first polishing with finer 5μm alumina power and then by 0.05μm alumina power (BUEHLER, MicroPolish). After each polishing step, the electrode is rinsed with DI water. The electrochemical cleaning is done by CV in a 2.2V scan range with 50mV/s scan rate in 0.1M $HClO_4$ acid electrolyte, which provokes violent gas evolution and strip off covalent bonded chemical. Lastly, before any electrochemical measurement, the electrode is scanned in the normal electrochemical window for several cycles until the standard CV features is very stable and obvious. The glassy carbon disk electrode is only cleaned by the mechanically polishing since it is relative inert material.

Two RRDE electrodes have been used in the experiments: a gold disk and platinum ring electrode and a glassy carbon disk and platinum ring electrode, both purchased from Pine Research Instrumentation. For the gold disk RRDE disk, the gold insert disk (AFED050P040AU) diameter is 5mm, the platinum ring (AFE6R1PT) inner diameter is 6.5mm, outer diameter is 7.5mm, the collection efficiency is 25%. For the glassy carbon disk RRDE (AFE7R9GCPT), the glassy carbon disk diameter is 5.61mm, the ring inner diameter is 6.25mm and the outer diameter is 7.92mm, the collection efficiency is 37%. Both of these two RRDE electrodes go through the cleaning process as described above. The disk electrode and the ring electrode go through the electrochemical cleaning procedure separately.

## Modified electrode preparation

Three kinds of modified electrodes have been prepared in this work. One is cobalt salen modified polycrystalline gold electrode. The other two are Pt/C catalyst and Au/C catalyst modified glassy carbon electrode. For the first modified electrode, for convenience, many experiments are done in a cobalt salen containing electrolyte environment; but for some special situations, a thin film modification method has been adopted to make a quasi-stable cobalt salen modified electrode. The thin film modification method is described as below. A clean polycrystalline gold disk electrode (polycrystalline gold RDE or polycrystalline gold RRDE) was been prepared first, then 15μL 2mM/L cobalt salen solution was deposited covered the surface of the Au electrode. Then, the electrode was dried for 30mins and a very thin layer film was formed on the surface of the electrode.

The Pt/C catalyst and Au/C modified glassy carbon electrode was prepared by depositing 12 μL ink on the surface of glassy carbon electrode. The ink was prepared using 5% Nafion solution (Sigma-Aldrich) in a 30/70 ionomer to catalyst ratio with methanol as solvent. The 30% Pt/C catalyst was purchased from BASF company, and the diameter of the nano Pt particle is around 2nm. The Au/C catalyst in this work was prepared by two different methods with two different nano particle size (Au/C-a, Au/C-b). The first preparation method (Au/C-a) is done by the most commonly used colloidal gold preparation method, Turkevich method.[91] According to this method, an aqueous solution of chloroauric acid ($H[AuCl_4]$, 88.4mg in 400mL $H_2O$) was heated to 70°C. Then, trisodium citrate solution (212mg in 4mL $H_2O$) is added into the preheated solution to start to reduce chloroauric acid, and the mixture was stirred for 3 hours at 70°C. After the solution is cooled down, an ethanol dispersion of carbon black (XC-72, Cabot) was added to the mixture, and the mixture was stirred for 20 mins then centrifuged. The remain was washed with ethanol and water, dried in vacuum to have the final power like catalyst. The gold to carbon ratio is calculated from the ratio of the material to be 30% wt. The size of the nano particles is around 18nm, calculated from Scherrer equation (equation 2.1) using the data from XRD experiment. The XRD experiment setting is shown in the latter section.

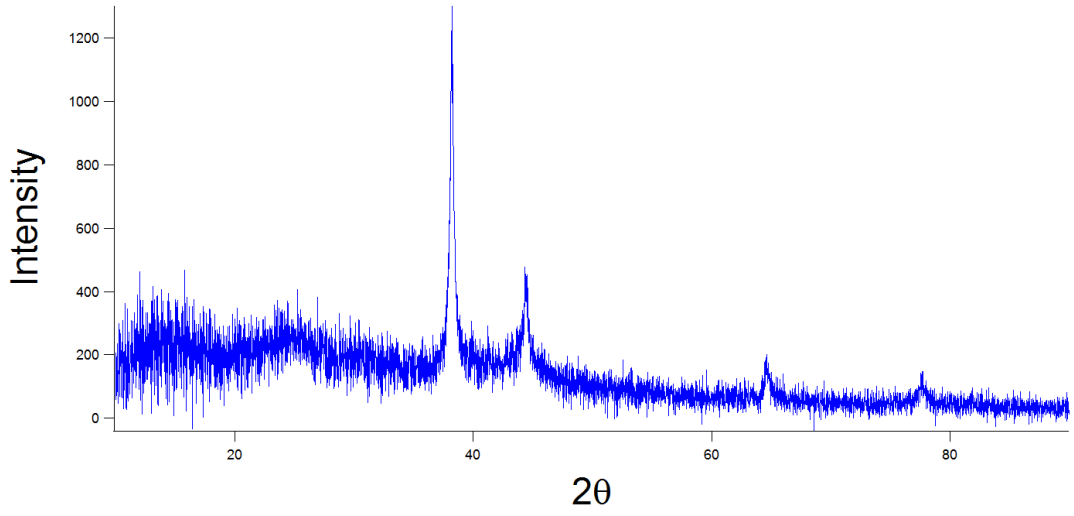


Figure 2.1 XRD patterns of Au/C-a, Peak Au (111) is locate at 38.12, and is used to calculate the nano particle size

$$\tau = \frac{K\lambda}{\beta \cos\theta} \qquad \text{(Equation 2.1)}$$

The second method to prepare gold on carbon catalyst is using the magnetron sputtering method. XC-72 and two 1 inch Teflon coated stir bars were placed inside a set of stainless steel cups attached to a vacuum compatible motor. A high purity gold target (Refining systems, 99.99%) was sputtered, at an applied power of 14W, for 160 mins, by direct current magnetron sputtering in an Ar atmosphere onto the continuously rotating carbon black. Gold loading was determined using Inductively Coupled Plasma (ICP) Optical Emission Spectrometer. Five ml's of freshly prepared aqua-regia (3:1 mixture of hydrochloric acid and nitric acid) was used to dissolve the Au from the samples for analysis. Then, the samples were centrifuged to separate the carbon support from the acidic liquid phase which was collected by decanting. The collected wash was combined then diluted

and used for ICP measurements. The ICP standard is prepared by the serial dilution of a gold standard purchased from Alfa-Aesar. The experiment result shows the Au loading was 4.77%. Compare with previous Turkevich method, this method is free of residual impurities like leftover reducing agent. The average particle size is estimated to be about 1.8nm, calculated from scanning transmission electron microscopy (STEM) data, as shown in Fig 2.2. (The catalyst and preparation method is from Gabriel M. Veith from ORNL)

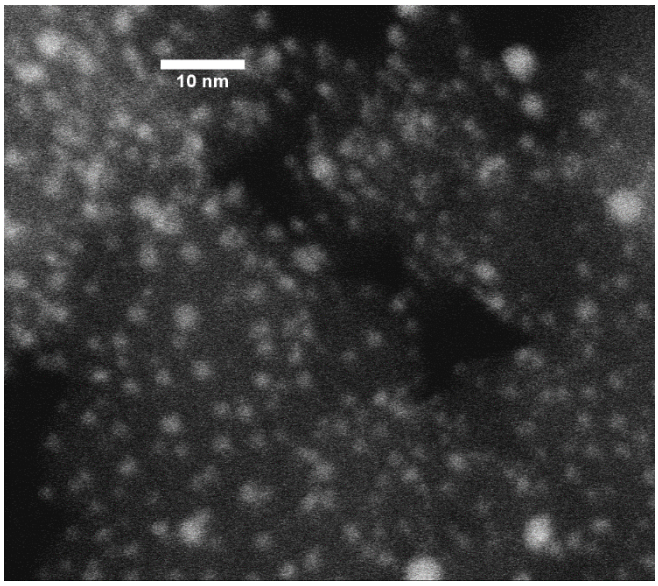


Figure 2.2 STEM images of gold particles on carbon black (Au/C-b)

## Electrochemical measurements

All experiments were conducted in a standard three-compartment electrochemical cell sealed from the ambient environment. For RDE experiment, a modulated speed rotator (model ARMSRCE, Pine Research Instrumentation) was used. For three-electrode cell systems, a potentiostat (SP-200, Bio-logic) is used to make the measurement, a multi-channel potentiostat (VMP3, Bio-logic) is used for RRDE four electrode system. A gold

wire counter electrode was separated from the working electrode by a porous glass frit. For measurement in alkaline electrolyte, a Hg/HgO reference electrode or a double junction saturated Ag/AgCl reference electrode are used; for measurement in acid electrolyte, a saturated $Hg/HgSO_4$ reference is used. For some experiments, the reference electrode was calibrated to the reversible hydrogen electrode (RHE) by sparging the cell with $H_2$ and measuring the open circuit potential (OCP) at a Pt working electrode. For RDE experiments, a Teflon plug with a bearing was used to cap the electrode entrance and fits snuggly around the shaft of a rotating electrode. During the experiment, either $O_2$ or Ar atmospheres were maintained with a slight positive pressure generated by a water or oil bubbler on the gas outlet from the cell.

For the alkaline electrolyte electrochemical measurement, alkaline solution was made by potassium hydroxide (Sigma Aldrich, 306568-500G), lithium hydroxide (Sigma Aldrich, 545856-100G) and Mili-Q water. A glass electrochemical cell (Pine instruments, RRPG085) with water jacket is used for temperature controlling experiments, and a heated water bath circulator is used to control the temperature. EDTA (E9884-100), as peroxide stabilizer, was purchased from Sigma-Aldrich. For the organic electrolyte electrochemical measurement, the glass electrochemical cell was dried in the oven to remove water. Organic electrolyte was made by acetonitrile (J.T.Baker, JT9255) and Tebrabutylammonium bromide (Sigma Aldrich, 426288-25G). The cobalt salen used in both aqueous and organic electrolyte is from Sigma Aldrich (274712-1G).

Before every electrochemical measurement, the potential was hold at OCV for 30 mins. For all the cyclic voltammetry (CV) experiments in this work, after the OCV potential

holding, the potential will scan from the OCV potential to the lower potential, then scan back after it reached the lower potential limit.

The tafel plots in this work are made by plotting the log (current density) vs potential from related RDE experiment kinetic region. The HCD (high current density) range tafel slope is calculated by selecting data points from 0.1mA/$cm^2$ to 1mA/$cm^2$. The LCD (low current density) range tafel slope is calculated by selecting data points from 0.01mA/$cm^2$ to 0.1mA/$cm^2$.

## FTIR measurement

FTIR measurement was carried out on a Vertex 70 (Bruker Coporation) on an ATR unit in a $N_2$ purged environment. For the purpose of verifying catalytic activity, cobalt salen was deposited on a piece of gold coated silicon wafer (Ted Pella Inc, No.16012-G) by drying a 15mL 2mM Cobalt salen solution on the surface. (Thin film modification) The gold coated silicon wafer is 5$cm^2$ cut from a 2 inch diameter piece. The gold layer thickness is around 50nm, and the silicon wafer is around 500μm. The Au layer is coated by vacuum evaporation system. The surface is not atomically flat, but has roughness in the nm range. Before each experiment, the sample container is purged with $N_2$ for 10 mins. An LN MCT mid-range IR detector was used, and a liquid $N_2$ cooling procedure is carried out before each use. A background scan was also taken before each sample measurement with the same measurement conditions. The scan range is from 350 to 8000 $cm^{-1}$ with 4 $cm^{-1}$ resolution. Although all the experiments were conducted in a $N_2$ purged environment, the influence of $CO_2$ still cannot be fully eliminated. The background scan and the experiment scan sometimes have different extent of $CO_2$ influence in the results. Subtracting the

background from experiment result sometimes created a small signal around 2300 $cm^{-1}$. Since our sample did not have the possibility to produce a peak around 2300 $cm^{-1}$, which intercross with $CO_2$ peaks. The $CO_2$ related peaks are all manually wiped out from the graph.

## XRD measurement

The XRD experiment is carried out on a Bruker D2 PHASER. The radiation source is from a Ni-filtered CuKα X-ray sealed tube with intensity of 30Kv/10mA, λ=0.154184. 2θ range is from $20^o$ to $75^o$, with $0.14^o$ and 0.5s per step. A background scan with the same experiment condition is conducted before the sample scan. Peak analysis of obtained patterns was performed using multi-peak fitting (Voigt fit) function of Igor pro software.

# Chapter 3

# Reversible ORR catalyst - I Reaction mechanism

## 3. 1 Background research

### 3.1.1 Quasi-reversible Oxygen reduction reaction on Au (111)

While ongoing efforts on searching for a better bifunctional catalyst for air battery, it has been somewhat overlooked that Au (111) is a good catalyst which that can process a two-electron quasi-reversible oxygen reduction. N.M.Markovic and his colleagues examined ORR and peroxide reduction catalytic activity in detail. It is found that Au (111) process a net two-electron reduction of oxygen, while Au(110) process a mixture of two-electron and four-electron reduction of oxygen and Au (100) process a four-electron reduction of oxygen within certain potential range.[92]

As seen from the Figure 3.1 below, there is almost no current on the cathodic scan in the voltammogram of Au (111), and the tiny current present should be due to the reduction of oxygen which comes from the self-decomposition of peroxide on the electrode surface. Therefore, one can conclude that peroxide is very stable on the surface of Au (111). On the peroxide oxidation aspect, all three crystallographic orientations show good catalytic activity. This suggests a quasi-reversible mechanism for ORR on both Au (110) and Au (111). The Ohsaka group has studied the above phenomena in detail and confirmed that quasi-reversible nature of gold-catalyzed ORR. (Fig 3.2)[93]

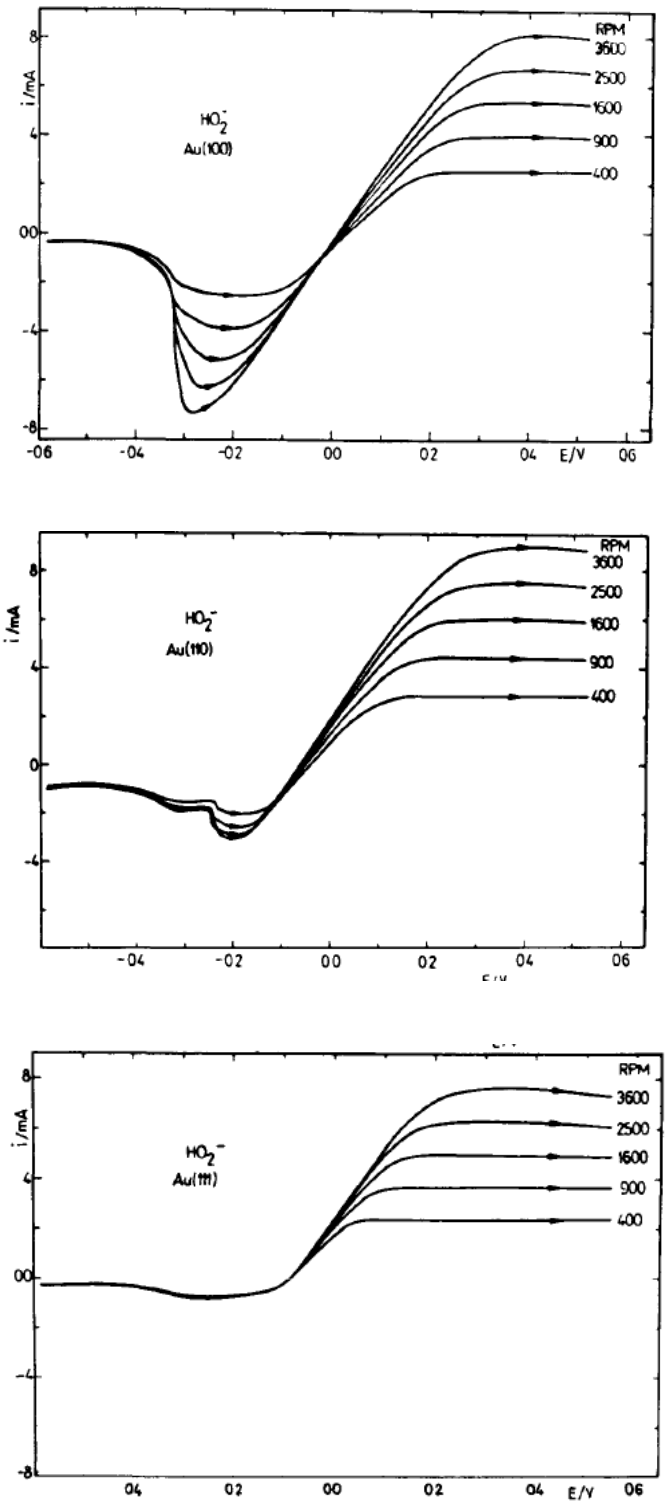


Figure 3.1Voltammetry curves for $HO_2^-$ reduction and oxidation on Au single crystal electrodes in $N_2$-saturated 0.1 M NaOH containing 8.5mM $HO_2^-$. Sweep rate:50mV/s; electrode area: 0.5 $cm^2$ [92]

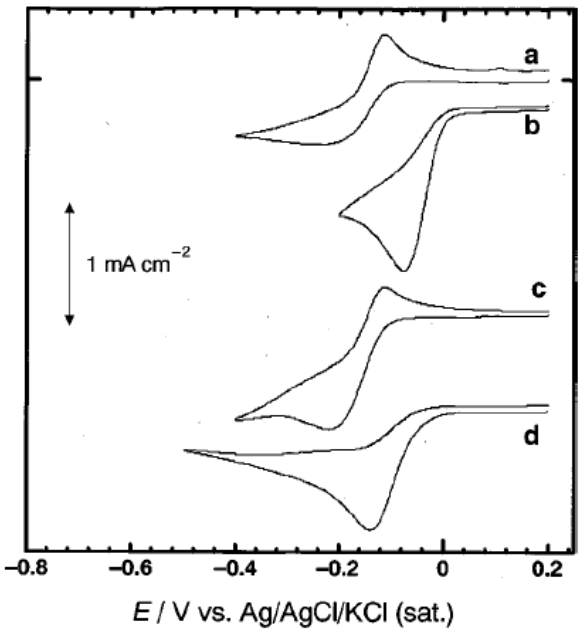


Figure 3.2 CVs for the ORR obtained at (a) Au(111) , (b) Au(110), (c) Au(100) single-crystalline, and (d) unmodified (bare) poly-Au electrodes in $O_2$ saturated 0.5 M KOH. Scan rate: 50mV/s. [93]

As can be seen in Figure 3.2, Au (100) produces a four-electron irreversible ORR similar to that observed for poly-crystalline Au, while Au (110) and Au (111) show a quasi-reversible case. And the ratio of cathodic peak current to anodic is almost equal to one for the Au (111) electrode while a higher ratio is obtained on Au (110), which also tells us that peroxide production is important here.

### 3.1.2 Oxygen reduction reaction on Au (100)

It has been acknowledged that Au (100) is one of the best ORR catalysts in alkaline media, showing activity comparable to that of Pt. ORR catalyzed by Au (100) proceeds via a four electron reduction of $O_2$ to $OH^-$ while the other two single crystalline planes catalyze two electron reductions of $O_2$ to $HO_2^-$. Additionally, the half-wave potential of ORR is nearly

200mV more positive for Au (100) when compared with that of the other two low-index planes.[92] The four-electron process inherent to Au (100), though desired in fuel cell applications, has been found to be very sensitive to surface structure and operates only over at a certain potential range. Two dominant factors, namely the AuOH layer formed by chemisorption of OH- and four fold symmetry sites on Au (100)-(1×1), are commonly considered to be as two prerequisites necessary for ORR via a four-electron process. The importance of $OH^-$ adsorption has been demonstrated by Strbac and Adzic.[94] Their work with various orientations of Au (*hkl*) in 0.1 M NaOH with RDE and RRDE illustrate the relationship between the potential range of this adsorption and the crystallographic orientation, as can be seen in Figure 3.3. Apart from the OH- formation, the positive sweep in the CV of Fig 3.3 also shows the feature of irreversible oxide formation and surface reconstruction, which will be discussed later. Results on ORR from this paper proves that the four electron oxygen reduction activity does firmly correlate with the specific adsorption of OH-. The authors propose that the 4-fold symmetry sites of Au (100) provide a more suitable surface for chemisorption of hydroxide relative to the close packed hexagonal lattices of other gold catalysts which favor physisorption. A similar argument can be made for the chemisorption of $HO_2^-$ on different gold surfaces, which is thought to be necessary for ORR by a four-electron process under alkaline conditions. These observations taken together may explain why the mechanism of ORR observed by Au (100) differs from that seen for Au (110) and Au (111).

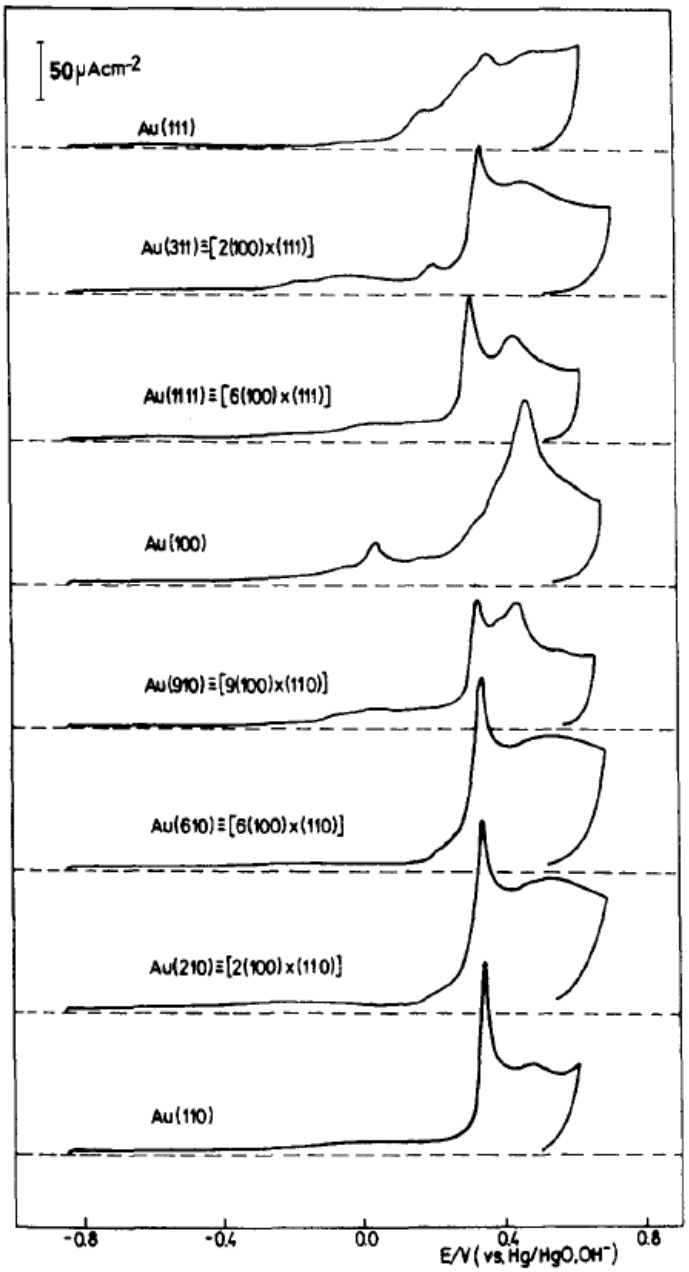


Figure 3.3 Positive going sweeps for various Au (hkl) surfaces in $N_2$-saturated 0.1M NaOH; Scan rate: 50mV/s[94]

### 3.1.3 Surface reconstruction phenomenon on Au electrode

The reconstruction of clean metal surfaces, including Pt, Au and Ir, when prepared under ultra high vacuum (UHV) condition is well-known. The surface atoms rearrange in order to achieve lower surface energy. In an electrochemical environment with enough negative potential below potential of zero charge (pzc), a similar surface rearrangement can occur.[95] Features of cyclic voltamograms on metal electrodes have long been assigned to surface reconstruction, an assumption later proved by the study of the electrode-electrolyte interface with the help of STM, LEED, RHEED technologies. [95,96,97,98] Low-index single crystalline electrode surfaces are much more stable than high-index planes under most conditions. As a result, research has focused on surface reconstruction phenomena for the low-index planes. The graph below shows the native and rearranged structures of three single crystal surfaces of Au.

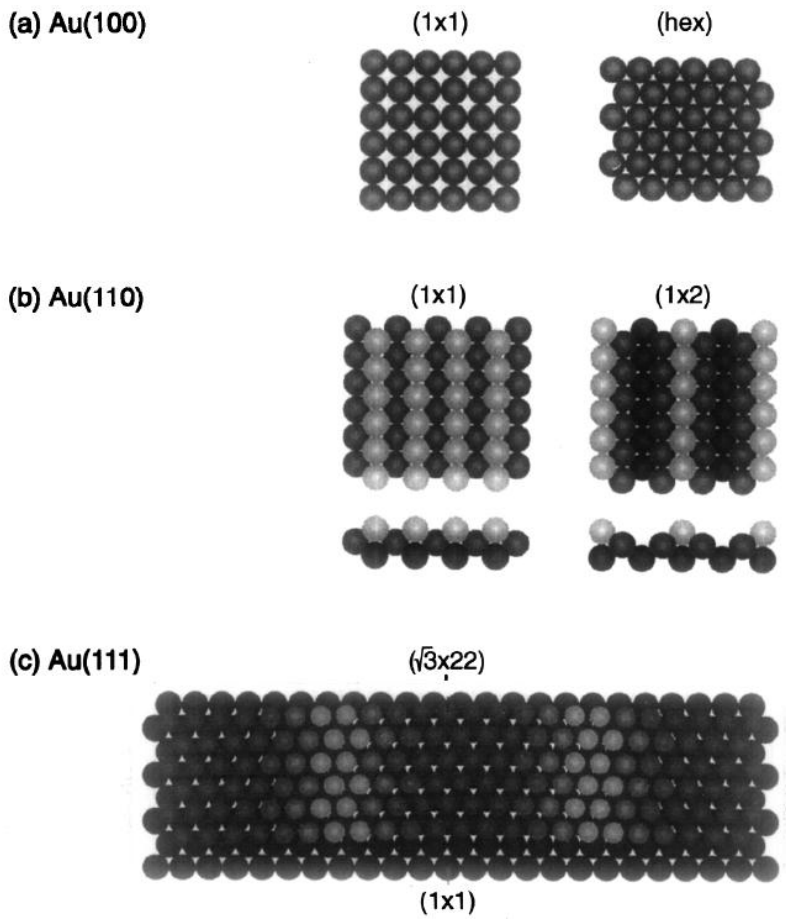


Figure 3.4 The structure of unconstructed and surface-rearranged gold single- crystal surfaces [99]

Au (100) reconstruct into a hexagonal close packed form, usually been called Au (100)-"hex" or termed "$(5 \times 20)$". This Au (100) reconstructed structure becomes an Au (111) similar structure with triangle coordinated sites. However, the actual reconstructed structure is slightly buckled and forms a corrugated surface. Au (110) surfaces typically reconstruct into a $(1 \times 2)$ structure with one row missing. At some occasions, a $(1 \times 3)$ structure with two row missing can be observed. [100,101] Both $(1 \times 2)$ and $(1 \times 3)$ structure will lead to a narrow micro-facet of a buckled Au (111) similar structure, as can been seen

from Fig 3.4 (b). Xueying Zhao et al. proved that glycine physisorption can induce a surface reconstruction on Au (110).

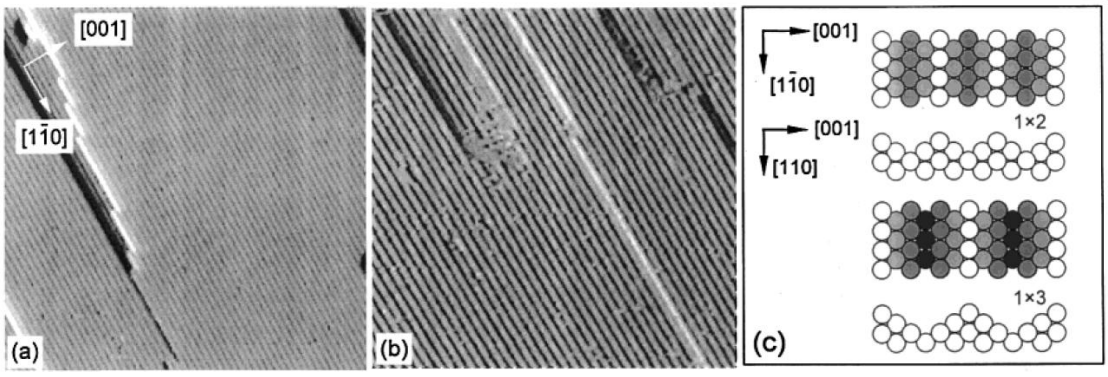


Figure 3.5 STM images (500Å × 500 Å) obtained from Au (110) surface in the course of low rate glycine deposition: (a) the clean Au (110) 1×2 surface before deposition, obtained with a bias voltage of -2.0V and a tunnel current of 0.6nA; (b) image (1.0V, 0.6nA) of the 1×3-reconstructed surface obtained at the low-rate deposition process; (c) (top half) top view (upper) and side view (lower) of the missing-row model of Au (110) 1×2 surface, (bottom half) top view (top) and side view (bottom) of the 1×3 reconstructed Au (110) surface.[100]

As can been seen from Figure 3.5, depending on the interaction time between glycine and Au surface, Au (110) $1 \times 2$ and Au (100) $1 \times 3$ can be successfully obtained and measured by STM. Although both of the buckled Au (111) similar structure got from reconstructed Au (110) and Au (100) surface is different from genuine (111) surface, their three coordinated sites structure still make their catalytic activity similar to Au (111) in some cases. This phenomenon will be discussed further in the following sections. [100]

In an actual electrochemical environment, Au electrode surface reconstruction is a result of many different factors. Generally, bare unreconstructed surfaces are in a meta-stable

state. Apply a controlling potential negative to the potential of zero charge (pzc) can reduce the activation barrier to induce reconstruction. Besides the negative potential, other species from the electrolyte can also play a vital role though the interaction at the electrode and electrolyte interface. Usually, specifically and nonspecifically adsorbing ions may have a impact on surface reconstruction through a chemical bond, but physisorption based interaction from neutral species or even omnipresent water can sometimes have a large influence on the surface energy.

### 3.1.4 The influence of Au surface reconstruction on ORR

As discussed before, the ORR is a good example of how an electrochemical reaction is sensitive to surface structure. Since the catalytic activity of ORR has such a significant difference on three low index single crystal, surface reconstruction on Au electrode can also greatly influence the catalytic activity.

A similarity between Au (100) and Au (110) surface reconstruction, as we summarized above is that, the reconstructed surface tends to have a larger buckled Au (111) surface. The surface reconstruction on a Au (111) surface itself does not show such a large difference with only more close packed surface atoms. Therefore, we can conclude that it is possible to fabricate an Au (111) similar electrode from a polycrystalline Au electrode with specific controlled surface reconstruction on the Au (100) and Au (110) domain. Then, the only difference between this special reconstructed Au electrode and a simple Au (111) single crystal electrode is that some domain of the reconstructed surface has more corrugation than an Au (111) single crystalline electrode.

The next important question is whether oxygen reduction behaves differently on this buckled Au (111) similar surface. The answer is yes, R.R.Adzic et al. used STM and XRD to directly compare oxygen reduction between Au (100) (1×1) surface and Au (100) hexagonal close packed surface.[102] They experimentally prove that four electron oxygen reduction and two electron peroxide reduction occurs on Au (100) (1×1) surface. Au (100) hexagonal close packed structure supports two electron oxygen reduction and is not active for $HO_2$- reduction. The author also proves that $HO_2$- itself did not have any influence on the reconstruction. These results correlate very well to the previous theoretical assumption. Chemisorption of $HO_2^-$ is only active on four fold symmetry sites; other three fold sites, corrugated or not, all have negligible activity towards $HO_2$- adsorption.

Except for the influence from the electrode surface change, the transition process of the surface reconstruction itself is also an interesting aspect to look into. The transition potential of reconstruction depends on both the surface structure and the electrolyte environment. Fig 3.6 is a demonstration of how the anion influences the reconstruction transition potential. We can see that, in some electrolyte environment, the transition potential is within the range where we usually characterize the oxygen reduction. However, further in-situ electrochemical surface experiments show that the transition process does not have a dominant effect here. Firstly, the kinetic region of oxygen reduction is much narrower than the potential range of surface reconstruction. Furthermore, the whole surface reconstruction process has been proved to be a much slower process than oxygen reduction with at least two orders of magnitude. [102,103,95]

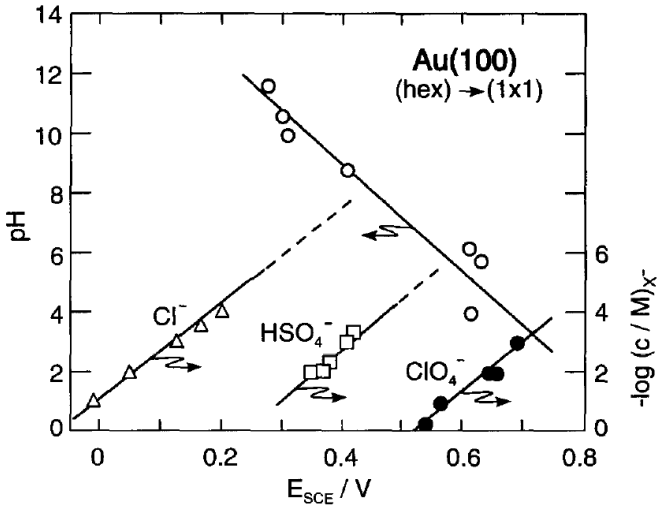


Figure 3.6 Transition potential for Au (100): (hex) ~ (1 ×1) as a function of anion concentration and PH. The (hex)-structure is stable only at potentials to the left of the respective line.[104]

### 3.1.5 Au (111)-like polycrystalline gold electrode

Since different crystallographic gold domains have effects over oxygen reduction reaction, people try to create different crystallographic orientation catalyst particles for different applications. For example, S.Othman et al. try to create Au (100) like nanoparticles for oxygen evolution.[105] Shouheng Sun's group from Brown University looks into the surface and structure effect on Au nanoparticles for oxygen reduction; they found that 8nm nanoparticles with good Au (111) facets and special facet angles have the highest specific activity over other particle sizes and commercial nanoparticles. Gold electrodes, like other noble metal electrodes, will go through a relaxation process after certain electrochemical reactions, and special orientation on the catalyst surface is hard to maintain forever. It is difficult to manufacture nanoparticles with one single crystal domains, nanoparticles with dominant single crystal domain are more realistic. In this case, chemically modified

electrodes can be a good way to help us to have more control over catalyst activity. Takeo Ohsaka's group focused on special chemical modified Au electrodes for oxygen reduction.[106–113] Some of their work showed that certain thiol compounds can form a sub-self-assembled-monolayers (sub-SAM) on the polycrystalline Au electrodes, and the selective adsorption feature of this modification makes it capable of blocking the catalytic activity of both Au (110) and Au(100), leading to switching the behavior of the poly-Au electrodes to that of single-crystal. [93,114,115] Fig 3.7 shows CVs of ORR on polycrystalline Au electrode modified by several thiol compounds with different surface coverage.

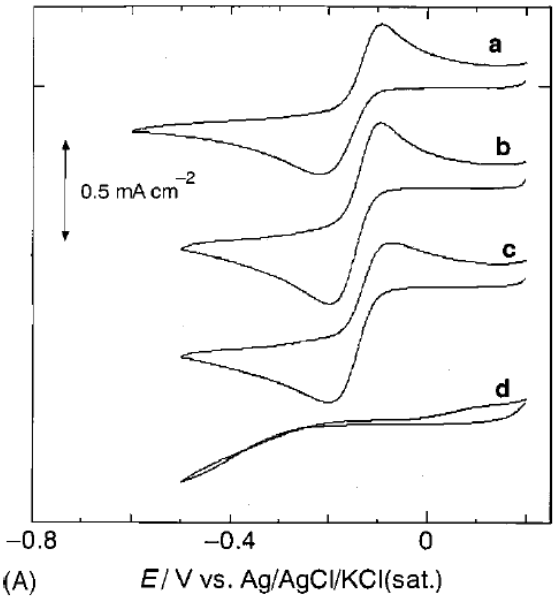


Figure 3.7 CVs for the ORR obtained at sub-SAM/Au electrodes fabricated with (a) CYST ($\Gamma_{CYST}$= 7.09 × $10^{-10}$ mol $cm^{-2}$), (b) MAA ($\Gamma_{MAA}$= 1.31 × $10^{-9}$ mol $cm^{-2}$), (c) CYSN ($\Gamma_{CYSN}$= 1.04 × $10^{-9}$ mol $cm^{-2}$) in $O_2$-saturated 0.5 M KOH. Curve (d) shows the CV for the ORR at a compact CYST SAM/Au electrode ($\Gamma_{CYST}$= 1.13 × $10^{-9}$ mol $cm^{-2}$). Scan rate: 50mV/s. [93]

The sub-SAM Au electrode is made from partial reductive desorption. This means weakly bounded chemisorbed thiol molecules from the Au (111) domain is believed to be stripped off from the poly-Au electrode; and the Au (110) and Au (100) are left covered. Thus, this sub-SAM behaves like Au (111) single crystal Au electrode with similar quasi-reversible feature on ORR.

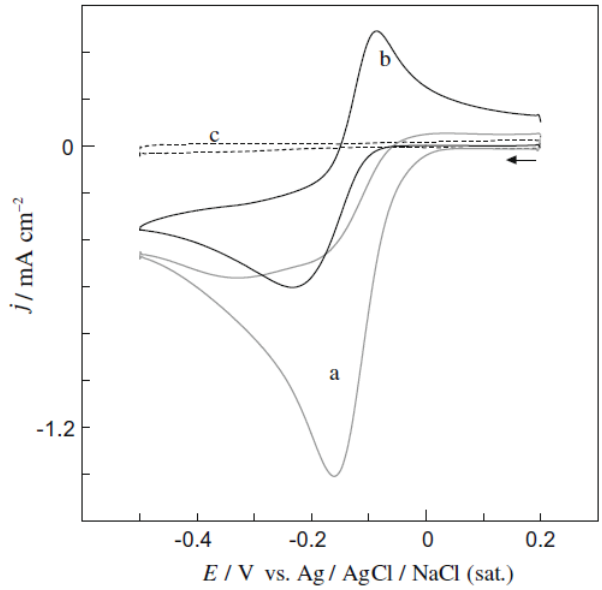


Figure 3.8 CVs obtained at the (a) bare Au (poly) and (b,c) sub $I_{(ads)}$/ Au (poly) electrodes ($\Gamma = 1.8 \times 10^{-9}$ mol $cm^{-2}$) in (a,b) $O_2$- and (c) $N_2$-saturated 0.1 M KOH solutions. Scan rate: 100mV/s.[116]

Since the above selective specific adsorption mechanism is based on the relative weak bonding of thiol on the Au (111) domain, other specific adsorption approaches have proved to be capable of partly modifying Au (110) and Au (100) on poly-Au electrode via the same mechanism. Halogen elements adsorption is commonly studied in many electrochemical systems since bromine and chlorine are good choice of oxidants. There is an acknowledgment that the specific adsorption bonding energy should follow the order :

$Cl^- < Br^- < I^-$ .Bromine and iodine are used for the sub-modification since they have stronger specific bonding energy.[116,117,108]

From the figure above, we can see that the poly-Au electrode behaves like Au (111) again by sub-modification. Although the author does not point out which cycle this is for the bare poly-Au electrode, the graph (a) should be the first cycle of the CV. This tells us how much surface space should available for the Au electrode. By comparing graph (a) and graph (c), it may indicate that, after this sub-modification, only partial of the surface (Au 111) participates in the oxygen reduction. No clear comparison of kinetic is given between the sub-modified electrode and the bare electrode. From the basic CV data, it seems the kinetics of the sub-modified electrode is equal to or a little worse than the bare poly-Au electrode, possibly because ORR kinetic on Au (111) is slower than Au (110) or Au (100). For both of these sub-modification (thiol and Iodine modified), the author used several different methods to verify the reaction mechanisms of ORR on these Au (111)-like electrode. Results from RRDE (Au disk, Pt ring) electrode shows that, althrough sub-modified Au electrode has poor kinetic of ORR and smaller peak current, the ratio of two electron peroxide production current is almost equal to the total current. This proves that the oxygen reduction on this sub-modified electrode is a two-electron process. The other strong proof comes from the use of peroxide and superoxide disproportion enzyme, dismutase (SOD) and catalase (Fig 3.9).[93] By applying them into the electrolyte, results show that the reversibility of ORR is totally ruined by the use of catalase, peroxide disporportion enzyme , but not affected by using dismutase (SOD) at all.

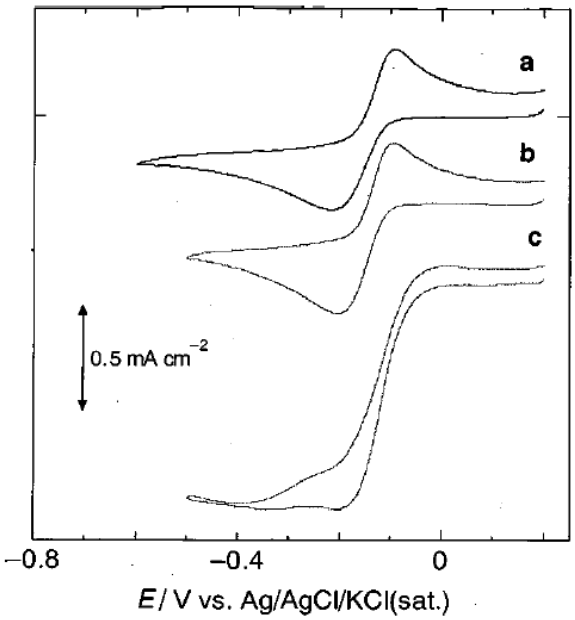


Figure 3.9 CVs for the ORR obtained at CYST sub-SAM/Au electrode ($\Gamma_{CYST}$= 7.09 × $10^{-10}$ mol $cm^{-2}$) in $O_2$-saturated 0.5 M KOH containing (a) 0.0 μM SOD + 0.0 μM catalase, (b) 0.03 μM SOD, and (c) 0.3 μM catalase. Scan rate: 50mV/s.[93]

## 3.2 Interaction between cobalt salen and Au in alkaline environment

The interactions between cobalt salen and different electrode material have been studied in many electrochemical systmes.[118–122,123] Carbon electrode or carbon paste modified electrodee is most commonly used to characterize the electrochemical activities of Cobalt salen. Since the cobalt is only chelated with the salen group, the valence changing features of cobalt is most obvious features of the voltammetry. In organic electrolyte environment, both $Co_2$+ / $Co_3$+ and $Co_1$+ / $Co_2$+ redox peaks can be seen from the voltammetry.[118] For the aqueous eletrolyte environment, only $Co_2$+ / $Co_3$+ valence change can be observed due to the limit electrochemical window.[123] To understand the interaction between cobalt salen and Au electrode in the alkaline environment, we use CV scanned over the full

electrochemical window to characterize all the features. Fig 3.10 (a) is a demonstration of how a polycrystalline Au electrode behave in an electrolyte environment of alkaline and cobalt salen.

Before this experiment, the Au electrode electrode goes though a standard electrochemical cleaning and mehanical polishing process as described in the experiment section. As can be seen from the Figure 3.10 (a), within the 1.7 V electrochemical window, we can see two main peaks on anodic scan and two main peaks in cathodic scan. On the anodic scan, the first peak from the range of (-0.6V~0.0V) can be attribued to the process of oxidation of $Co_2+$ to $Co_3+$ from cobalt salen complex. The second peak from the range of (0.05V~0.5V) can be attributed to the possible specific adsorption of OH- and oxide formation. By contrast, the two peaks on the cathodic scan correspond to the reverse process of the two peaks in the anodic scan. The peak from the range of (-0.1V~0.2V) can be attributed to the process of OH- and oxide stripping. The peak from the range of (-0.5V~ -1.0V) correspond to the process of reduction of $Co_3+$ to $Co_2+$ from cobalt salen compound. The two peaks of $Co_3+$ / $Co_2+$ redox couple in this graph has a peak seperation of roughly 300mV, indicates this is a quasi-reversible process. Since this is in alkaline solution, the two relative peaks above 0.0 V should be a combination of OH- and oxide formation and stripping process. According to the discussion in the former section, the fact that there is no obvious OH- specific adsorption region suggest there is fewer Au (100) based domains exist on the Au electrode surface. The very small peak around 0.05 V has two possbilities. One is a nearly buried OH- adsorption peak. The other reason can be the adsorption of an electroactive $Co_3+$ species. Another experiment (Fig 3.11) is specifically set up to verify this assumption.

Comparing experiment (a) and experiment (b) in the Figure 3.10, we can also see the difference between CVs with or without having cobalt salen in the electrolyte environment. Compare with Figure 3.10a, Figure 3.10b does not show the redox peaks of cobalt salen in the lower potential region, but the OH- adsorption and oxide formation region is largely constrained. Based on the fact that the corresponding stripping region still remains with the same magnitude, we can assume the enhancement part is due to the ireversible oxide formation. On the other hand, this enhancement also indicates that, Au has a much stronger interaction with oxygen containing species, which can be a very important factor for our further understanding on ORR. This direct comparison can give us a basic understanding of the surface specific adsorption species situation in the inner Helmholtz layer. This will help us in the reaction mechanism discussion later.

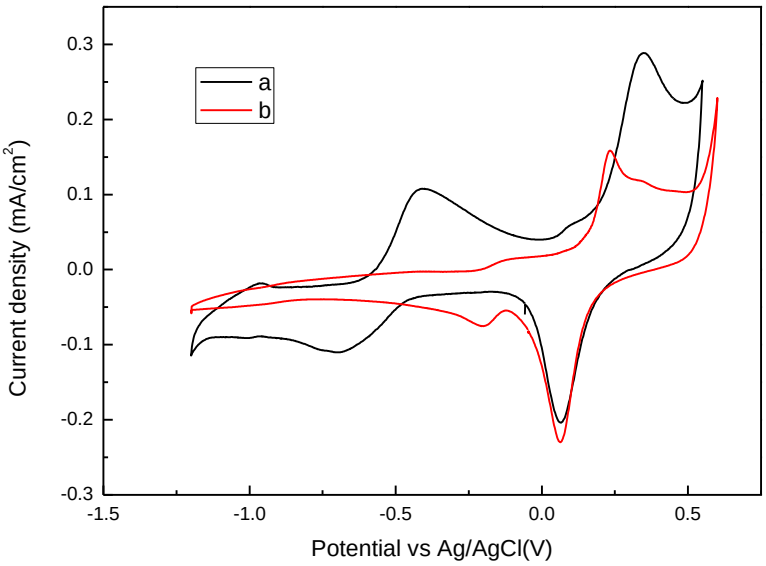


Figure 3.10 CV obtained on Au (poly) electrode in (a. 1M KOH+ 2mMcobalt salen b. 1M KOH) $N_2$ saturated electrolyte. Scan rate: 50mV/s.

Since the previous experiment (Fig 3.10 a ) focused on the properties of the redox couple of $Co_3$+ / $Co_2$+ and whether a follow-up electrochemical adsorption is exist, the scan range for the CV is reduced and features of gold oxide formation and stripping are eliminated. A forty-cycle continuous scan CV in the same electrolyte environment is shown below.

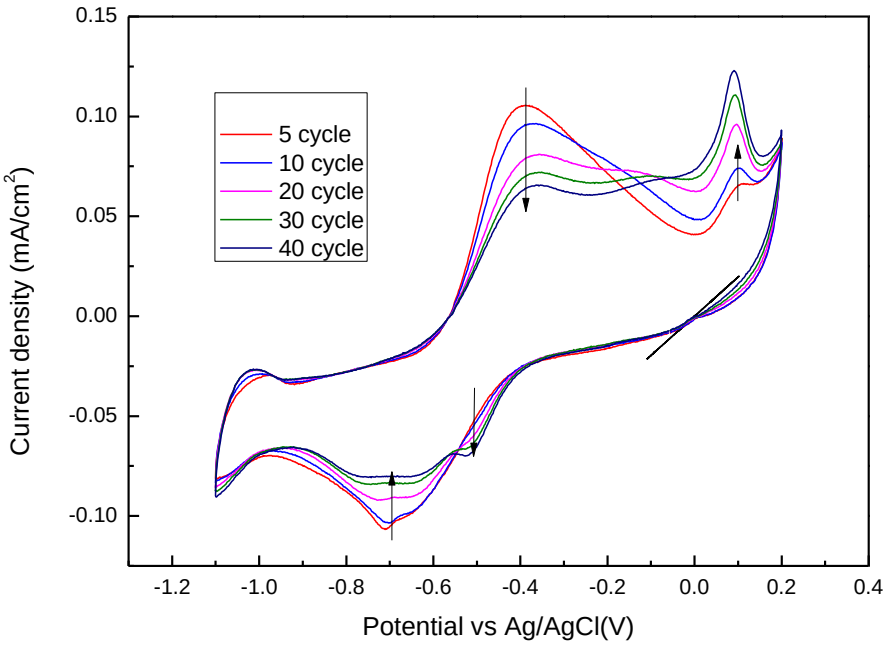


Figure 3.11 CV of several cycles picked from 40 cycles continuous CV on Au (poly) electrode. Scan rate: 50mV/s, electrolyte: 1M KOH +2mM cobalt salen (purged 30mins $N_2$ before experiment)

As can be seen from Fig 3.11, there are four trends of the peak shape along with continuous CV cycles. The two original large redox peaks as described in the last graph gradually vanished cycling. However, a small peak around 0.1 V in the anodic scan and another small peak around -0.5 V in the cathodic scan gradually appeared and are enhanced with cycling. As $Co_3$+ / $Co_4$+ is not possible in this potential region, the most probable cause for the

emerging peaks along with decay of the $Co_3+$ / $Co_2+$ redox peaks is the specific $Co_3+$ adsorption and partial desorption. The phenomenon of peak current density of $Co_3+$ / $Co_2+$ redox couple gradually decreasing could be because of a gradual coverage of the other species on the electrode surface. The gradually enhanced new anodic scan peak can be the accumulated $Co_3+$ species on the electrode surface. The cathodic emerging peak is much smaller than the anodic emerging peak, which means this could be a gradually growing adsorption process. This is also reasonable for the above postulation that the surface is gradully blocked. In this case, this proposed gradual adsorption induced electrode surface blockage needs to be prevented from interfering with any other desired electrochemical process.

## 3.3 Oxygen reduction reaction on cobalt salen modified Au electrode

As we previously discussed before, both gold and cobalt salen have been researched to be possible candidate to replace Pt an better oxygen reduction catalyst. Oxygen reduction on a Au electrode depends on the specific planes where the reaction happens. The mechanism of oxygen reduction can be either four electron reduction or two electron reduction. Cobalt-Schiff base complexes are well-known for their property of reversible coordinating dioxygen. Because of this property, scientists tried to use them as oxygen reduction catalyst.[118,120,123,124] Since there is an acknowledged that the limiting step of the reduction process is the adsorption of dioxygen to the catalyst surface,.[118,125] Among the cobalt-schiff base complexes, the best known is N,N'-bis(salicylaldehyde)-ethylenediimino cobalt (II), commonly called, cobalt salen. Recently we found out that a cobalt salen modified Au electrode can combine the features from the Au electrode, cobalt salen and the special

interaction between them to create a catalyst with a unique property towards oxygen reduction. We just showed how Au electrode behaves in electrolyte environment with cobalt salen present, when purged with nitrogen. However, more interesting properties show up when the same electrolyte system is purged with oxygen. Fig 3.12 and Fig 3.13 is a CV of comparison of a Au electrode in a 1M KOH and 1mM cobalt salen electrolyte when purged with nitrogen and oxygen.

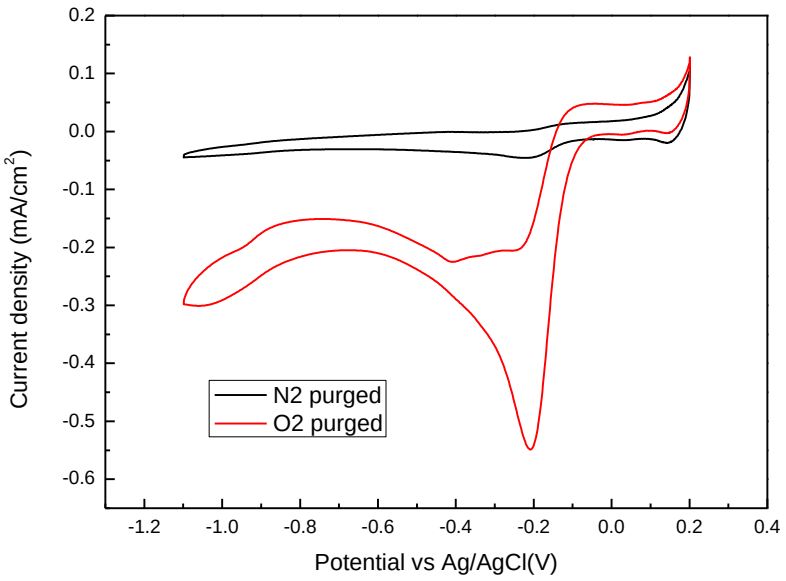


Figure 3.12 CV of comparison of a Au electrode in a 1M KOH electrolyte when purged with nitrogen and oxygen  Scan rate: 50mV/s

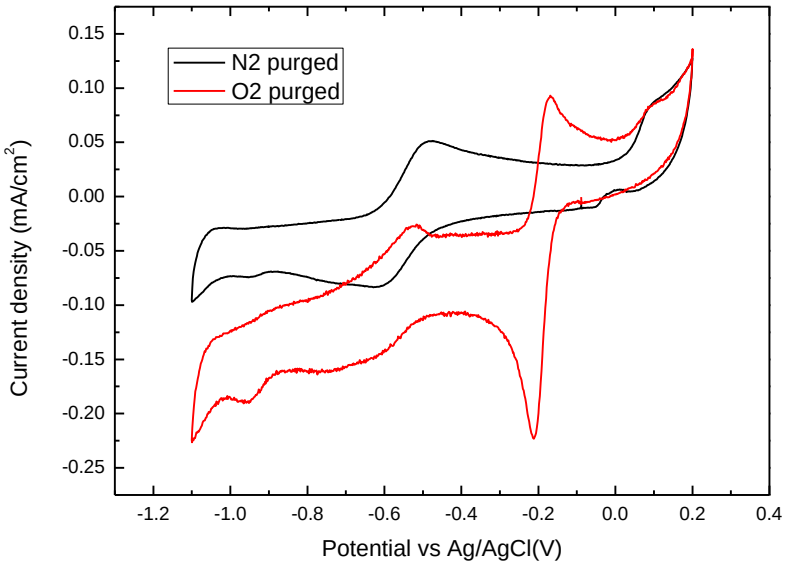


Figure 3.13 CV of comparison of a Au electrode in a (1M KOH + 1mM cobalt salen) electrolyte when purged with nitrogen and oxygen  Scan rate: 50mV/s

As can be seen from the Fig 3.13, except for peaks from $Co_3$+ / $Co_2$+ redox couple and the gold oxide formation peak, a reversible redox peak appears around -0.2V. Based on the reaction potential and the fact that these peaks only show up in the oxygen saturated solution, we temporarily assume that these two new redox peaks are for oxygen reduction. The $Co_3$+ / $Co_2$+ redox peaks exist at the same time with oxygen redox peaks also eliminate the possibility of $Co_3$+ / $Co_2$+ redox peaks swith positively to a higher potential. Thus, in this situation, we assume that we achieve an uncommon oxygen reduction property, this is an oxygen reduction with very good reversibility in aqueous electrolyte. To further understand the reversibility of the oxygen reduction on this particular electrode, we reduce the scan range to a smaller scale, which is symmetric with respect to the redox formal

potential and omits the influence of the redox couple of $Co_3+$ / $Co_2+$. Fig 3.14 is the specific CV for characterizing the properties of the new redox couple in a reduced range.

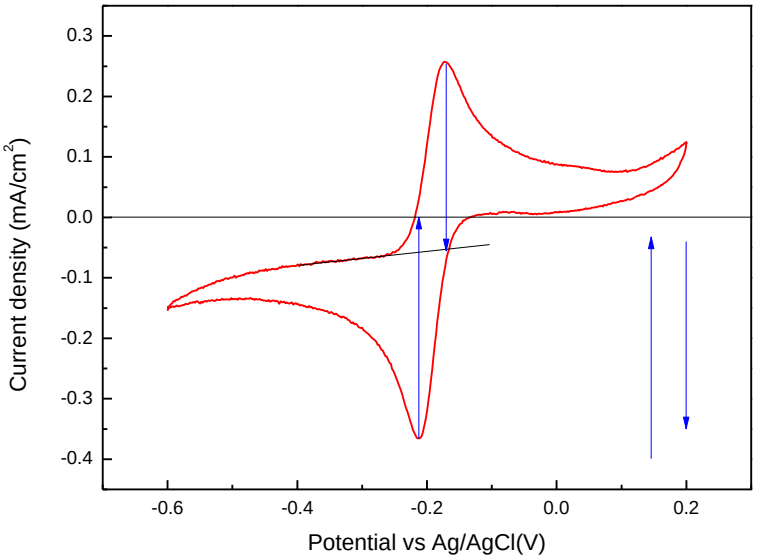


Figure 3.14 CV of ORR Au (poly) electrode in electrolyte (1 M KOH + 1mM cobalt salen), Scan rate: 50mV/s ,IR corrected

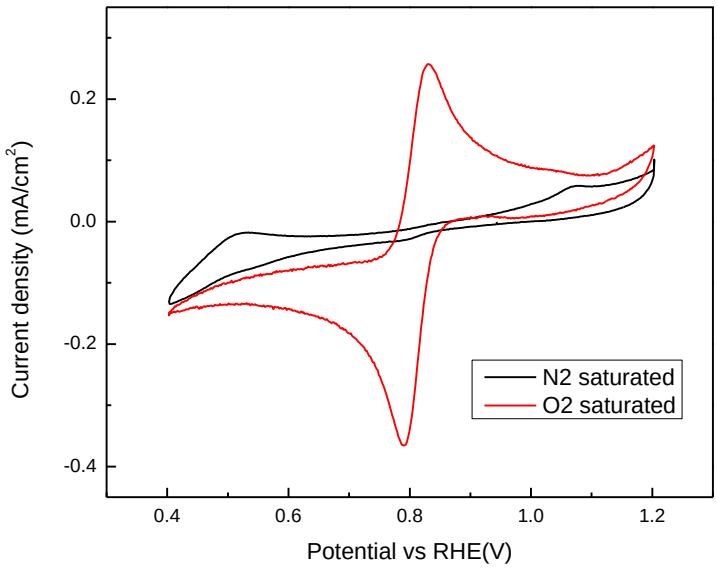


Figure 3.15 CVs of ORR Au (poly) electrode in electrolyte (1 M KOH + 1mM cobalt salen) , Scan rate: 50mV/s ,IR corrected, potential vs RHE

As can be seen from the graph, after reducing the scan range, the anodic peak is enhanced with much a higher peak current density than the previous larger scan range CV, which demonstrates much better reversibility for the reaction. This indicates that the reaction mechansim in the cathodic direction may be a electrochemistry-chemistry (EC) mechansim. In this case, the cathodic reaction product has a chemistry process after the electrochemical reaction that consumes the electrochemical reaction product, so the smaller anodic peak stands for more cathodic product is consumed in a larger time scale of previous CV. Combined with other experiment results (shown later), the EC mechaism here is hydroperoxide self-decomposition, and the redox couple here is $O_2$/ $O_2^{2-}$. Since this CV is particularly used for characterizing this redox couple, several details of this CV are discussed below to qualitatively understand this redox couple.

First, the shape of the CV indicates a highly reversible case and the peak separation is about 36mV, this should be most probably a two electron redox reaction. Secondly, for a two electron redox process, the separation peak potential difference , 36mV ≈ 58mV/2 means this is a nearly reversible case. Finally, the oxidation peak current is slightly smaller than the reduction peak current, the ratio of peak reduction current density over peak oxidation current density is 1: 0.81. This also proves that this is a quasi-reversible case and the cathodic reduction product has a EC mechanism. For further verifying the reversibility of this redox couple, the variation with scan rate situation has been measured, shown below. (Fig 3.16)

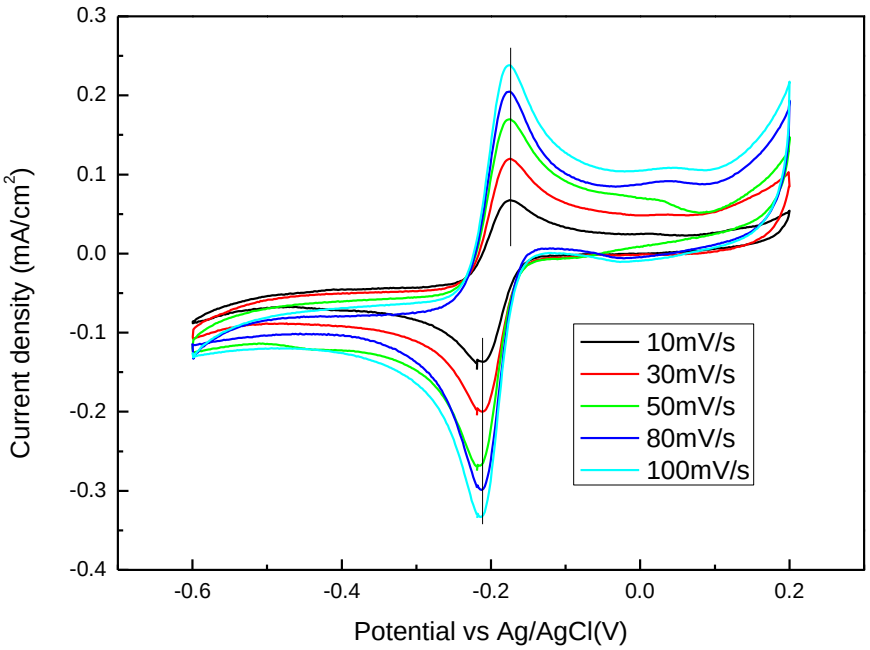


Figure 3.16 CVs of various scan rates on Au (poly) electrode in a reduced scan range particular for oxygen reduction redox peaks. Electrolyte: 1 M KOH + 1mM cobalt salen, IR corrected

Variation of scan rate is a basic but very useful method in CV. By changing the scan rate, the experiment is altering the balance between the speed of electron transfer and reactant transport. The difference between a reversible redox process and a quasi-reversible redox process is the speed of hetergeneous electron transfer. For the reversible case, no matter what the scan rate is, the hetergeneous electron transfer rate is fast enough to reach equilibrium. Thus, the CV's peak potential will not change along with the scan rate change, which is one standard to verify whether the redox couple is electrochemical reversible or not. From Fig 3.16, we can see that, the peak potential separation almost dones not shift with one order of magnitude increase on scan rate. This is reversible case according to this standard and also correspond very well with our previous assumption.

## 3.4 EC mechansim: catalytic case

Another important aspect that needs verification is the suspicious EC mechanism as discussed before. The smaller anodic peak in larger time scale is not an absolute proof for a EC mechansim, especially for what kind of EC mechanism. Using a relatively slow scan rate CV is a common method to varify a EC mechanism. By having the electrochemical reaction happen at a super slow rate, we can maximize the influence of follow-up chemical reaction which is not very obvious in normal scan rate.

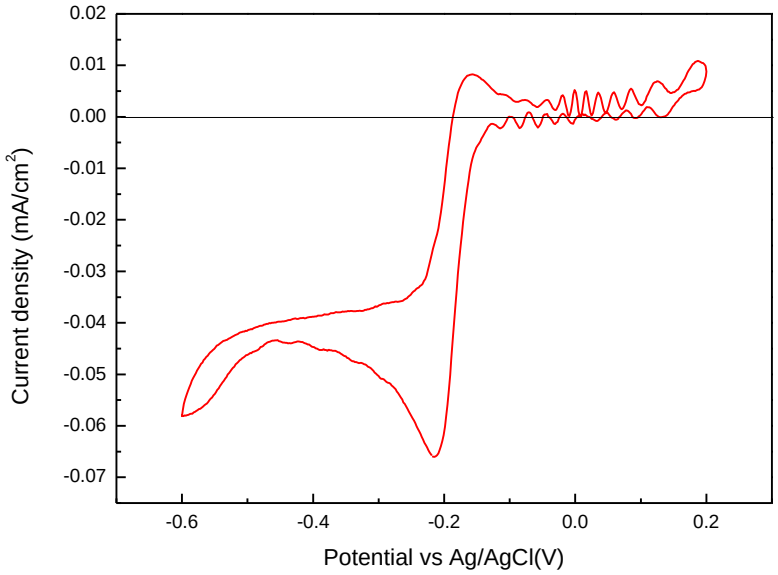


Figure 3.17 CV with 1mV/s scan rate on electrode in a reduced scan range particular for oxygen reduction redox peaks. Electrolyte: 1 M KOH + 1mM cobalt salen

Fig 3.17 is a illustration of how the previously described system behaves in a slow scan rate CV experiment. We can see that the anodic peak decays in this situation. This is because of the follow up reaction consumes the reaction product as previously mentioned. When the electrochemical reaction rate demaned also slows down, the previous relatively slow follow up reaction starts to play a major role. The other interesting aspect is that the reduction current shows a near steady state feature. This is concluded from the fact that reduction current does not fall off much after it passes over the reduction peak potential. Since oxygen diffusivity in the system is not changing, then a possible explaination is the EC mechanism here is actually a catalytic case. The catalytic case means that the second step of EC mechanism, the chemical process, produces reactant for electrochemical process. Thus, oxygen needs to be produced after the chemical process and the reduction current

can reach steady state more easily because of the excess oxygen on the electrode surface. The most likely reaction mechansim based on this behavior is, two electron oxygen reduction producing peroxide and peroxide self decomposition. Therefore, summarizing all the discussion above, the whole reaction mechanism can be written like this:

$$O_2 + H_2O + 2e^- \rightleftarrows HO_2^- + OH^-$$

$$HO_2^- \rightarrow OH^- + \frac{1}{2} O_2$$

Besides the slow scan rate method, we also adopted the so-called " sample and hold" method to verify the reaction mechansim. The general way to proceed in this experiment is described as below. When the potential is scanned to certain point, hold the electrode potential at that point and accumlate the "sample" at the electrode surface in the meantime; after enough "sample" accumulates, go on scanning the potential with the same rate and complete the original CV experiment and continue the second cycle without any potential hold. The second cycle behaves differently from the first cycle depending on the "sample" accumlating on the surface. Experiments with different potential holding point and comparison between first and second cycle are very good for revealing reaction mechanism involving follow-up reaction.

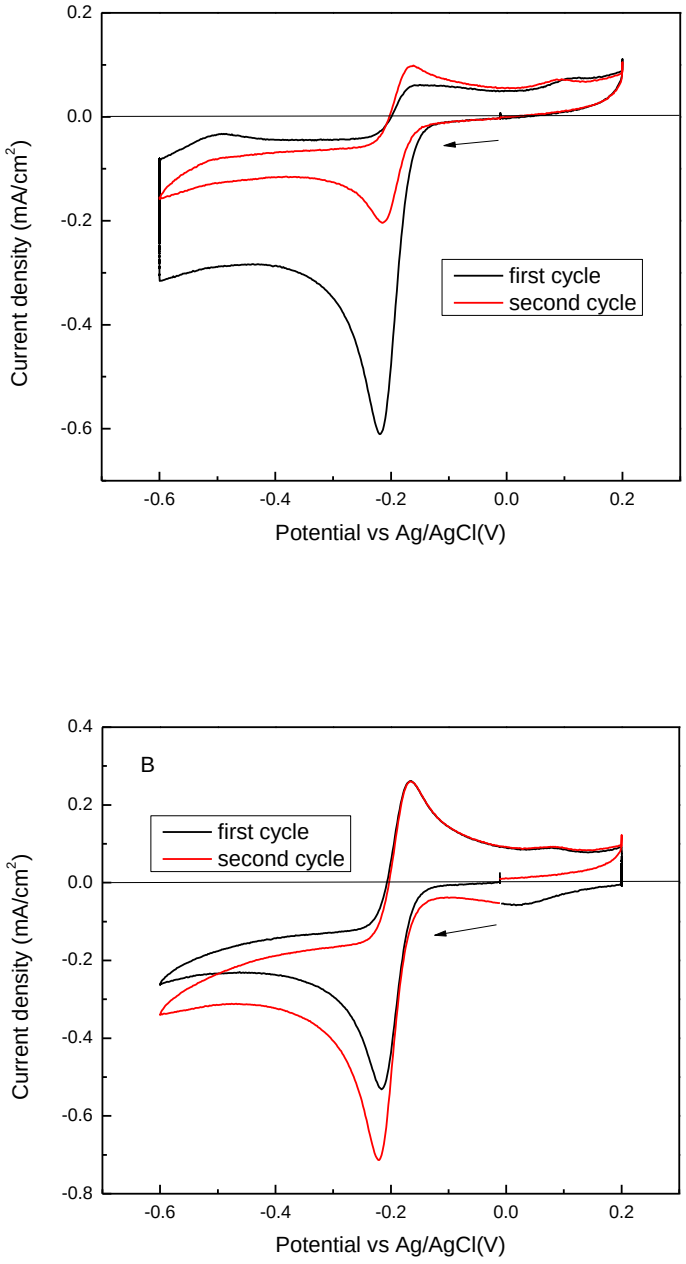


Figure 3.18 (A) Two cycles of CV, the first cycle holds potential at -0.6V for 5mins (B) Two cycles of CV, the first cycle holds potential at 0.2V for 5mins (Electrode: polycrystalline Au, electrolyte: 1MKOH+ 2mM cobalt salen, scan rate: 50mV/s)

In Fig 3.18, both graph A and graph B hold potential at specific point for 5 mins, the second cycle run in the same electrolyte without any potential holding. Graph A holds potential at -0.6V for 5 mins, the reduction current decays over this time, then the anodic peak almost disappear when it scans back. According to the previous postulated catalytic EC mechanism, the peroxide decomposition can explain the disappearance of the anodic peak very well. We can also see that the second cycle has a much smaller current than the first cycle because the peroxide decomposition only produces half the oxygen as the peroxide oxidation does and some oxygen will diffuse away during the 5 mins potential holding time, but the second cycle still retains very good reversibility. In graph B, the first cycle stops at 0.2V and oxidizing peroxide for 5 mins, the second normal cycle has a larger oxygen reduction current than the first cycle. The larger current density of the second cycle indicates the oxidation product in the anodic scan is oxygen, this is a strong side proof for the anodic scan peroxide oxidation we assumed before. Another interesting point is that the oxidation current goes to zero after hold for 5 mins, this indicates that peroxide is only available in a limited amount from the previous cathodic scan.

## 3.5 RDE and RRDE experiment

Rotating disk electrode (RDE) and rotating ring disk electrode (RRDE) are the most common and useful tools to characterize electrocatalysis. We also adopt both of these technologies to further understand this catalyst.

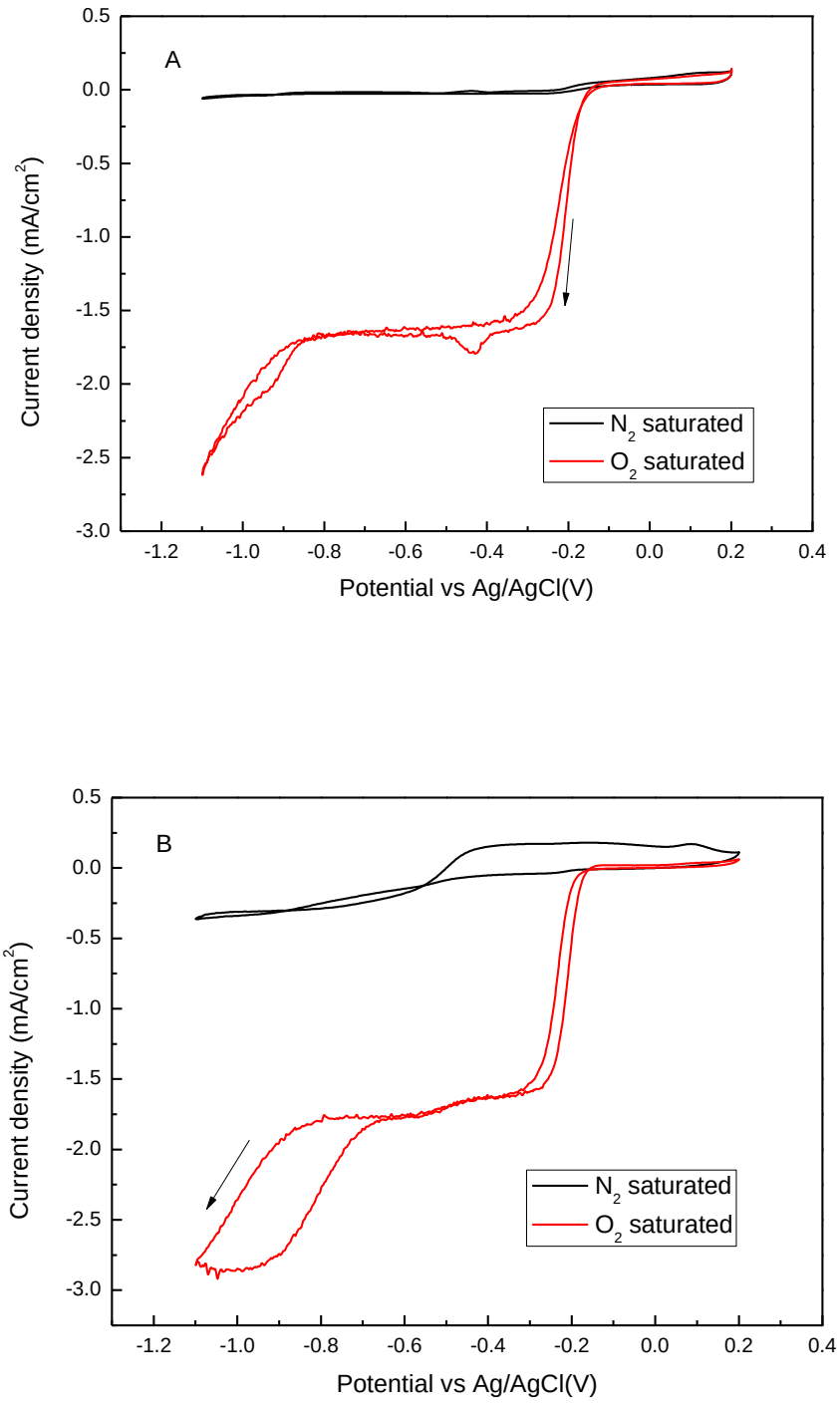


Figure 3.19 RDE experiment comparison on Au (poly) electrode in (A. 1M KOH B.1M+2mM cobalt salen) electrolyte. (Scan rate: 50mV/s, 1000 rpm)

RDE is the most popular hydrodynamic electrochemical technique. By having the electrode rotate as certain speed, the liquid flowing field is well defined on electrode surface. Steady state can be attained rather quickly, and the influence of mass transfer to the electron transfer kinetics is reduced. Fig 3.19 is a RDE comparison of the Au electrode in alkaline electrolyte with or without cobalt salen, we will discuss the shape differences of these graphs here and later discuss the kinetic differences. We can see that the steady state current density of these two graphs is very similar, the difference comes from the anodic scan. In the $N_2$ saturated electrolyte with cobalt salen situation, a cobalt salen oxidation peak starts between -0.5V and -0.6V, and a steady state of $cobalt^{2+}$ oxidation is reached beyond that potential. In the $O_2$ saturated electrolyte with cobalt salen situation, the anodic scan current is influenced by complex factors. On one hand, the cobalt salen is still playing a significant role; on the other hand, the RDE experiment caused the peroxide to leave electrode after been produced and influence the anodic current when it scans back.

RRDE is well established and widely used technology for measuring electron transfer number for ORR. Au disk electrode without further modification with Pt ring is also ideal situation for accurate measurement. Our RRDE experiment results exactly match our assumption that the polycrystalline Au electrode in this special electrolyte environment processes a two electron reduction of ORR in certain potential range. Fig 3.20 (A) shows the steady-state voltammogram of a polycrystalline Au electrode in electrolyte (1M KOH+ 1mM cobalt salen) and how the electron transfer number change with potential.

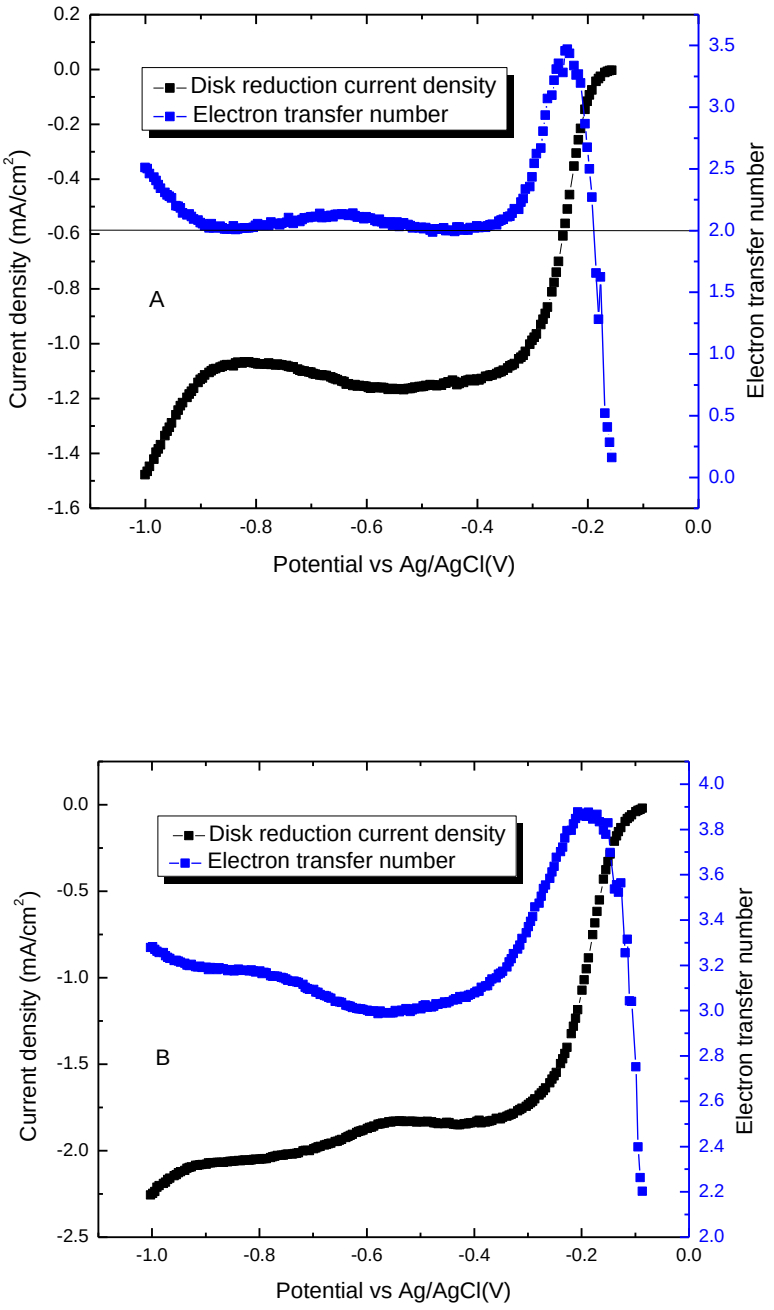


Figure 3.20 (A) Black dots: Steady state voltammogram of Au (poly) in electrolyte (1M KOH+ 1mM cobalt salen) saturated with oxygen. Blue dots: Electron transfer number change with potential. (B) Black dots: Steady state voltammogram of Au (poly) in1M KOH electrolyte saturated with oxygen. Blue dots: Electron transfer number change with potential. Scan rate: 50mV/s, 1000 rpm, background subtracted.

The equation used to calculate the electron transfer number is shown as below.

$$N = 4I_{Disk}/(I_{Disk} + I_{Ring}/n)$$

(N, electron transfer number; $I_{Disk}$, reduction current on the disk electrode;

$I_{Ring}$, peroxide oxidation current on ring electrode; n, collect efficiency)

In Fig 3.20 (B), the oxygen reduction current density stabilized at -1.2mA/cm$^2$ from 0.9V to 0.35V; at the same time, the electron transfer number of this reduction reaction also stabilized around 2.1. The transition range before the steady state current between 0.2V and 0.35V shows the electron transfer number fail from 3.5 to 2.1 along the with the cathodic scan of the potential. The potential range after 0.9V also shows an increase of electron transfer number from 2.1 to 2.5.

On the other hand, in Fig 3.20 (A), the oxygen reduction current stabilizes at a higher current density of 2.0 mA/cm$^2$. The electron transfer number goes down from 3.9 to 3.1 from transitional potential range 0.2V to 0.35V before steady state potential range, then electron transfer number gradually increases along with the potential cathodic scan.

As discussed before, the polycrystalline Au electrode is a mixture of different crystallographic planes on the surface. Therefore, the electron transfer number is around 3.0 is very reasonable in Fig 3.20 (A). This means that both four electron reduction and two electron reduction are happening at the same time. In the other electrochemical system of Fig 3.20 (B), we previously assumed the oxygen reduction is a two electron reduction process, and the result from RRDE experiment exactly matches this assumption. It is shown that the two electron oxygen reduction reaction is the dominant mechanism within

approximately 500mV potential range. This potential range is wide enough for further development to apply this catalyst in a real electrochemical cell.

To understand the influence of oxygen transport on the ORR reaction mechanism, experiments of variation of rotation speed of RRDE electrode are also conducted. As seen from Fig 3.21 (A), the disk current and ring current both increase as we increase the electrode rotation speed. After we calculated the electron transfer number at each rotation speed, we found out that the ORR is not greatly influenced by the rotation speed of the electrode. For all the three rotation speeds, the electron transfer number in the potential range of (-0.3V~ -0.9V) remains around two. We can also observe a slight increase of electron transfer number in the potential range of (-0.3V~ -0.7V) for the rotation speed of 1000 and 1600. A popular explanation for the influence of rotation speed on the electron transfer number to the surface modified electrode is that the reaction intermediate can be further reduced in the condition of faster mass transport, because faster mass transport can drive the reactant to the inner space for further reaction to happen. However, for our plain Au polycrystalline electrode in a cobalt salen present electrolyte environment, all the active sites for the reaction are exposed to the reactant at any electrode rotation speed. So we can expect the influence of rotation speed in this situation can be related to the undetected peroxide production for higher rotation speed. Our experimental rotation speed range is from 500 rpm to 1600rpm, so we can expect that this catalyst ORR reaction mechanism is not greatly influenced by the oxygen mass transport. This is also very helpful for us to further apply this catalyst.

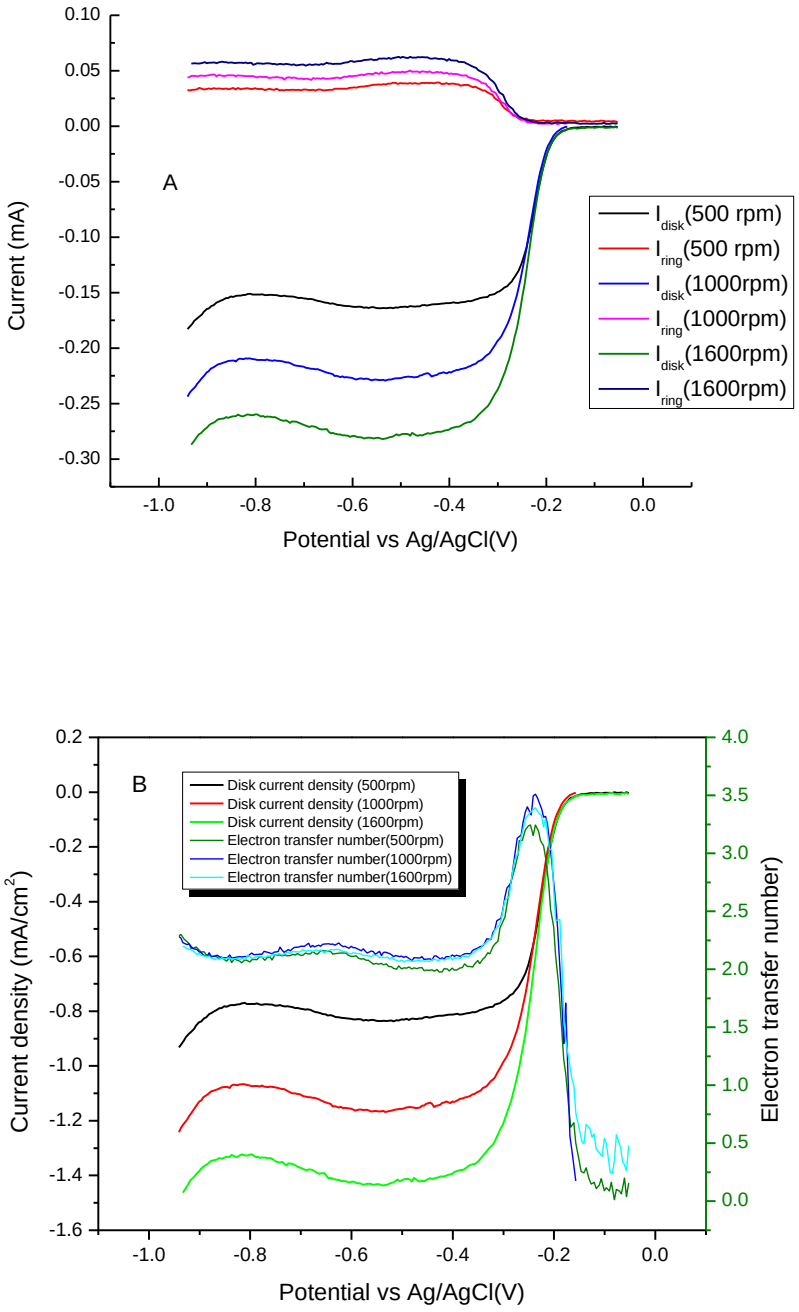


Figure 3.21 (A) Au disk current (background subtracted) and Pt ring current of RRDE electrode verse potential with the rotation speed of 500rpm, 1000rpm and 1600rpm in the electrolyte (1M KOH+ 1mM cobalt salen) saturated with oxygen; (B) Disk current density and electron transfer number verse potential converted from Fig 3.21(A).

## 3.6 Cobalt salen induced surface reconstruction on Au electrode

Our initial experiment discovery of this special catalyst is based on the oxygen reduction performance on the polycrystalline Au in potassium hydroxide and cobalt salen solution. When comparing the experiment results under the same condition with or without cobalt salen in the electrolyte, it seems that cobalt salen is the key element that contributes to this change. Furthermore, when polycrystalline Au and cobalt salen are used as catalyst for oxygen reduction individually, their catalytic activity is very different from combining them together.[118 126] Thus, we suggest the reason for the good reversibility of ORR is based on the combination of Au and cobalt salen together. However, we still cannot fully understand the reason why this unique combination can convert oxygen reduction to a very reversible process. Combining some related previous research from other scientists and some of our own experiment results, we believe that cobalt salen induced Au surface reconstruction is probably the origin of the reversible oxygen reduction. Polycrystalline means there are several different crystallographic orientations on the surface. Catalytic activity on the polycrystalline electrode surface should be a result of combination of catalytic activity on all kinds of orientation on the surface. Fig 3.20 is a perfect example of this. As we previously discussed, oxygen reduction on Au (111) surface is a quasi-reversible two electron oxygen reduction. Although, when comparing our experimental results and reported Au (111) oxygen reduction, our catalyst shows much better reversibility than Au (111), we think that the nature of the two electron reversible oxygen reduction is related to the Au (111) plane. This relation is due to the special interaction between the cobalt salen and the polycrystalline Au electrode, so that the unique feature of

Au (111) planes shows up. There are two possible ways the Au polycrystalline electrode will show the feature of Au (111) ORR. The first way is by specific adsorption on the selective planes. As formerly described, some previous work from Ohsaka's group is exactly this kind of modification.[116,114,93] Both thiol and bromine can form strong covalent bonds, but the bonding strength on the Au (111) plane is relatively low. After applying a very precise selective desorption on the Au (111) plane, the polycrystalline Au electrode becomes partially covered. However, the prerequisite of this method is the strong specific adsorption that can make Au (100) and Au (110) based planes inactive. The key element we have, cobalt salen, is a neutral organic compound and does not show any specific adsorption feature in the CV, as shown and discussed in Fig 3.10. We can use our experiment result to further verify this assumption. The first reason why this is not because of specific adsorption is the active electrode surface area for ORR in the presence of cobalt salen is not obviously smaller in the results of our experiment. We discussed this in the former section by comparing stationary CV graph, but stationary CV is not a good method for quantitative comparison. Now we use comparison of RDE experimental result sto make this point, which is a more persuasive proof. Fig 3.22 is an illustration of RDE polarization curve difference between a sub-modified electrode and a bare electrode. We can see from the graph that the sub-modified electrode has a much smaller steady state current density, indicating that the active surface area is much smaller than that of a bare Au electrode. However, in Fig 3.23, our experiment shows that the steady state current density is almost the same with or without cobalt salen in the alkaline solution. This suggests that the active surface area of ORR in the presence of cobalt salen is not reduced.

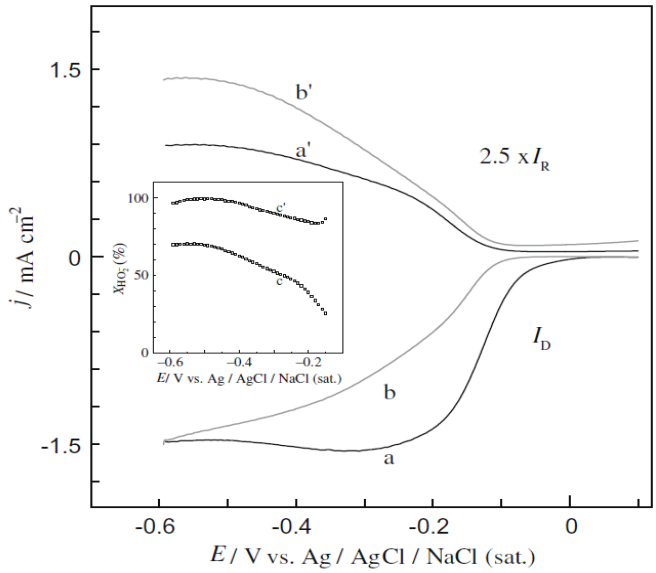


Figure 3.22 CVs obtained at the (a) bare Au (poly) and (b,c) sub $I_{(ads)}$/ Au (poly) electrodes ($\Gamma = 1.8 \times 10^{-9}$ mol $cm^{-2}$) in (a,b) $O_2$- and (c) $N_2$-saturated 0.1 M KOH solutions. Scan rate: 100mV/s. 1400 rpm. [116]

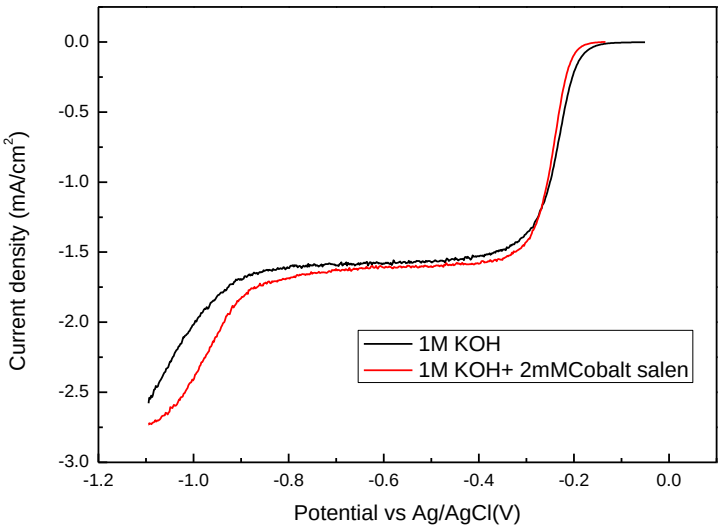


Figure 3.23 Polarization comparison of Au (poly) in alkaline electrolyte environment with or without cobalt salen. Scan rate: 10mV/s, 1000rpm. Background subtracted.

One interesting question about this result is why the steady state current density should be the same while the ORR electron transfer number is decreasing by almost one. One possible answer for this is because the cobalt salen is solvated in the solution phase, and the reversible bonding of oxygen makes the solubility of oxygen in the alkaline solution increased. The diffusivity of oxygen in the electrolyte is also not a simple situation. A slightly increase in diffusivity of oxygen is also a possibility.

Another reason we should verify the possibility of specific adsorption is the experiment in Fig 3.11 shows that $Co^{3+}$ does show sign of specific adsorption. We also design a special experiment to show that the reversible oxygen reduction activity is irrelevant to the presence of $Co^{3+}$. A polycrystalline Au electrode is electrochemically and mechanically cleaned. It is then tested in a pure alkaline solution and shows very typical crystalline Au catalytic activity on ORR. Then a 10 μL (1M KOH + 2mM cobalt salen) solution is deposited on the electrode surface and dried for 30 mins, a thin polymer film is formed by this method. We put this thin film-modified electrode back into the 1M KOH solution saturated with oxygen. Fig 3.24 is a comparison of ORR CV before and after this modification.

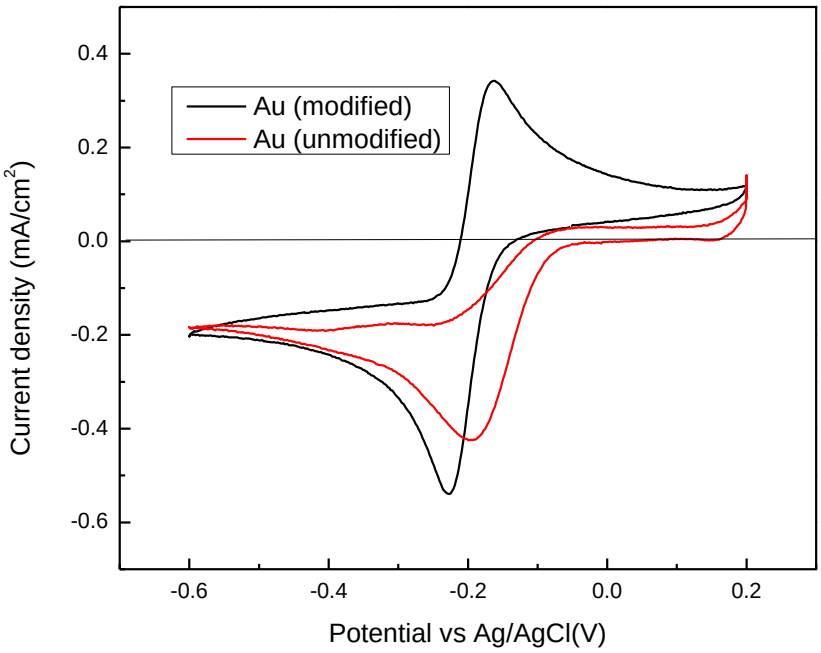


Figure 3.24 Red line: CV of Au (poly) in 1M KOH electrolyte satuarated with oxygen. Black line: the same Au (poly) deposited 10 µL (1M KOH + 2mM cobalt salen) solution and dried for 30 mins, then tested in the same 1M KOH electrolyte. Scan rate: 50mV/s (both are extracted 3$^{rd}$ cycle from original continuous CV)

This experiment is a strong proof that the reversible oxygen reduction catalytic activity is because of the direct interaction from cobalt salen not the specific adsorption of cobalt salen ($Co^{3+}$). The cobalt salen on the electrode surface has not been through any electrochemical process, there is no $Co^{3+}$ on the surface at all. The other point this experiment indicates is that the redox current is not related to the cobalt salen solvated in the solution but a surface modification changes the oxygen reduction reaction mechanism.

Therefore, we eliminate one possibility that will make the electrode behave like a Au (111) surface. The other possibility which can also make the polycrystalline Au electrode behave

like a Au (111) surface is cobalt salen induced surface reconstruction. This mechanism means that the surface layers of polycrystalline Au electrode will go through a surface reconstruction to form a Au (111) like structure because of the presence of cobalt salen on the surface. Previous research on surface reconstruction on Au surfaces from other groups suggests that it is possible to use an organic compound to induce this kind of reconstruction.

Table 3.1 Influence of adsorbed organic molecules on the potential for the Au (100)- (hex) to Au (100)-(1×1) structure transition in 0.01 $Na_2SO_4$ + 1 mM organics. ($E_T$ vs. SCE)[99]

| molecule / 1 mM | | $E_T$(hex→1x1) |
|---|---|---|
| phtalazine | 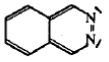 | -155 mV |
| pyridine |  | -10 mV |
| pyridazine |  | -5 mV |
| pyrazine |  | +240 mV |
| uracil | 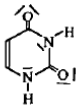 | +255 mV |
| pyrimidine |  | +266 mV |
| **0.01 M $Na_2SO_4$** | | **+350 mV** |
| cumarone |  | +350 mV |
| phtalide |  | +430 mV |
| coumarine | 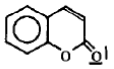 | +450 mV |

Table 3.1 is an illustration of how an organic compound can influence the transitional potential for Au (100) reconstruction. According to this table, coumarine is capable of increasing the transition potential of Au (100) reconstruction to 450mV higher than SCE potential. This transition potential is much higher than the potential of oxygen reduction and oxygen evolution in our system. We assume the similar structure, salicyladehyde, which is the basic component of cobalt salen, is also capable of lifting the transition potential. This means that it is possible to use a special adsorbate to convert Au (100) planes on the polycrystalline Au electrode to Au (100) - (hex) planes and have oxygen reduction and oxygen evolution reaction happen on it. As previously mentioned, Au (100) - (hex) structure is an Au (111) similar structure. Oxygen reduction proceeds by a two electron reduction on this catalyst surface. Therefore, this suggests our assumption that cobalt salen induced surface reconstruction is possibly the reason why Au (poly) can process a two electron reduction mechanism in the potassium hydroxide and cobalt salen electrolyte environment.

## 3. 7 ORR kinetics and reaction mechanism on cobalt salen modified Au electrode

Compare to the quasi-reversible ORR on Au (111), the kinetics on the modified Au electrode are much faster. This is also one of the advantages of this catalyst over other bifunctional catalyst. To understand why this is a totally reversible case, we need to separately investigate the kinetics of oxygen reduction and peroxide oxidation. Here, we first characterize the kinetics of oxygen reduction by comparing the kinetic on modified

Au electrode with the normal gold electrode. We extract a Tafel plot from previous RDE experiment data (Figure 3.19), as shown in Figure 3.25.

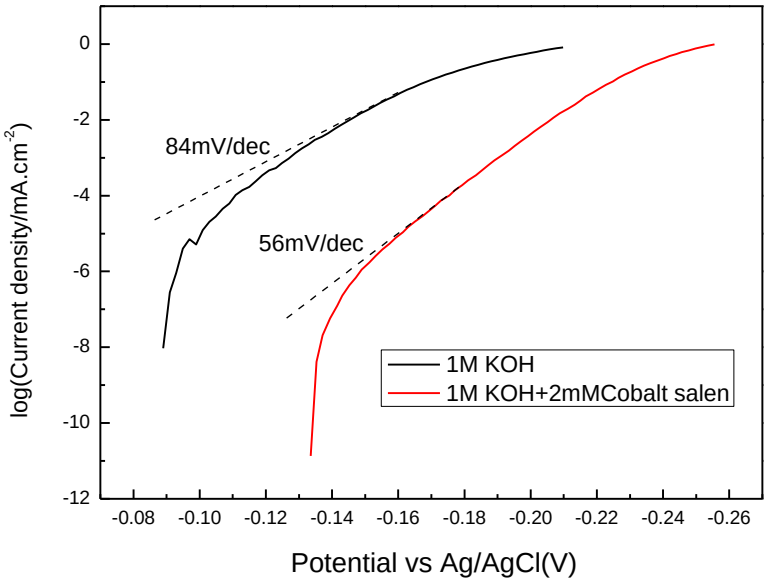


Figure 3.25 Tafel plot extracted from Fig 3.19

The Tafel plot of a polycrystalline gold electrode in 1mol/L KOH solution shown here is a little smaller than some results that been reported previously. Some values from other labs are between 90 to 108mV/dec in the HCD (high current density) range.[127,128] The value we measured is 84mV/dec in HCD range, 40mV/dec in the LCD (low current density) range. (The selection of HCD and LCD range is described in the experiment section). The tafel slope obtained in the alkaline electrolyte environment with cobalt salen is much better than any reported value on any size and shape Au catalyst. Among different models that describe ORR mechanism, the Damjanovic model is a popular one. According to this model, the common tafel slope value from 90mV/dec to 108mV/dec, meaning the ORR on bare gold

surface is limited by the first electron transfer.[126,128] Other studies of the ORR on nano gold particles also indicate the rate limiting process is the first electron transfer. Popular interpretation suggests this rate limiting process is the chemisorption of oxygen onto the gold surface. However, our experiment result shows that, in the alkaline electrolyte environmental with cobalt salen, the electrode has a tafel slope value of 56mV/dec at HCD range, and 36mV/dec at LCD range. Since the usual limiting step in ORR is chemisorption, the improvement after the modification could indicate that the chemisorption of oxygen is greatly enhanced. The difference between this catalyst and the normal bare Au electrode is the presence of cobalt salen on the surface. We suggest that this phenomenon is related with the reversible to bonding of oxygen of cobalt salen. As we mentioned early, cobalt salen is an example of well known synthetic reversible oxygen carriers cobalt-Schiff based complexes. Figure 3.26 is an illustration of how oxygen is reversiblly bonded with cobalt Schiff based complexes.

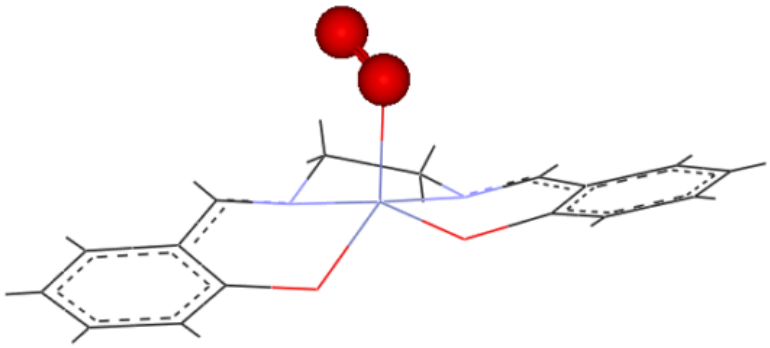

Figure 3.26 Illustration of oxygen reversible bonding oxygen

To explore the relationship between reversible bonding oxygen on cobalt salen and how this improves oxygen chemisorptions on Au, we need to further explore the interaction

between cobalt salen and Au. Our previously discussed experiment result suggests that no strong interaction is found between cobalt salen and Au. This suggests that cobalt salen is not specifically chemisorbed on Au. And cobalt salen is a neutral compound, there is no ionic interaction either. The only possible interaction left is physisorption. Physisorption usually refer to species adsorbed on the surface by weak van der waals forces. The distance between adsorbate and adsorbent varies greatly for different molecules, and this distance could be much larger than chemisorptions. In electrochemical terms, we suggest that cobalt salen should be within Outer Helmholtz Layer (OHL). This is a very important conclusion, because we now know that there are chemi-bonded oxygen with cobalt salen within OHL, which, by modern electrochemical theory, should have influence on the ORR on Au.

Another aspect to discuss is that how the cobalt salen molecule stands on the Au surface. Based on the chemical structure in Fig. 3.26, the chelated cobalt ion stands out from the salen ligand, and the oxygen molecule bonds to the salen structure vertically. We make an assumption here that Co ions are opposite where salen and Au interacts. Thus, the mechanism by which is oxygen reduced may have a different pathway on this modified Au than on plain Au. The limiting step of the ORR on plain Au electrode is the oxygen chemisorption step, shown below:

$$O_2 + e^- \rightarrow O_2^-(ads)$$

Kinetics of chemisorption is related to the interaction between the catalyst surface and oxygen. The volcano plot is usually used for understanding the relationship between the level of interaction and the reaction rate.[131] Before the volcano peak, the metal surface has relatively low d-band energy center and has weak chemisorption. After the volcano peak,

the catalyst surface forms too strong of a bond with O or OH species, which will poison the catalyst surface. For an ideal ORR catalyst, Pt is believed to be the best by having the intermediate adsorption characteristics for four electron ORR. According to the volcano plot of Fig 1.4, Au (111) is not on the right side of volcano plot for both two electron ORR and four electron ORR. Since our assumed reconstructed Au electrode has similar behavior with Au (111), we can generally conclude that the reaction is limited by the weak interaction between Au and oxygen. Therefore, if we can enhanced the interaction between catalyst and oxygen which means a stronger oxygen chemisorption, we can quicken the kinetics. The usual method to control the chemisorption of oxygen on the catalyst is by tuning d-band electron density. And the popular ways to achieve that are alloying different catalyst, core-shell structure, as discussed in the introduction chapter. The surface modification method we use stands for the other kind of approach. By changing the electrode surface double layer, you can also influence how oxygen interacts with the catalyst. The previous discussion on the difference of ORR in acid and alkaline condition is one evidence of this approach. Now, we are proposing a theory that using cobalt salen as modified molecule to pre-interact with oxygen for further chemisorption. To understand this theory, we need to first look at the status of oxygen at different level of chemisorption. The molecule length of oxygen is convenient reference for comparing to characteristic distances for different catalysts. For example, free oxygen molecule bond length is 1.21 Å, the O-O bond length when $O_2$ adsorbed on Au (111) is calculated to be 1.29 Å, and on Au (100) is 1.37 Å.[129] With larger bonding energy with the catalyst, the oxygen molecule is more stretched. This means oxygen is more strongly adsorbed on Au (100) than Au (111).The same applies to other well studied catalyst. The O-O bond length of $O_2$ adsorbed

on Pt (111) and Pt (100) were calculated to be 1.36 Å and 1.37 Å respectively.[130] Since both Au (100) and Pt are both at better positions at the left side of the volcano plot than Au (111), their larger molecule length with better reaction rate also means that stronger chemisorption. Based on Figure 3.25, the cobalt salen modified Au (111) like electrode surface also has very fast kinetic. We attribute this to the phenomenon that the oxygen molecule bonded with cobalt salen has lower electron density and is a better electron accepter compare to normal oxygen molecule. Using DFT calculation, the oxygen molecule length when bonding with cobalt salen complexes is in the range of 1.28 ~ 1.29 Å. This is exactly the same with the molecule length of oxygen when chemisorbed on Au (111). The means the extent of how oxygen oxygen molecule stretched is exactly what it needs to be when chemisorbed on Au (111). We hypothesize that this coincidence is related to the fast kinetics we measured. In this theory, Au electron density is not increasing because of cobalt salen, but the oxygen molecule becomes more stretched and is more readily to have interaction with the catalyst. In general, we believe that the pre-interaction between oxygen and cobalt salen can greatly enhance the oxygen chemisorption process. Based on this situation, we propose two follow up reaction mechanisms based on the transfer of oxygen or electron. The first mechanism is more similar with the normal ORR mechanism on Au. After reversible bonding with cobalt salen complexes, the stretched oxygen transfer to the Au surface and chemisorbs very quickly, then receive another electron to become peroxide, as shown in Fig 3.27. The other mechanism is related to electron tunneling phenomenon. Although the distance between cobalt salen and Au is not certain, its structure has the possibility to be in the vicinity of the catalyst surface. Therefore, after the oxygen bonds with cobalt salen, the cobalt can become the reaction center and

finish the first electron reaction with tunneling electron transfer, as shown in Fig 3.28. The evidence for the first model is related with all the experiments of ORR on reconstructed Au electrode. The evidence for the second model is related with ψ surface phenomenon of electrochemistry.

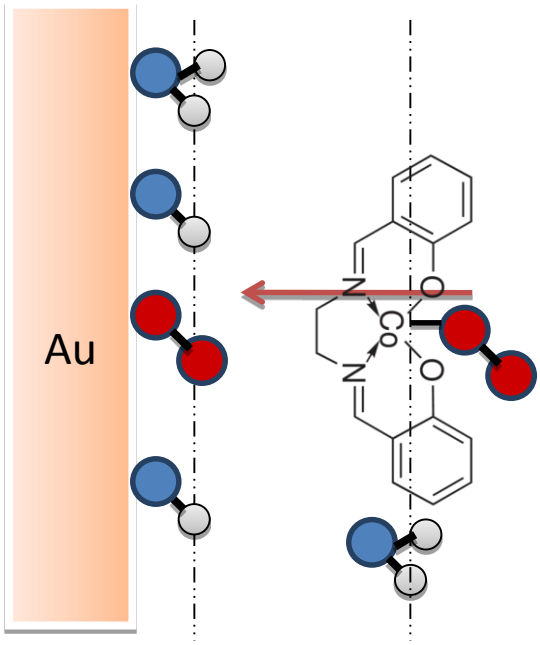


Figure 3.27 Illustration of how stretched oxygen transfer from cobalt salen to Au surface

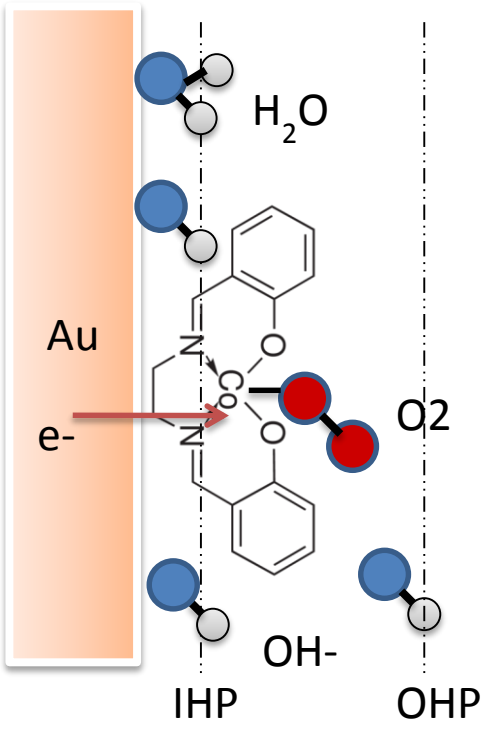


Figure 3.28 Illustration of how electron transfer from Au surface to cobalt salen by tunneling phenomenon

## 3.8 IR surface characterization on modified electrode

Our proposed reaction mechanisms are based on having cobalt salen on the Au surface. A characterization experiment, which proves the critical molecule is cobalt salen, is very important. Although we estimate that the cobalt salen does not have strong interaction with Au, and we also think that other molecule in the electrolyte will not cause any unexpected change to cobalt salen itself, we still need an experiment to prove this. A special FTIR experiment was designed for this purpose.

As described in the experiment section, a gold silicon wafer covered with very thin layer cobalt salen is prepared. The cobalt salen is first in liquid phase than dried to solid phase,

thus it has enough time to fully interact with Au. An ATR FTIR experiment is first conducted on the surface of the wafer to confirm the surface molecule. (Fig 3.29) Then, the exact same gold silicon wafer is transfer to a standard electrochemical cell for a standard ORR CV measurement. (Fig 3.30)

As can be seen from Fig 3.29, a sharp peak appears around 2900 $cm^{-1}$ and a series of peaks appear in the traditional fingerprint region, between 1600 $cm^{-1}$ and 700 $cm^{-1}$. Though cobalt is chelated with the salen group, and this interaction is not very strong. It is difficult to characterize the presence of Cobalt in this molecule from the observed peaks. However, the salen group has identical IR peaks, and we can correlate them very well with our experiment data to show that there is a salen structure molecule on the surface. In the fingerprint region, the peaks at 1600 $cm^{-1}$, 1300 $cm^{-1}$, 700 $cm^{-1}$ can each correspond with C=N, C-O and C-C bond. The sharp peak at 2900 $cm^{-1}$ can be explained with a strong stretching signal by C-$H_2$ connected with N.

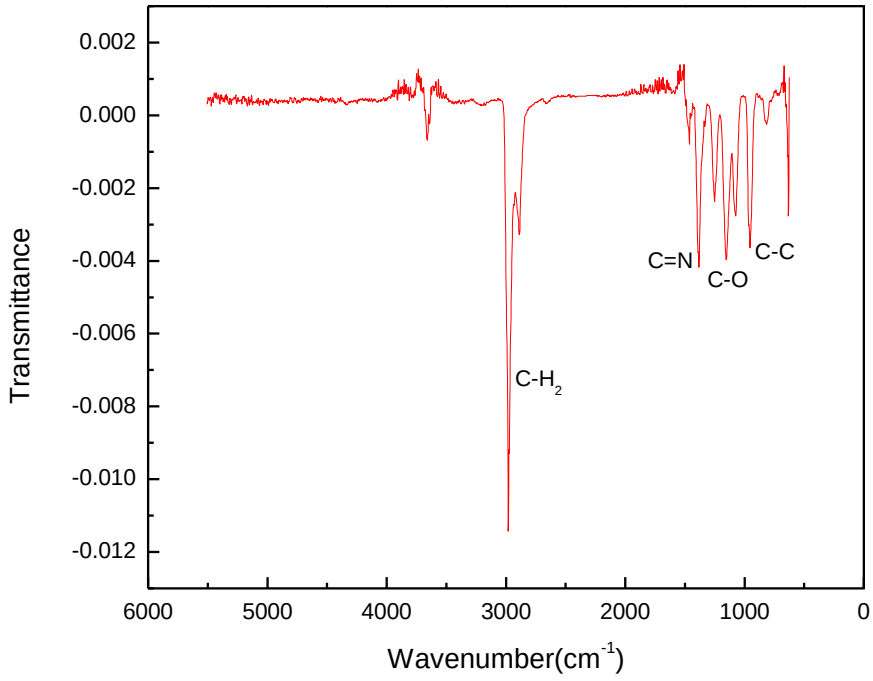


Figure 3.29 FTIR spectra of cobalt salen on silicon Au wafer.

After we verify that the cobalt salen is on the surface, the next step is to verify the ORR catalytic activity on the exact same wafer. A special electrochemical cell is made for this experiment. The working electrode connection wire is used to directly connect with one side of the Au-coated wafer, and a holder is used to keep the wire connection out of the electrolyte but keep the main body of the wafer plate within the electrolyte. The surface area of the Au wafer dipped into the electrolyte is around 2 $cm^2$. The normal experimental conditions with $O_2$ and $N_2$ saturated 1M KOH electrolyte are used. The result, as shown in Fig 3.31, demonstrates a very similar result compared with a normal cobalt salen modified Au electrode. The most obvious difference is in the cathodic scan of the CV where ORR occurs: the ORR reaction is stronger in the lower potential range. The detailed reason for

this is unknown, but this could be partly attributed to the silicon surface dipped into electrolyte at the same time.

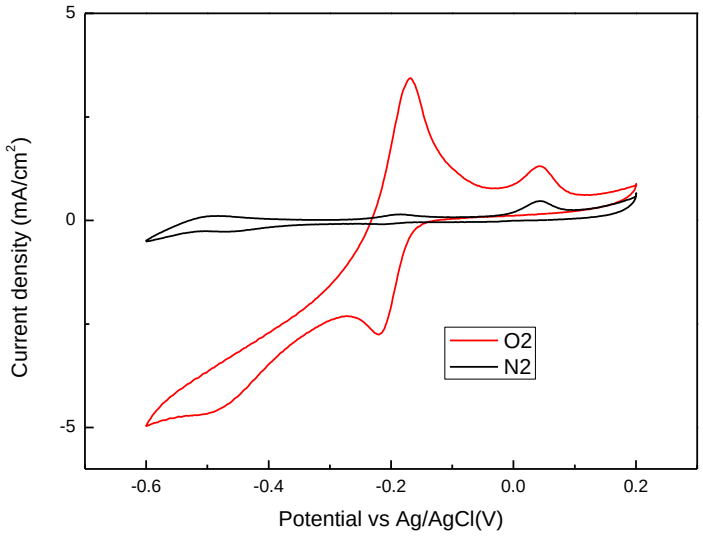


Figure 3.30 CV comparison of cobalt salen modified Au silicon wafer in 1M KOH saturated with $O_2$ (black) and $N_2$ (red). Scan rate: 50mV/s

# Chapter 4

# Reversible ORR catalyst -- II

# Characterization and preparation method

## 4. 1 Temperature influence on oxygen reduction reaction

### 4.1.1Base voltammetry of Au (poly) at different temperatures

In order to understand better how the catalyst performance is influenced by the temperature, we need to first understand how ORR on polycrystalline gold is influenced by the temperature. To understand the difference within the CVs which characterize the ORR, we need to understand the differences between base voltammetry measurements at different temperatures. T.J. Schmidt and P.N.Ross did thorough research on temperature effects on single crystalline gold electrode. [132] From Fig 4.1 we find some features that all the single phases have in common. The most obvious feature is potential shift of oxide layer formation and stripping. The oxide formation potential shifts negatively and oxide stripping potential shifts positively. This implies that the oxidation process is becoming more reversible with increasing temperature, which is a common feature for noble metals in aqueous electrolyte.

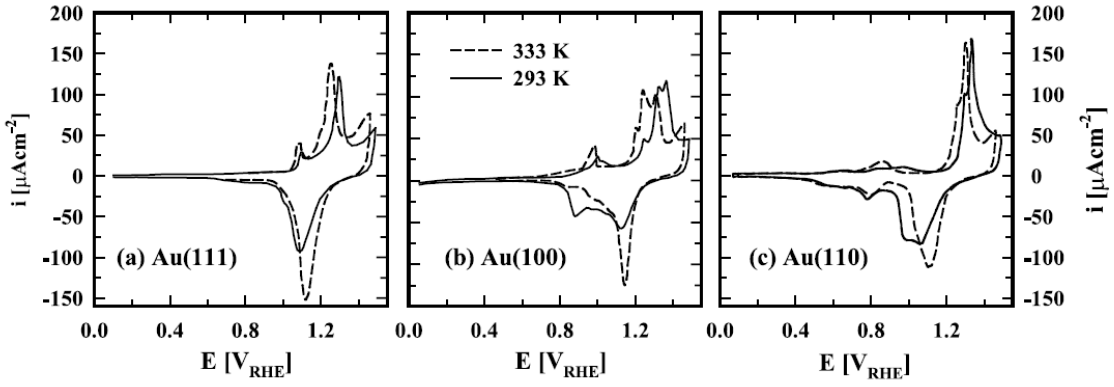


Figure 4.1 Base voltammetry at 293K (solid line) and 333 K (dashed line) on (a) Au (111), (b) Au (100) and (c) Au (110); 0.1 M KOH, 50mV/s.[132]

The other feature that can also be found from all these three graphs is that $OH_{ad}$ adsorption is also shifted negatively. It is a more obvious feature for Au (100) and Au (110), but it all happens on all three single crystalline phases.

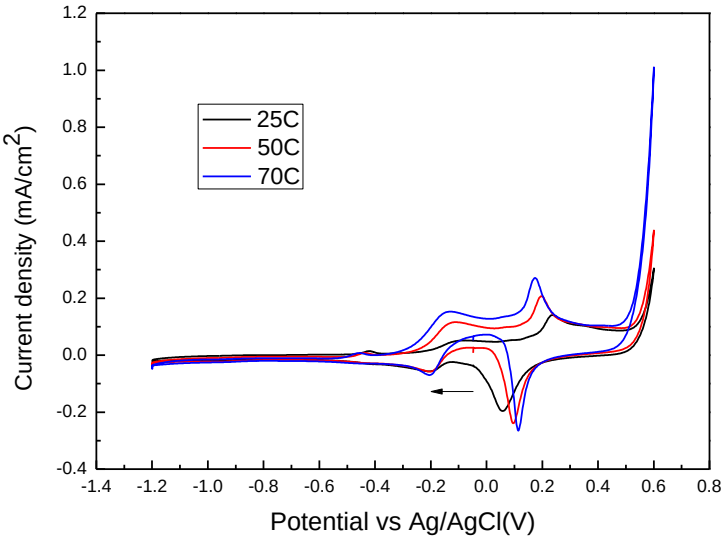


Figure 4.2 Base voltammetries of Au (poly) at three different temperature levels, scan rate: 50mV/s. Electrolyte: 1M KOH saturated with nitrogen.

To study the temperature influence on our polycrystalline Au electrode, we further characterize the electrode with three temperature levels, at 298K, 323K and 343K. As shown in Fig 4.2, the feature of how temperature influences the base voltammetry is very similar to what T.J. Schmidt et al. show in the their work. The gold oxide formation process is gradually becoming more reversible at increasing temperature. And the $OH_{ad}$ adsorption is gradually shifted to more negative potential. The positive shifting of the oxide stripping makes the gap become gradually deeper between -0.2V and 0.1V along with the increasing temperature. The obvious feature of the $OH_{ad}$ adsorption potential shift implies that this polycrystalline surface has Au (100) and Au (110) as the majority of exposed sites, which indicates that this is a very typical polycrystalline Au electrode. The reason why we are interested in these features is that they all happen within the region where ORR and OER occurs. As we discussed before, $OH_{ad}$ adsorption and oxide formation can both greatly influence these two reactions. Another important point about the temperature influence on surface reconstruction is the surface reconstruction transition potential changes with temperature.

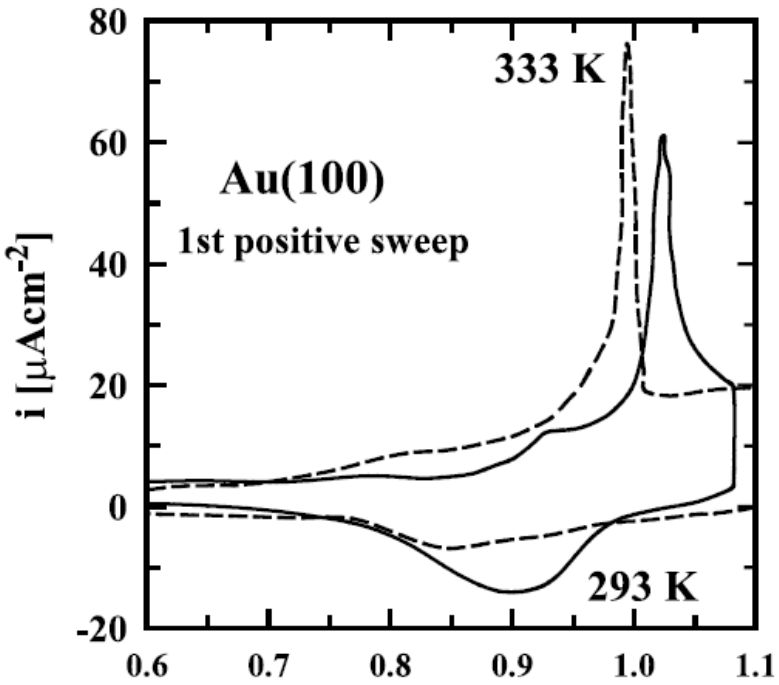


Figure 4.3 Magnification of the first voltammetric sweep after emersion at ca. 0.1V on Au (100) at 293 (solid line) and 333K (dashed line); 0.1M KOH, 50mV/s. [132]

Fig 4.3 shows the first sweep of how Au (100) behaves when scaned positively over 0.1V at 293K and 333K. The reason for this sharp peak is that the Au (100) surface is hexagonally reconstructed forming a ($5 \times 27$) surface. The sharp peak is associated with the surface reconstruction to Au (100) ($1 \times 1$) because of $OH_{ad}$ adsorption when sweeping from negative potential. As shown from Fig 4.3, the surface reconstruction is shifted negatively along with the increasing temperature. Since the $OH_{ad}$ adsorption is also shifted negatively, this indicates that $OH_{ad}$ adsorption could induce the surface reconstruction.

### 4.1.2 Temperature influence on ORR on gold electrode

In the last section, we discussed the influence of temperature on gold electrode behavior without oxygen and without modification. The next step is to see the influence of temperature on the ORR on gold electrode. Fig 4.4 shows the ORR CV experiment results for the same polycrystalline gold electrode at different temperatures.

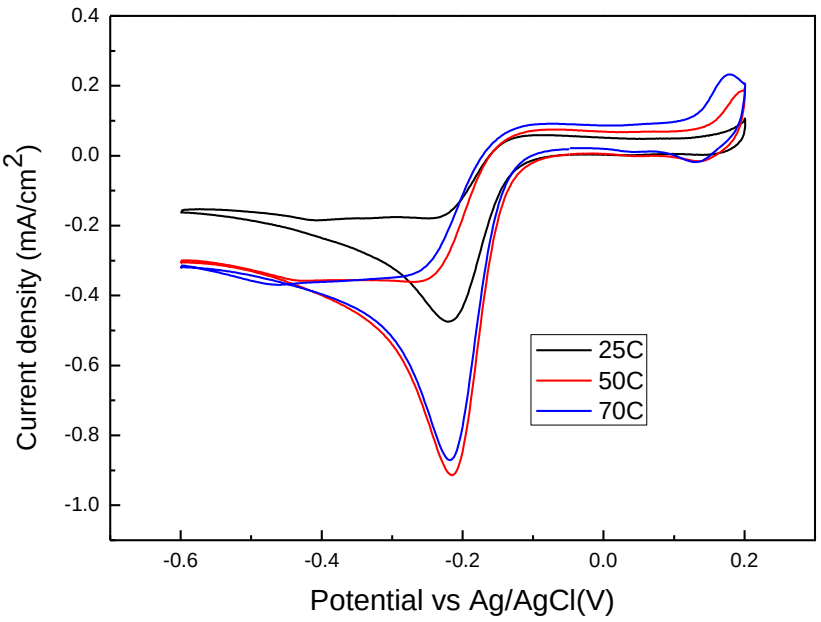


Figure 4.4 CVs of ORR on Au (poly) at three different temperature levels, scan rate: 50mV/s. Electrolyte: 1M/L KOH saturated with oxygen.

As shown in the graph, the gold electrode has better catalytic activity on the ORR at higher temperatures of 50$^{o}$C and 70$^{o}$C, but has very little difference between 50$^{o}$C and 70$^{o}$C. This is in accordance with T.J. Schmidt et al. work. They use an RRDE electrode with a single

crystal gold electrode and platinum ring to verify the peroxide production tendency with increasing temperature, as shown in Fig 4.5.

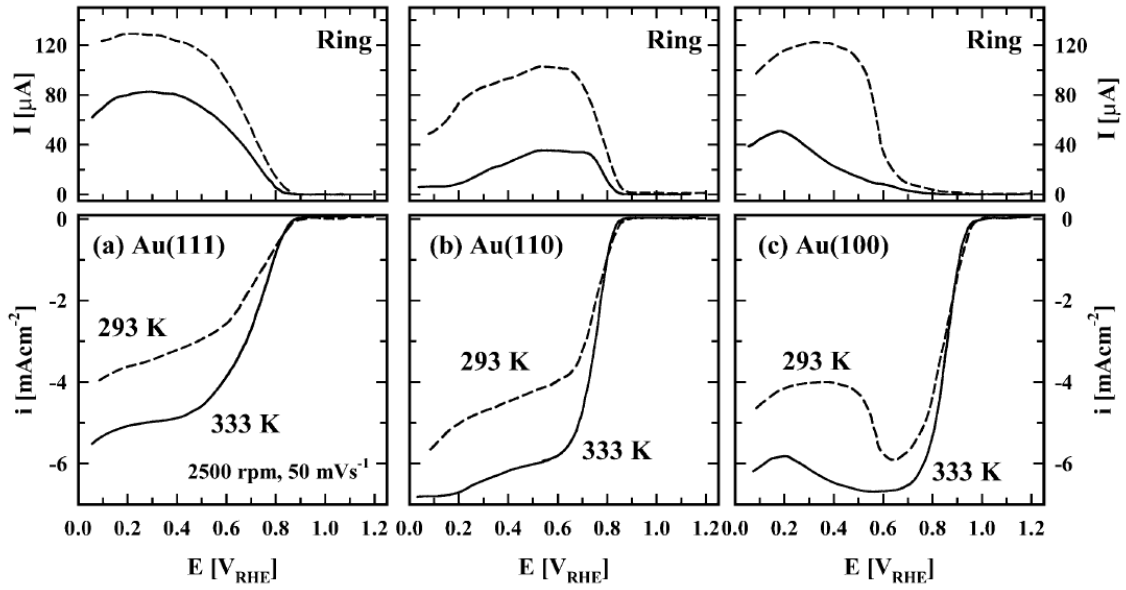


Figure 4.5 ORR polarization curves (lower panel) along with the ring currents for peroxide detection (upper panel) at 293K (dashed lines) and 333K (solid lines) on (a) Au (111), (b) Au (110) and Au (100); 0.1M KOH, 50mV/s, 2500rpm.[132]

As shown in Fig 4.5, at higher temperature the peroxide production is greatly reduced while the ORR peak current density is greatly increased. This means the ORR reaction pathway follows a four electron reduction much more than the two electron reduction at higher temperature. Especially on Au (100) and Au (110), peroxide production almost vanished. Since these changes happened on well defined single crystalline Au electrode surfaces, the conclusion is that chemsorption of hydroperoxide is favored at high temperature on all gold electrode surfaces. This indicates that Au is a good alternative to platinum in alkaline fuel cell application in high temperature operation.

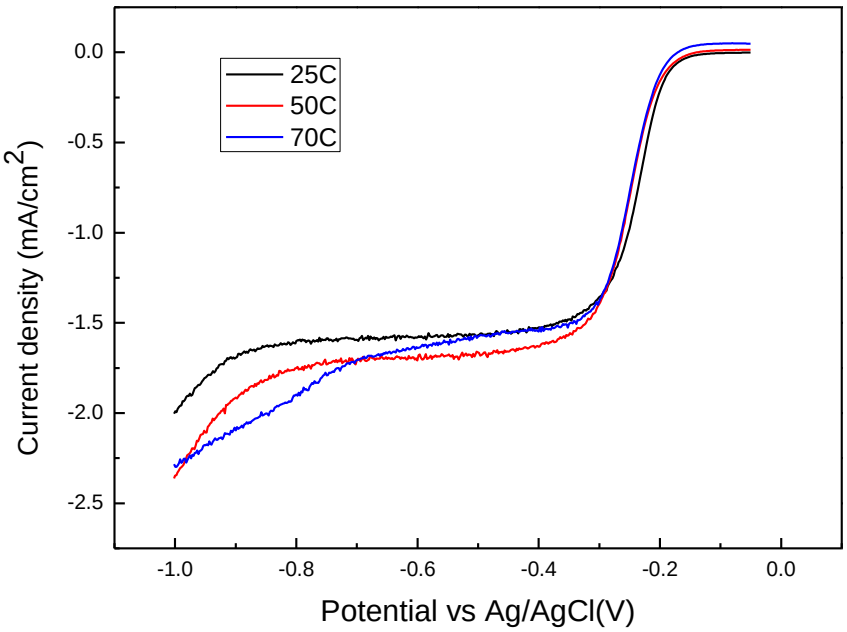


Figure 4.6 ORR polarization curves on Au (poly) at three different temperature levels. 1000 rpm, scan rate: 10mV/s, background subtracted, electrolyte: 1M/L KOH

The polarization curves obtained by RDE experiment on this same Au (poly) differ somewhat from those on the single crystal electrode. The steady state current density from high temperature experiment does not have a very obvious higher current density difference. The detailed reason for this is still unknown, but that the peroxide ions are much further reduced is still apparent in the potential range between 0.5V and 1.0V.

### 4.1.3 Temperature influence on reversible ORR catalyst

There are two reasons why it is important to know how temperature influences ORR on this cobalt salen modified electrode. One obvious reason is to verify the best working temperature range for this catalyst to have a reversible ORR catalysis property. The other

reason is to verify the separate roles of Au and cobalt salen on the catalytic activity. Our previous discussion assumes that Au is mainly responsible for the reversible nature of the catalytic activity, and cobalt salen is responsible for the reactant centralization and better reaction kinetics. A hypothetical mechanism is that cobalt salen can induce the gold electrode to undergo surface reconstruction when it is on the surface. A pure polycrystalline gold electrode's catalytic activity for peroxide production is greatly changed by increasing temperature. Therefore, if the cobalt salen modified gold electrode shows the same tendency with respect the peroxide production, this indirectly indicates that Au may be responsible for the reversible nature of the catalyst.

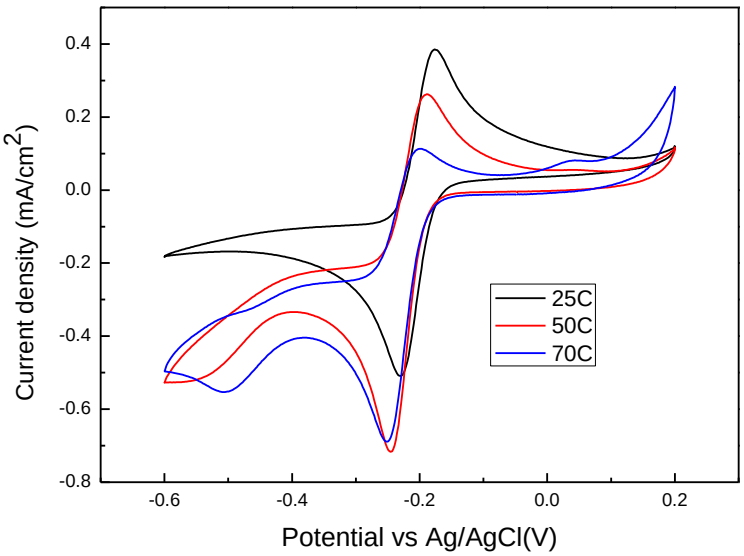


Figure 4.7 CVs of ORR on Au (poly) at three different temperature levels, scan rate: 50mV/s. Electrolyte: (1M KOH+2mM cobalt salen) saturated with oxygen.

Figure 4.7 shows the temperature influence on the catalytic activity of a polycrystalline gold electrode in an alkaline environment with cobalt salen. The tendency is very clear and behaves in accord with our previous assumption on the separate roles of Au and cobalt salen. The further reduction of hydroperoxide ions is enhanced with increasing temperature. Unlike the behavior of the catalyst at 25$^{o}$C, the same catalyst has much higher reduction current density at 50$^{o}$C and 70$^{o}$C. The solution is maintained saturated with oxygen, and the variation of solubility of oxygen in the solution is very small. Therefore, the higher reduction current is mainly caused by the further reduction from hydroperoxide to hydroxide. And the catalyst at 70$^{o}$C has a steeper reduction curve than the catalyst at 50$^{o}$C. This also implies that the chemisorption of the hydroperoxide on the Au surface is favored by higher temperature, regardless of surface atom arrangement. The anodic peak current density is also decreasing with increasing temperatures; this is evidence of less production of peroxide.

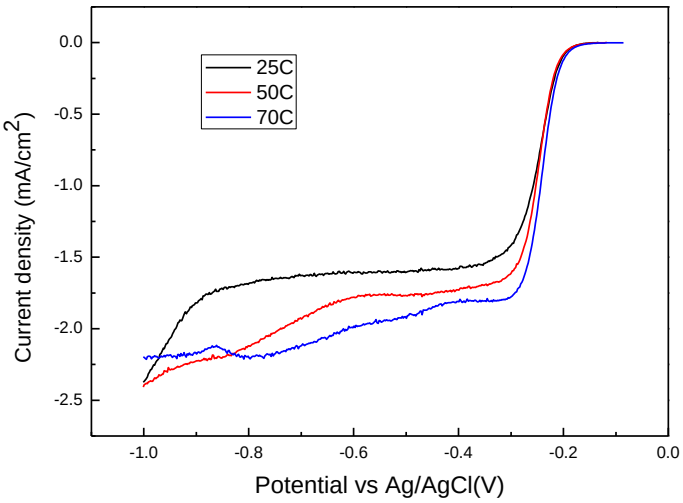


Figure 4.8 ORR polarization curves on Au (poly) at three different temperature levels in (1M KOH+2mM cobalt salen) solution. 1000 rpm, scan rate: 10mV/s, background subtracted.

As we discussed before, the steady state current density with or without cobalt salen in the electrolyte is almost the same. The reason for this behavior lies in the oxygen solubility difference compensating the reduced electron transfer number. However, the polarization curves in the alkaline cobalt salen electrolyte environment show much higher current density at high temperature (323K and 343K) than in pure KOH solution. This can be interpreted by the reason that the solubility of oxygen in alkaline cobalt salen solution is indeed higher than pure alkaline solution.

## 4. 2 The influence of pH on the reversible ORR catalyst

As we briefly introduced in the first chapter, the different concentrations of H+, OH- and working potential shift have great influence on the mechanism of ORR. Generally, ORR in alkaline is more facile than ORR in acid. However, for different catalysts, the influence is different. Gold is well known for having a different catalytic activity on Au (100) in alkaline, but this difference disappears when it comes to acid electrolyte. The reason why most people focus on the ORR on gold in alkaline is not only that Au (100) can catalyze four electron reduction in a certain potential range in alkaline, but also that the onset potential of the ORR in acid is much lower than in alkaline with reference to the reversible hydrogen electrode (RHE). O.V.Tripachev et al. did a polarization curve comparison on ORR on Au(poly) and nano Au particle on carbon. As shown in Figure 4.9 the onset potential shift negative approximately 500mV for Au(poly) electrode and 600mV for the nano Au particle, while the electrochemical window shifts 825mV.[133]

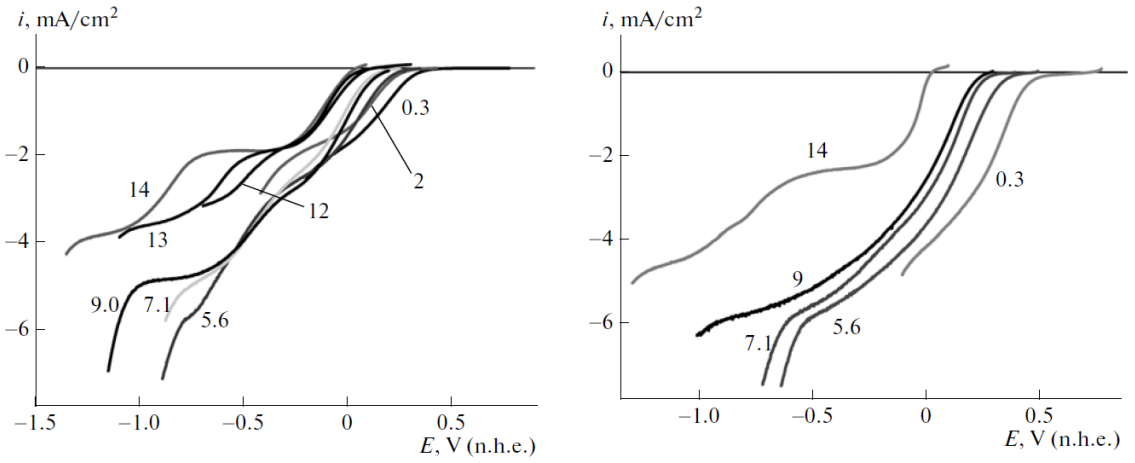


Figure 4.9 Polarization curves of $O_2$ reduction on polycrystalline (left) Au and nanoparticles of Au/C (right) at different PH values. [133]

This indicates that the fuel cell voltage will lose at least more than 200mV when the electrolyte switchs from alkaline to acid when using Au as ORR catalyst. Therefore, Au in acid electrolyte is normally not the best choice for fuel cell or battery applications. Furthermore, our experimental results show that there is no reversibility in acid for this catalyst. If this catalyst only works in alkaline environment, then we need to determine the right pH range for this catalyst to be able to perform well. All of our previous experimental result were obtained in 1M KOH solution. We then designed a series of experiments to verify the catalyst activity in different concentrations of alkaline solution. In this experiment, a same modified electrode was used in a series of different CV experiments. The alkaline solution is saturated with oxygen prior to the experiment. The experiment starts with the lowest concentration and proceeds to the highest concentration, so that the lower amount of solution from former experiment will not affect later experiment. The electrode is deposited with 10μL 2mM/L cobalt salen solution and dried between every

experiment to insure the modification is stable enough. The CV comparison is shown as in Fig 4.10.

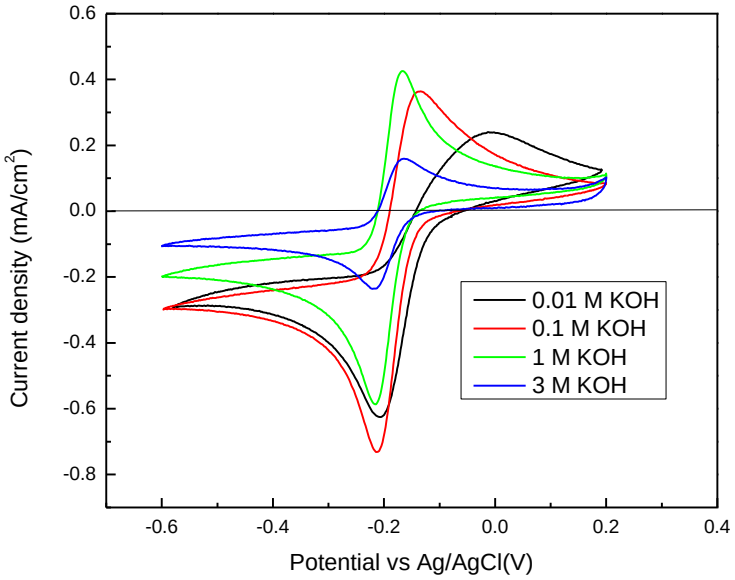


Figure 4.10 CVs of cobalt salen modified Au electrode in different concentration of KOH saturated with oxygen.

First of all, from the shape of the CV, we can tell that the catalyst works well in 1 mole and 3 molar solutions. The current density difference between these two concentrations is mainly because of the oxygen solubility difference.[134] For the 0.1 mole and 0.01 molar alkaline solutions, the reversibility gets worse with lower concentration. There are two possible reasons for this: (1) when the alkaline concentration is low, the composition of the double layer near electrode surface is changed; the mechanism of peroxide oxidation on this catalyst can be very sensitive to the double layer structure. (2) the product produced

by this catalyst after oxygen reduction is hydroperoxide ($HO_2^-$), and $HO_2^-$ can decompose into oxygen and hydroxide.

$$HO_2^- \rightarrow OH^- + \frac{1}{2} O_2$$

Therefore, it is reasonable that the decomposition rate of hydroperoxide can be influenced if the hydroxyl radical concentration becomes one or two orders of magnitude smaller.

## 4.3 Peroxide oxidation on cobalt salen modified Au electrode

As discussed previously, the kinetics of peroxide oxidation on cobalt salen modified Au electrode seems to be very good. This is also one of the reasons why the ORR on this catalyst is nearly reversible. To specifically investigate the peroxide oxidation catalytic activity of this catalyst, we need to characterize this catalyst in a peroxide solution. 6mM $H_2O_2$ + 1M KOH solution was made as described in the experiment section. As shown in the following graph, a similar CV experiment is conducted in this new electrolyte environment.

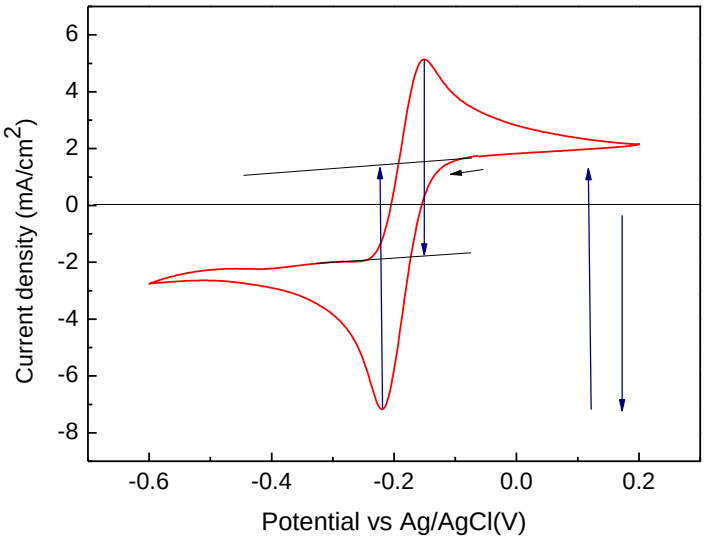


Figure 4.11 CV on reconstructed Au (poly) in (6mM H2O2 + 1M KOH) solution. Scan rate: 50mV/s

Figure 4.11 shows that, in a peroxide rich alkaline electrolyte environment, oxygen and peroxide form a very good redox couple. It also shows some features that are very different from the CV in a peroxide-free environment. First, the magnitude of the current density in the graph is much higher than for the CV in pure alkaline environment. This is because the solubility of oxygen in 1 molar KOH solution is around 1 millimolar. According to the Randles-Sevcik equation:

$$i_p = (2.69 \times 10^5) n^{3/2} A D^{1/2} C^o v^{1/2}$$

The peak current density is directly proportional to the peroxide concentration in the solution. On the cathodic scan, the oxygen concentration on the electrode vicinity should be the same as the peroxide concentration in the solution. Therefore, the oxygen concentration in this new electrolyte environment in the vicinity of the electrode is around

6 times higher than for pure 1M KOH solution. This explains the peak current density difference between two experiments. The other important feature is that the ratio of peak reduction current density over peak oxidation current density is 1:0.78, which is similar to the CV in pure 1M KOH solution on the modified electrode. The obvious oxidation peak on this unmodified electrode occurs because this is a peroxide rich environment. The EC (electrochemical-chemical) mechanism in the previous experiment is not valid in the new electrolyte environment. The original follow up chemical process, hydroperoxide self–decomposition, is greatly restrained in this situation, and the peroxide ion concentration near electrode cannot be influenced by this very small amount of self-decomposition process. The higher reduction peak current density is because the oxygen reduction on the unmodified Au electrode is still three electron ORR and this will create a higher current density than the two electron peroxide oxidation. The last important feature of this CV is that the peak potential difference in this graph is around 70mV, which is larger than for the CV on the modified Au electrode but smaller than that for the reconstructed Au (poly) electrode in pure 1M KOH solution. The trend of peak potential difference changes with scan rate and also suggest that the reversibility of the $O_2/O_2^{2-}$ redox couple in this case is between the these two situation, as shown in Fig 4.12. The exact reason for this feature is not very clear. However, we can still discuss the possible reasons why the peak potential difference changes.

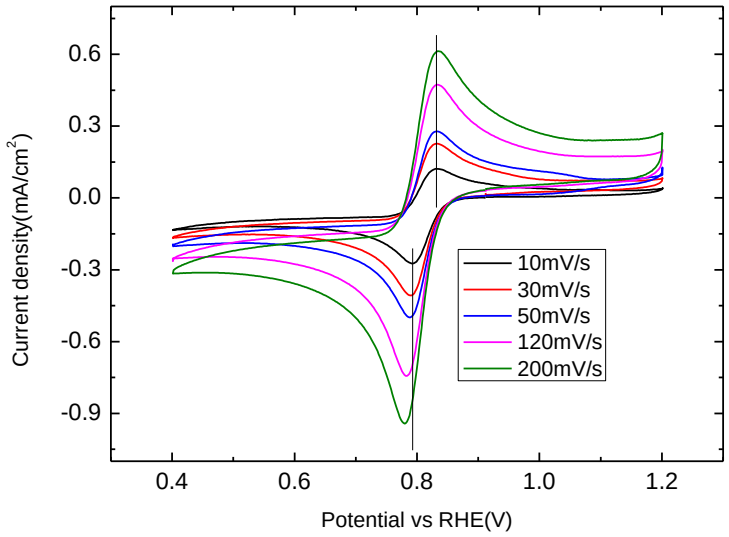


Figure 4.12 CV of various scan rates on reconstructed Au (poly) in (6mM H2O2 + 1M KOH) solution.

One possible reason is that, since peroxide is stable on the reconstructed Au electrode surface, the presence of peroxide in the double layer of ions on the electrode surface can influences the transport of other peroxide ions and oxygen. The other way to understand this is that the reconstructed Au electrode actually has better kinetics in a peroxide environment than without it. This generally implies that heterogeneous electron transfer rate is slower when peroxide is not in vicinity of the electrode.

In the last, the most important part is to test how peroxide oxidation is enhanced on the cobalt salen modified Au electrode. Since peroxide self-decomposition is faster when cobalt salen is in the solution, a thin film modification method is used again to have the Au (poly) electrode been modified by cobalt salen. The same reconstructed Au electrode is used in this experiment also. The difference between CV with and without modification on the electrode is shown in figure 4.13.

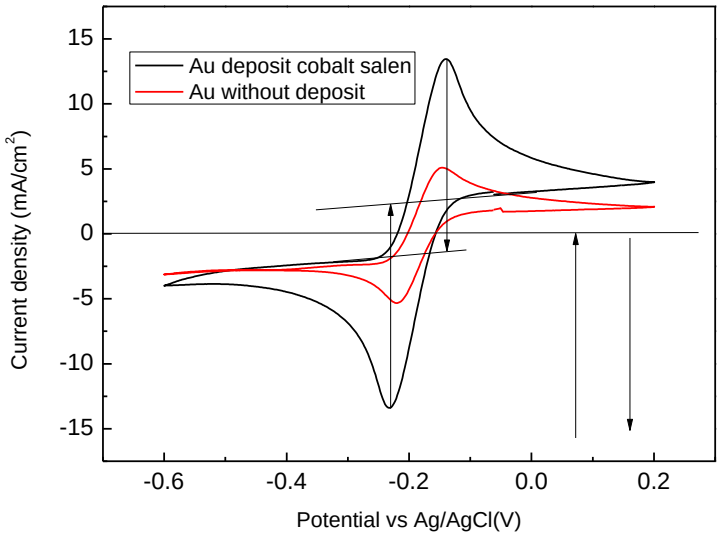


Figure 4.13 Red line: CV of Au (reconstructed) in (1M KOH+6mM $Na_2O_2$) electrolyte satuarated with oxygen. Black line: the same reconstructed Au deposited 10 µL (1M KOH + 2mM cobalt salen) solution and dried for 30 mins, then tested in the same (1M KOH+6mM $Na_2O_2$) electrolyte. Scan rate: 50mV/s (both are extracted 3rd cycle from original continuous CV)

As can be seen from the graph 4.13, the peak current density of the CV at the same scan rate and in the same electrolyte environment is different. The peak potential difference between the oxidation and reduction is not obviously shifted, which implies that the reaction mechanism is not changed. A possible interpretation for this is a similar reversible bonding of peroxide with cobalt salen like oxygen reversible bonding with cobalt salen. Peroxide ions or hydroperoxide ions have a one electron difference in terms of valence state. Although there has not been any therotical calculation to prove this, reversible bonding with little different bonding energy may be possible. If this assumption is proven valid from further research, we can expect a peroxide concentration phenomenon near electrode. This phenomenon can explain the difference from the previous graph. Compared

to the CV difference in pure 1M KOH solution (Figure 3.14), the bigger difference in current density in peroxide environment after modification is because the peroxide concentration in this electrolyte is much higher than oxygen concentration in 1M KOH solution. The other important feature is that the ratio of peak reduction current density over peak oxidation current density increases to 1:0.97. This indicates that the ORR on the modified Au electrode should be two a electron reduction, which agrees with the two electron peroxide oxidation reaction. Therefore, in a peroxide rich alkaline electrolyte environment, the reaction mechanism is two electron quasi-reversible ORR without follow-up reaction.

## 4.4 Electropolymerization cobalt salen on polycrystalline Au electrode

No matter what actual mechanism is working to change the oxygen reduction reaction mechanism to such a reversible process, our experiment confirms one fact: that this astonishing phenomenon is due to the combination of Au electrode and cobalt salen on gold surface. Thus, further improvement to immobilize cobalt salen complexes on Au surface is necessary. As we want this immobilization to be irreversible, the best way to achieve this composition is to form a covalent bond between cobalt salen and the Au surface. One way to directly modified complexes on Au is using thiol as connection atom. However, based on the normal thiol modification property, we think this method may not be the best way to immobilize cobalt salen. First, stability issues compromise thiol modified surfaces with respect to the ORR. SAMs (self assembled monolayers) need very good orientation and close packing on the Au surface to have enough van der waal's force between the molecule to maintain long term stability. SAMs are usually not good for

ambient operation. $O_3$ is one of the main reasons for the desorption of thiol from Au surface according to the following reaction:

$$RS - Au + H_2O + O_3 \rightarrow RSO_3H + HO - Au$$

Secondly, having long chain SAMs may jeopardize the catalytic property of the original catalyst. Connecting sulfur directly to Au may cause undesired surface reconstruction, and the chain length of what normal SAMs require for stability is too long to allow intimate connection between cobalt salen and Au. Therefore, we prefer other methods over SAMs. For other methods of immobilizing cobalt salen, we divide them into two categories: modifying cobalt salen on the carbon support and solidifying cobalt salen. Unlike Au, carbon is more easily modified and allows different choices for the connection molecule. This modification will not jeopardize the Au surfaces. For solidifying cobalt salen, we can modify cobalt salen to ensure it not only retains the same properties but is also insoluble. We can polymerize the cobalt complex on the catalyst surface to make it form a network and also to make it insoluble. Among all these methods, we suggest that electropolymerization could be the best way to achieve our goal.

Electropolymerization is a valuable tool for the development of the modified electrodes. First, electropolymerization is a simple method for to deposit a target monomer on the electrode surface. Second, an electropolymerized film is a kind of a molecular wire or net. It is more stable compared to both adsorbed and covalently linked modifiers. Third, the electropolymerized monomer sometimes possesses unique features compared to the monomer itself. Electropolymerization is typically achieved upon oxidation or reduction of organic compounds. The oxidation potential of salen is out of the aqueous

electrochemical window, so the electropolymerization of cobalt salen is carried in an organic electrolyte environment, as described in the experiment section.

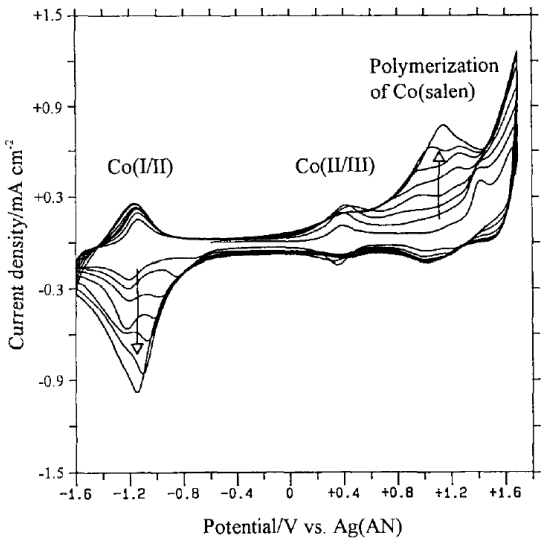


Figure 4.14 Current-potential curves showing progress of oxidative polymerization of Co (salen) on BHPG (high density pyrolytic graphite, apparent area 0.20cm$^{-2}$). Solution: Ar saturated AN solution with 2mM Co(salen) and 50mM $TMABF_4$. Scan rate: 0.1V/s.[120]

Fig 4.14 is one example of how to use cyclic voltammetric method to induce a salen complex to electropolymerize on a high density pyrolytic graphite (BHPG) electrodes. At around 1.35V, the current peaks for Co(salen) polymerization develop, while Co (2/3) and Co (1/2) peaks appeared at around 0.4 V and -1.2 V, respectively, the former diminished while the latter increased by repeated scans. A greenish film is found on the graphite electrode after the process. From these two plots, we should generally have an idea how a cobalt salen electropolymerization process should be carried out. And a very important conclusion is drawn by the comparison of these plots and the plots of electropolymerization

of cobalt salen on Au (poly) electrode. Fig. 4.15 shows twelve cycles of the CV process of the electropolymerization on a polycrystalline gold electrode.

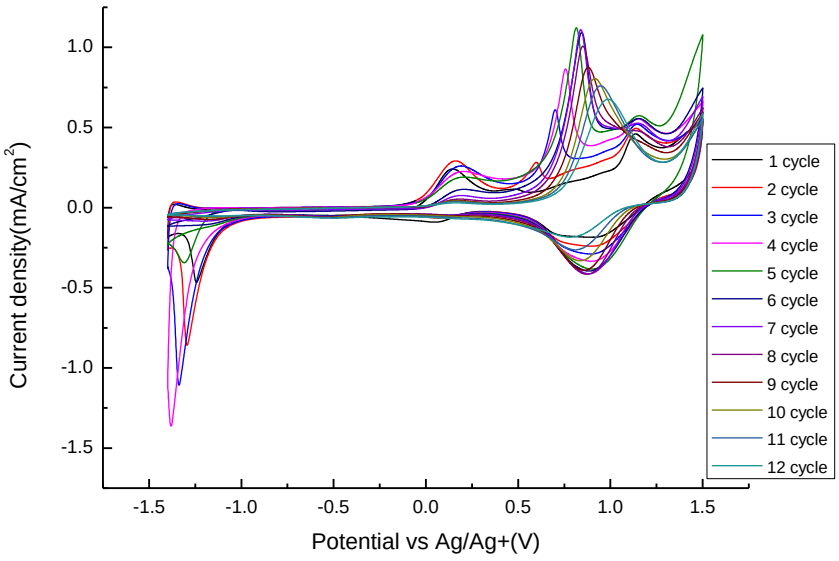


Figure 4.15 12 cycles of CV on Au (poly) electrode surface. Electrolyte: TBATF and cobalt salen in acetinitrile. Scan rate: 50mV/s

The first most obvious new feature in this graph is the shifting of $Co^{2+}$ oxidation potential after the electropolymerzation. The process of Co (salen) on BHPG does not show any shift like that shown in the graph 4.15. This tells us, along with the evidence that the film is growing on every cycle and the oxidation of $Co^{2+}$ is becoming more difficult, why the oxidation potential is shifting to the positive. The oxidation peak gradually merged into the range where electropolymerization happens. The other obvious new feature of this graph is that the $Co^{2+}$ oxidation peak is not only shifting, but also very sharp for every peak when compared to Fig 4.14 This new feature may suggest that a possible strong surface reconstruction is happening along with electropolymerization when the CV is conducted.

This might be a much stronger Au surface reconstruction, because the interaction of cobalt salen and the Au surface should be much stronger than only having cobalt salen in the solvent phase and interacting with the Au by physisorption. Polymerization is also a good way to bring about a surface reconstruction because the strong interaction between molecule and surface also changes the surface energy with potential change. Therefore, we might achieve two goals at the same time with the CV eletropolymerization process. One is having cobalt salen forming a stable insoluble film on the surface to stabilize the combination of cobalt salen and Au; the other is that we also achieve a more stable Au surface reconstruction. The stability test will be discussed later. After modifying the polycrystalline Au surface using electropolymerization method, the electrode is tested in 1M KOH electrolyte again to verify the effect on ORR. We find very encouraging results.

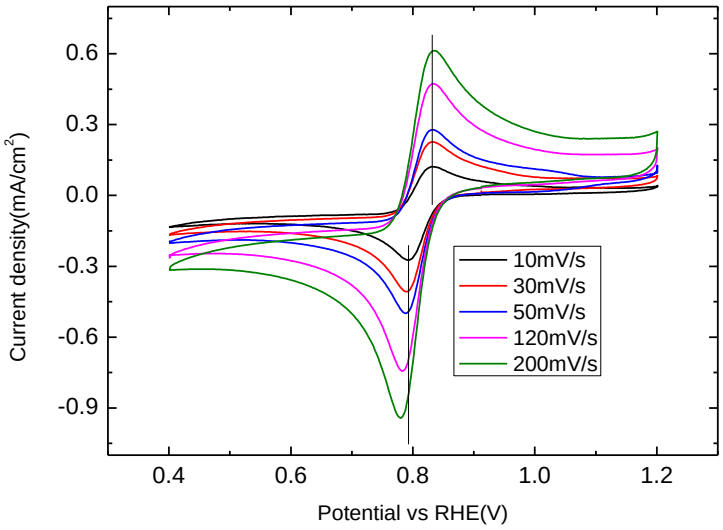


Figure 4.16 CV of various scan rates on Au (poly) electropolymerized with cobalt salen Electrolyte: 1M KOH Scan rate: 50mV/s, IR corrected.

From Fig 4.16, we can see that the reversibility of the ORR is still good, but the reduction potential shifts a little more along with the increase of scan rate than in the experimental data of Fig 3.16. This could be due to the property of reversible bonding to dioxygen molecule is weakened after the electropolymerization process. The other significant change after this modification is mainly related to stability. There are two reasons why the stability is greatly enhanced here. The first is that the electropolymerization process forms a network of chemical interactions between Au electrode and each monomer. Electropolymerization can be seen as a combination of electrodeposition and polymerization. The difference between electropolymerization and electrodeposition is new σ carbon bonds are formed between each monomer. Thus, the polymer film formed on the electrode is not only insoluable but also a three dimensional network of σ carbon bonding. This is the reason why cobalt salen is immobilized on the surface. The second reason is the modification process can induce a much more stable surface reconstruction. Electropolymerization results in a close packing of cobalt salen on the surface. This will cause a much stronger interaction between cobalt salen and Au electrode surface layer. This also perfectly fits the general surface reconstruction hypothesis.

The following experiment provides an indirect proof that the reversible ORR is because of the reconstructed Au (111) similar surface and the better kinetics of ORR and OER is because of cobalt salen modification. The experiment is carried out by directly mechanically polishing the electropolymerization-modified Au electrode without any electrochemical cleaning or any other cleaning procedure. (Fig 4.17) The point of this experiment is that removing the surface cobalt salen on the surface would cause a Au surface structure change.

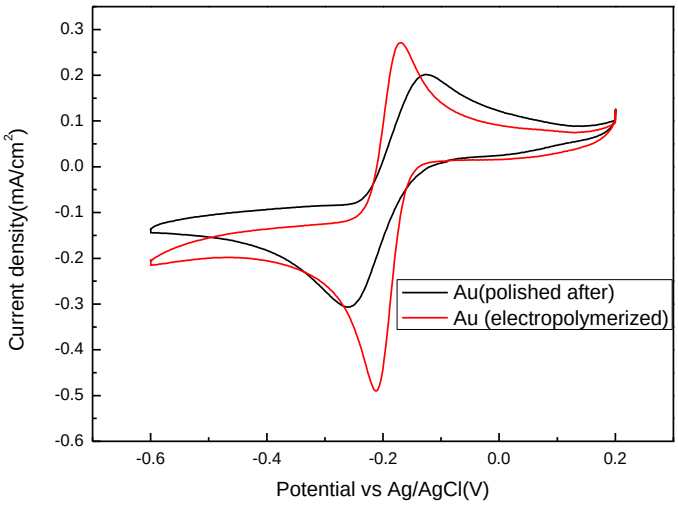


Figure 4.17 Comparison of ORR CV before and after mechanical polish a cobalt salen electropolymerized Au electrode Electrolyte: 1 M KOH Scan rate: 50mV/s

The peak potential separation of the CV after mechanically polishing the Au surface is around 100mV, this is exactly the peak potential separation it should be on Au (111) surface. This specially prepared electrode shows a very typical quasi-reversible ORR process. The following scan rate dependence experiment shows the peak current density and peak potential difference is proportional to the square root of scan rate, as shown in Fig 4.18. This also indicates that this is a very typical quasi-reversible reaction.[135]

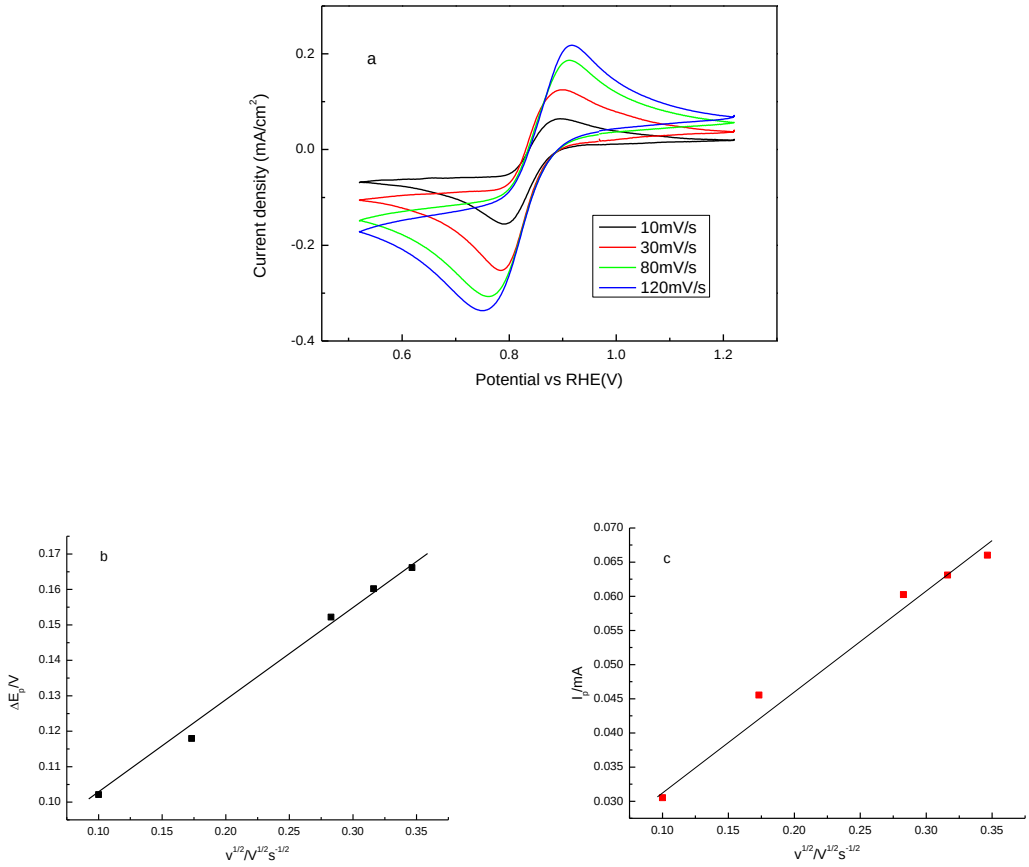


Figure 4.18 (a) CV of various scan rates on Au (poly) cobalt salen electropolymerized and polished. Electrolyte: 1M LiOH Scan rate: 50mV/s, IR corrected; (b) The relation between peak potential difference and square root of the scan rate from graph (a); (c) The relation between peak reduction current density with square root of scan rate from graph (a).

## 4.5 The influence of electropolymerization on catalytic stability

Our discovery proves that the combination of Au and cobalt salen can make oxygen reduction behave like a reversible reaction. To characterize this catalyst, most of our experiments were done in an alkaline solution containing cobalt salen since cobalt salen is soluble in aqueous solution. However, we need to try to preserve the peroxide after it is

produced so that we can use it to recharge the battery, and having cobalt salen dissolved in the electrolyte is not very realistic for the real battery based on this catalyst. On one hand, because heterogeneous catalysis only happens at the interface, it is not necessary to have cobalt salen in the solution phase even if we want to preserve the peroxide in the liquid phase. On the other hand, the cobalt in the cobalt salen complex is capable to catalyze peroxide self-decomposition. The cobalt in the solution has the capability to be oxidized to $Co^{3+}$, and $Co^{3+}$ is also capable to be reduced to $Co^{2+}$. Then the $Co^{2+}$ can have like a two-step series reaction like Haber-Weiss reaction. The Haber-Weiss reaction is a two-step series reaction that can generate hydroxyl radicals from hydrogen peroxide and superoxide, as shown below:

$$Co^{3+} + \cdot O_2^- \rightarrow Co^{2+} + O_2$$

$$Co^{2+} + H_2O_2 \rightarrow Co^{3+} + OH^- + \cdot OH$$

Figure 4.19 shows the result of an experiment that uses an electrochemical method to measure the peroxide decomposition rate in a cobalt salen alkaline solution.

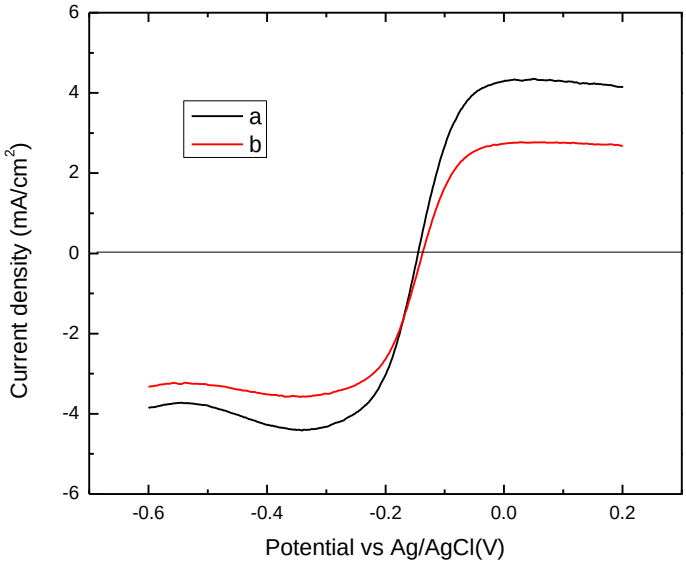


Figure 4.19 Polarization curves comparison of peroxide oxidation performance on Pt in the electrolyte (a. 1MKOH+ 2mMCobalt salen+6Mm$H_2O_2$ solution b. same electrolyte with "a" after been preserved for 10 hours.). Scan rate: 50mV/s, rpm: 1000

Peroxide oxidation on Pt is widely used in RRDE because it shows a good linear correlation between the amount of peroxide and measured current. In this experiment of Fig 4.19, we do a repeat experiment (b) 10 hours after the first peroxide oxidation polarization curve (a). Then we compare the steady state current density and find that the peroxide amount was greatly reduced. Therefore, we cannot have cobalt salen in the electrolyte to maintain the presence of cobalt salen. We next ask 'what is the stability of the catalyst when you already have cobalt salen on the Au and do not have cobalt salen in the electrolyte phase?' We use deposited and dried electrode method (described in the experiment section) to verify the catalytic stability, as shown in Figure 4.20.

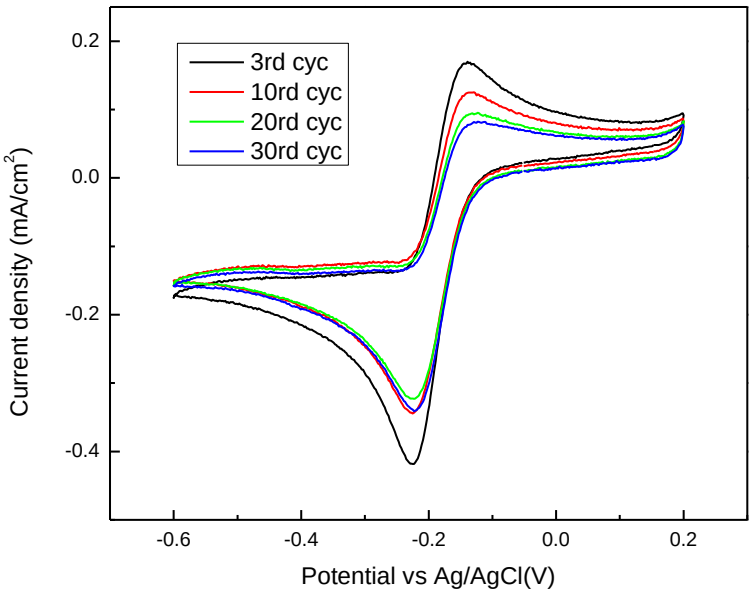


Figure 4.20 Electrode: Au (poly) deposited (1M KOH + 2mM cobalt salen) solution and dried for 30 mins .Electrolyte: 1M KOH saturated with $O_2$, Scan rate: 50mV/s

As shown from Fig 4.20, the catalytic stability of peroxide oxidation current decays very rapidly in a pure alkaline environment. This will be due to the gradual diffusion of cobalt salen away from the Au electrode. Losing contact with cobalt salen is actually changing the surface energy, causing the preferred surface reconstruction to revert to the original atom orientation. The electrode will gradually move to the normal polycrystalline Au electrode ORR catalytic activity. This also agrees with our previous suggestion that there is no strong interaction between cobalt salen and Au.

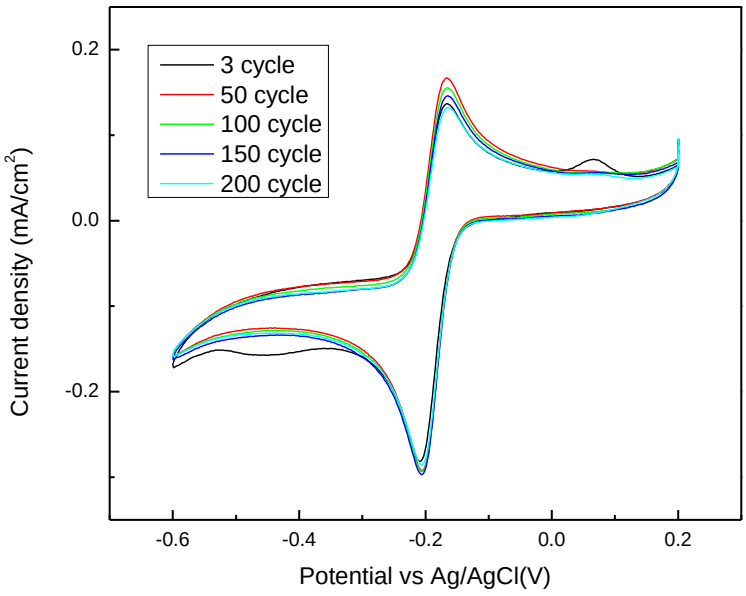


Figure 4.21 Electrode: Au (poly); Electrolyte: 1M KOH +2mM cobalt salen; Scan rate: 50mV/s

Fig 4.21 is a comparison experiment for Fig 4.20. In this experiment, the same electrode has been running CV in a cobalt salen containing alkaline electrolyte for 200 cycles. This is not only a good comparison for the experiment in Fig 4.20, but also a very good accelerated stability test for proposed catalyst in this work. Bifunctional catalysts are well known for low catalytic stability.[7 55,56,58,59,62] Apart from other factors that may jeopardize the catalyst stability, most bifunctional catalysts show a stability issue because the working potential range is too large. An ideal bifunctional catalyst for aqueous air battery needs to have a working potential range of over 1.3V (each direction polarized for 300mV), which is much higher than the one direction ORR catalyst. In this work, the working potential range required for this catalyst is only 600mV (considering the same extent of polarization), and this is a big advantage of this two electron reversible air electrode chemistry over

conventional aqueous air electrode chemistry. Also, from Fig 4.21, we find that the catalytic stability of this catalyst is very good in this potential range.

The next goal for stability is to immobilize cobalt salen on the Au surface and achieve the same stability as with the experiment with cobalt salen in the solution (Fig 4.21). According to the previous section, electropolymerization of cobalt salen has been conducted in organic electrolyte and similar catalytic activity has been achieved by this immobilization method. Here, 250 cycles of accelerated stability test is conducted in an alkaline electrolyte without cobalt salen, as shown in Fig 4.22.

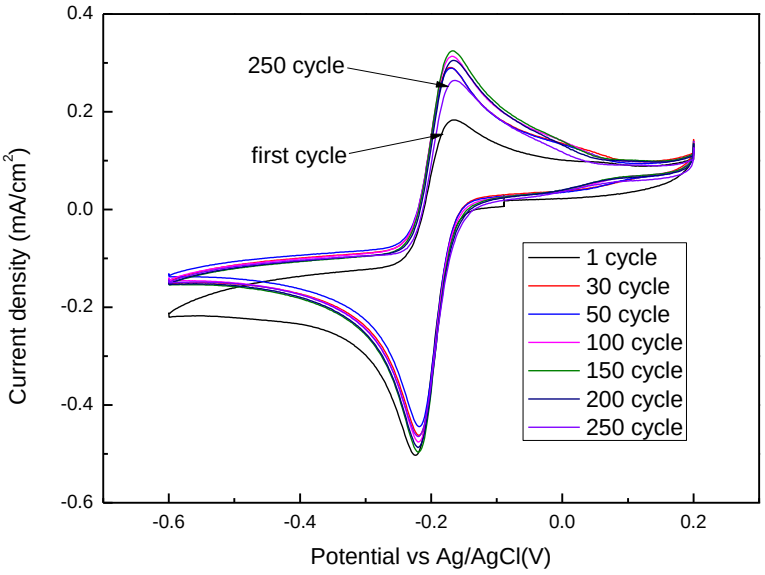


Figure 4.22 Electrode: Au (poly) electropolymerized with cobalt salen; Electrolyte: 1M KOH; Scan rate: 50mV/s

From the result, we can see that the catalytic activity is very stable in general. The first cycle, as pointed out in the graph, shows relatively poor reversibility. That is probably

observed because the thin polymer film on the surface of gold electrode does not cover the Au surface as evenly as physisorption does. This situation requires a break-in process for the polymer film. After the break in process, the catalytic activity shows good stability.

## 4.6 The influence of nano Au on the oxygen reduction catalyst activity

Since catalysts provide a surface for the chemical reaction to take place, nanoparticles with their extremely large surface area are very important in the catalyst industry, Especially for the heterogeneous catalysis where the catalyst is a different phase to the reactants, nano catalyst is almost a necessity. The use of nanoscale catalysts opens up a number of possibilities of improving catalytic activity and selectivity. Besides the increase in surface area, the catalytic properties of catalyst can also be greatly influenced by nano size. Both the bulk atom to surface atom ratio and the edge to surface ratio are greatly increased. Since the catalyst working mechanism often is based on the interaction between the catalyst and the reactant, the particle edge catalytic activity is different from particle surface. Therefore, when these two ratios increase to several magnitudes larger than the bulk phase, this will have a great influence on catalytic activity. In this case, since electrocatalysis, by nature, is a heterogeneous catalysis process, we can expect the nano size will also have big influence on catalytic activities.

For the oxygen reduction catalyst in electrochemistry, the size of the catalyst has been proved to have an impact on catalytic activity.REF For different catalysts, the influence of size on the ORR catalytic activity is very different. The most well studied catalysts are Pt and Au, and they present different trends. Antoine etc. showed that, from 2.5nm to 28nm, the oxygen reduction kinetics in acid on Pt particles decreased.[136] The work of Genies et

al. also reported a three-fold reduction in activity in alkaline electrolyte when platinum particles decreased in size from 24nm to 2nm.[137] The difference in catalytic activity is attributed to excess $HO_2^-$ on the surface, which desorbed without further reduction. For Au catalysts in electrocatalysis, the size tendency is the opposite in general. Au is also famous for the 'magic numbers,' which implies that certain size and crystal facets have much higher catalytic activity then other numbers. Wei Tang et al. did a detailed comparison between 3nm and 7nm Au nano particles, found out that 3nm particles have 2.5 times better catalytic activity than 7nm particles and the electron transfer number is decreased from 4 electron transfer to 2 electron transfer.[138] Samuel Guerin et al. use a combinatorial approach to study the Au particle size effect on ORR with two different supports.[139] For both carbon and titanium dioxide supports, in the range of 1.4nm to 6.3nm, the oxygen reduction decays rapidly for particle sizes below 3nm. For most methods of preparing Au nano particles, certain chemicals are added in the preparation process to prevent nanoparticle aggregation into bigger sizes. However, these methods need extra treatment, like heat treatment, to remove the coating. This will also influence the catalyst. In order to minimize the influence of post treatment and understand better the particle size influence. Youngmin Lee et al. used a single solution phase synthesis method.[140] The key point of this method is not only using tert-butylamine borane as reducing agent but also using oleylamine as both reducing agent and stabilizing agent to make nano Au particle. They showed size-dependent ORR activity with smaller nanoparticle sizes or highly discordered Au nanoparticle being more active. [138–147] As we discussed previously, the Au (100) phase proceeded by 4 electron reduction in alkaline solutions compare to other facets, which is very different from other noble metal in ORR electrocatalysis. Thus, the

enrichment or absence of Au (100) caused by certain preparation methods sometimes influences the catalytic activity. Also, different internal crystalline orientations will result in different shapes of Au nanoparticles, and also influence catalytic activity to some extent.[145] In general, people found different results when studying Au nano size influence on ORR because of the preparation method difference.

In the previous chapter we showed that the combination of Au and cobalt salen works as a bifunctional air electrode catalyst. In order to further apply this catalyst in a electrochemical cell, we need to prove that this catalyst combination also performs the same when the Au particle size is reduced to nano scale. In view of the large surface area of the nanoparticles, making a modified nano Au particles is necessary for the cell applications. As mentioned previously, nano gold particles with size over 8nm generally has similar catalytic activity to bulk phase Au. Therefore, our first experiment is making a nano Au particle size in the range of 8nm to 25nm. One of the simplest ways to produce Au nanoparticle of this size is use trisodium citrate as reducing agent to reduce hydrogen tetrachloroaurate in solution. In this method, the size of the particle is controlled by the reaction time and temperature. After three hours reaction, the particle size is approximately between 15nm to 20nm. The actual particle size is measured by XRD experiment, as described in the experiment section.

The previous method, having cobalt salen interact with Au from solution phase, is not suitable for the nano Au catalyst. For practical consideration, a nano Au particle needs to be deposited on an electronically conductive support, carbon or Titanium oxide. Here, we use carbon black, Vulcan XC-72, for the experiment. Since carbon supports provide most

of the surface area for the electrode and are two electron ORR catalysts, we are not using cobalt salen solution to modify the Au on carbon catalyst. The alternative method we tried is to have cobalt salen dissolved in the ink to form an electrode.

The ink composition and preparation method is described in experiment section. Depositing the ink onto RDE electrode also follows the previous description. To verify whether cobalt salen and Au nano particle have a strong interaction, the easiest method is a continuous CV in nitrogen purged alkaline solution. The following graph shows a continuous 40 cycles CV just after this electrode was immersed into the solution.

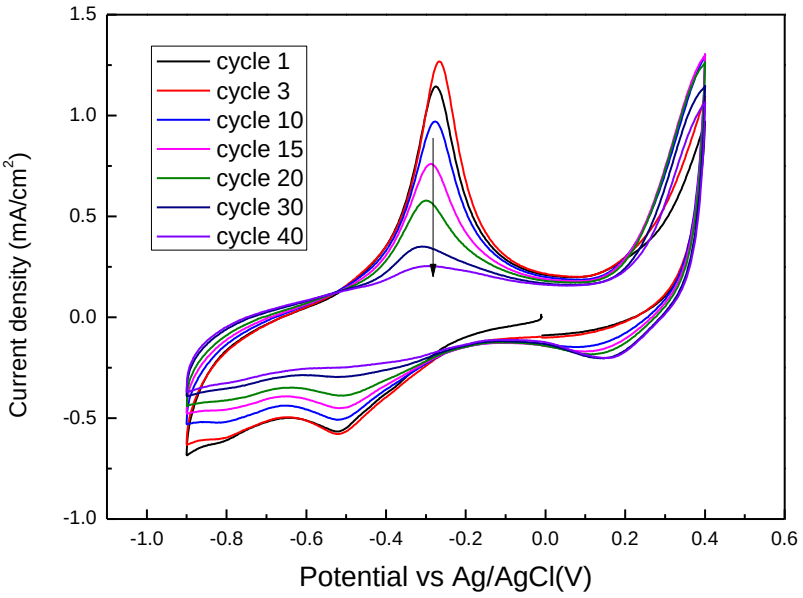


Figure 4.23 Continuous 40 cycles of CV on Au/C (with cobalt salen in the ink) in $N_2$ saturated 1M KOH solution.

The tendency showed in this CV indicates the interaction between cobalt salen and electrode is getting weaker with time after immersion into solution. The cobalt salen which

was previously dissolved in the solution diffusse into the bulk alkaline solution. However, based on the hypothesis we developed, this interaction should have sufficient influence on the surface properties of Au nano particles tochange the ORR catalytic activity of the catalyst.

To verify this, a comparison experiment is designed. Using the same Au on C powder, another ink with the same composition except for the cobalt salen was made. The catalytic activity of these two catalysts was tested under the same conditions.

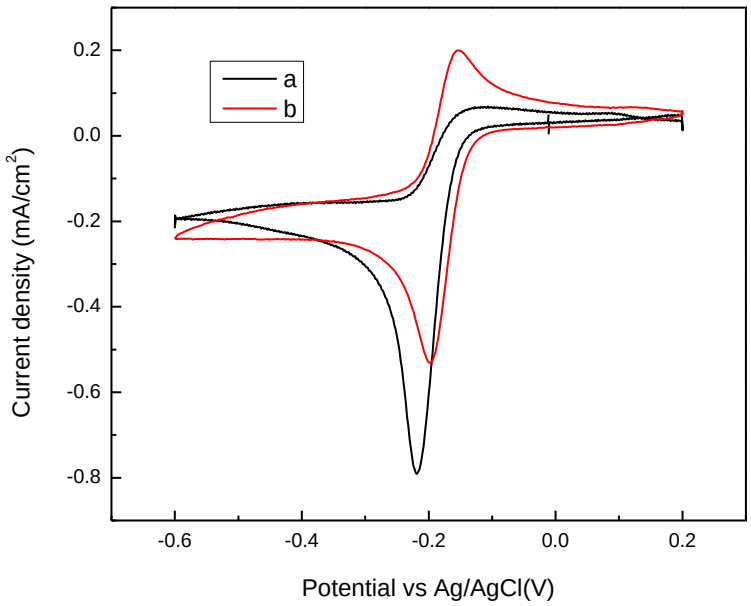


Figure 4.24 Comparison of ORR CV on (Au/C-a) catalyst (a. without cobalt salen b. with cobalt salen in the preparation ink) in $O_2$ saturated 1M KOH solution.

In a pure 1M KOH solution, this comparison experiment shows exactly the same difference with previous results on bulk Au electrode. The catalyst made from ink without cobalt

salen shows no sign of reversibility and almost no sign of peroxide oxidation. On the other hand, the catalyst made from ink with cobalt salen shows very good reversibility and peroxide oxidation. However, the reversibility for Au on a carbon catalyst modified with cobalt salen does not show reversibility similar to the bulk Au electrode. Two possible reasons for this are that (1) the carbon support is actually producing peroxide but not oxidizing it back, so the overall reversibility of the electrode is not very good and (2) the surface area of nano Au in specific area is larger than for the bulk Au electrode and the peroxide produced is more likely to be further reduced.

## 4. 7 The influence of peroxide stabilizer

Based on the previous discussion, the oxygen reduction process on this catalyst is an EC mechanism, hydroperoxide ($HO_2^-$) is produced by electrochemical oxygen reduction, then chemically decomposed in alkaline environment. To better benefit from the advantage of two electron reversible ORR chemistry, peroxide needs to be preserved as much as possible to reduce the battery recharge overpotential and also gain fast recharge speed. The peroxide preservation in alkaline media is well studied in paper and pulp industry. Hydrogen peroxide is widely used in paper and pulp industry as a bleaching agent due to its "green" feature. The most common way to use hydrogen peroxide to bleach the pulp is by having 2% wt hydrogen peroxide in alkaline solution.[148–150] For this case, they also have the same problem of peroxide self decomposition, and use peroxide stabilizer to maximize the use of peroxide. [151–153] Peroxide self decomposition is believed to be significantly hastened by Fenton processes caused by transition metal ions.[154] Therefore, most peroxide stabilizer is a strong transition metal ion defunctionalizer. The most commonly used peroxide stabilizer

is sodium silicate. Its complex stabilizing mechanism can stabilize peroxide with or without transition metal ions. The other alternative, such as DTPA and EDTA, are very strong transition metal ion complexing agents or chelating agents.

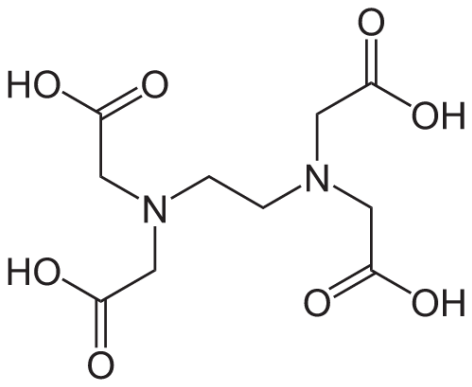


Figure 4.25 Chemical structure of EDTA

For convenience, EDTA (Fig 4.25) is selected as electrolyte additive, and a comparison experiment is designed to see the effect of peroxide stabilizer. In cycle voltammetry, the peroxide oxidation peak is the most direct evidence of how much peroxide is preserved. Compare with Fig 3.14, we can see that the oxidation peak current density is equal to the reduction peak current density. The ratio of peak reduction current density over peak oxidation current density is 1:0.99 in Fig 4.26. This means the peroxide produced in the oxygen reduction process is all oxidized back without losing any. And this is also a direct proof that, for this catalyst, the oxygen reduction process is a pure two electron reduction process, for all the reduction product can be oxidized back without going to higher overpotential. This experiment shows that using peroxide stabilizer is necessary for the

rechargeable air battery technology. However, our initial data here does not mean that EDTA will be the most ideal stabilizer since the time scale of CV is very short.

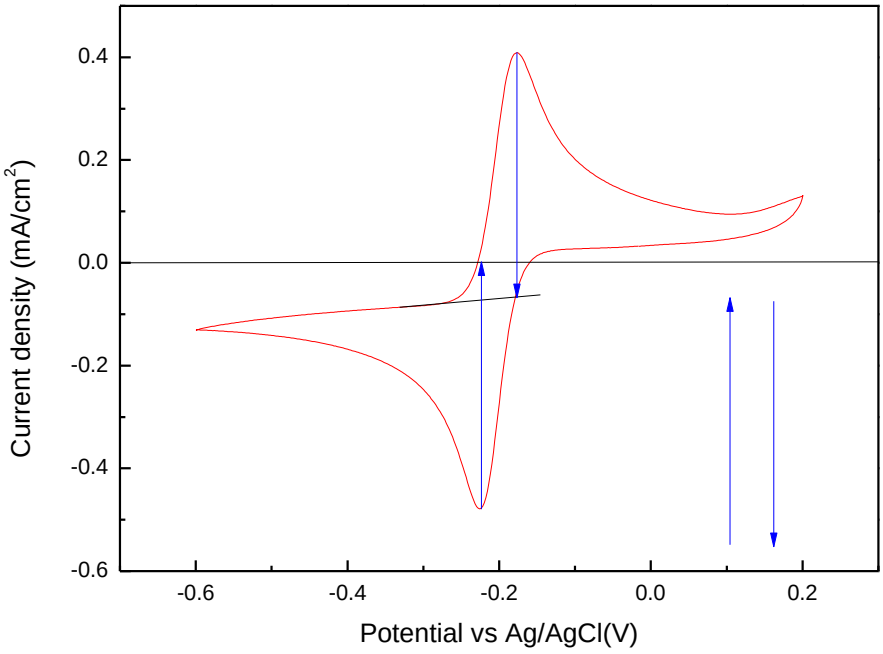


Figure 4.26 CV of cobalt salen modified Au electrode in 1M KOH+1M EDTA electrolyte saturated with oxygen. Scan rate: 50mV/s.

# Chapter 5

# The influence of cation to ORR in alkaline environment

As previously mentioned, one of the new features for the aqueous Li-air battery is that the electrolyte environment that is based on lithium salt or lithium hydroxide. Also, along with the battery operation, the electrolyte concentration is changed by the dissolved reaction product. For alkaline Li-air battery, LiOH is the reaction product, and it is accumulated and increases the concentration in the cathode along with discharging if no additional procedure is added for LiOH to be salted out. The ORR reaction here is similar with the ORR in alkaline fuel cell, except the electrolyte is LiOH instead of KOH and the concentration of the electrolyte is increasing with reaction. ORR reaction in alkaline environment has been investigated for many years along with the development of alkaline fuel cell and zinc-air battery. However, the influence of different cations and the influence of alkaline concentration on ORR have not been very well studied previously.

The influence of cations on the ORR is a relatively new research field. There are two approaches to develop an ORR metal catalyst: one is tuning the electronic properties of the surface metal atoms, the other is changing the components and structure of electrochemical double layer. The majority of research efforts on electrochemical double layer have long been focused on studying the direct chemisorbed species within interior Helmholtz layer, including, anions[155], oxygenated species[12] and supporting electrolytes. It has been acknowledged that these strong chemisorptions play a decisive role on catalytic activity since they can greatly influence how a reactant interacts with catalyst surface. On the other

hand, the influence of cation and other species within the outer Helmholtz layer has rarely been studied. The cation has usually been considered as having an interaction with water and hydroxide. The strength of these interactions is between strong covalent interactions and very weak electrostatic interactions, generally called non-covalent interactions. Although these non-covalent interactions don't greatly influence the ORR, there are some minor changes on the catalyst surface activities due to different cation. N.M.Markovic et al. first proposed a model about these non-covalent bonds influence to ORR.[85] They suggest a formation of $OH_{ad}$-$M^+(H_2O)x$ (M= $Li^+$, $Na^+$, $K^+$, $Cs^+$) cluster which could potentially block $O_2$ adsorption, and the bond formation and concentration of these clusters increases in the same order as hydration energies ($Li^+ << Na^+ < K^+ < Cs^+$). They later used surface X-ray scattering data to calculate that barium cations are located at 3.4 Å away from the surface (a distance between fully chemisorped and fully hydrated); this indicates the formal non-covalent interactions, and the ORR results also suggest that the cation influence is much more obvious on Pt than Au.[156]

The influence of concentration on the ORR is also a new but important research topic, especially for the alkaline lithium air batteries. Previous research did not focus on the concentration influence of LiOH but on the concentration influence of NaOH and KOH, which is widely used in fuel cell and zinc air battery. Allen J. Bard et al. use CV and transient amperometry to study the diffusion coefficient, solubility and electron transfer number. They show that the electron transfer number will decreases with the increase of the concentration.[157] In this work, we use CV to look at the chemisorption of different species on the catalyst surface. Figure 5.1, 5.2, 5.3 are CV comparisons of cation ions with different concentration of alkaline electrolyte. We also use polarization curve and tafel plot

from RDE experiment to study the electrochemical performance in the environment of LiOH in different concentrations. Pt/C is chosen as a research catalyst, since it is the most well understood ORR catalyst.

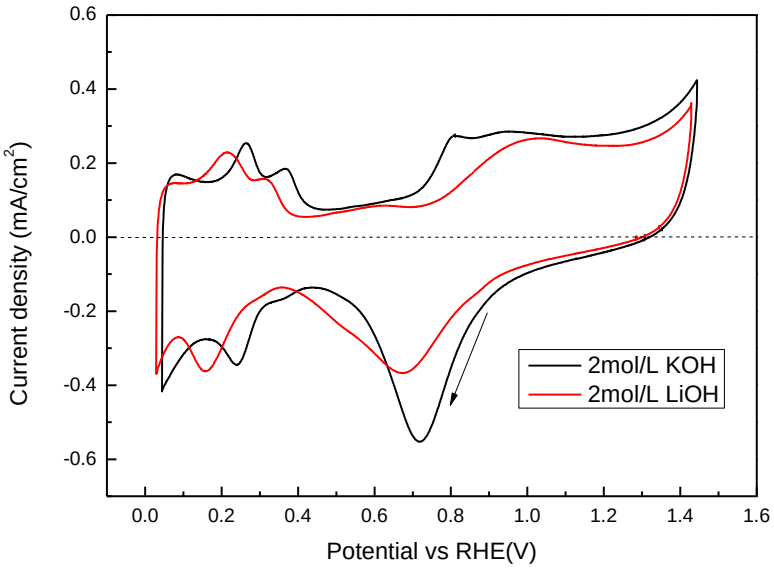


Figure 5.1 CV of Pt/Vulcan catalyst in 2 mol/L KOH and 2 mol/L LiOH electrolyte saturated with $N_2$ in a scan rate of 10mV/s

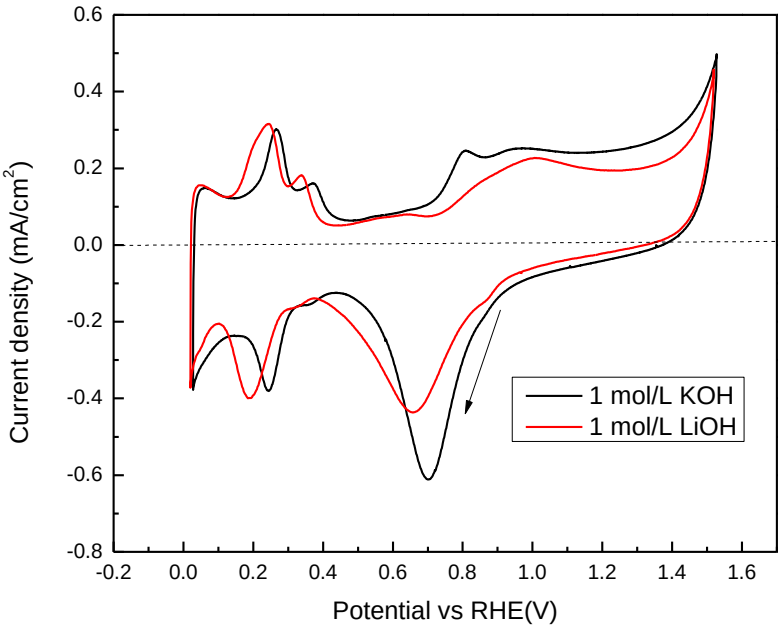


Figure 5.2 CV of Pt/Vulcan catalyst in 1 mol/L KOH and 1 mol/L LiOH electrolyte saturated with $N_2$ in a scan rate of 10mV/s

Figure 5.1 is a CV comparison of Pt/Vulcan catalyst in 2 mol/L KOH and 2 mol/L LiOH electrolyte saturated with $N_2$ in a scan rate of 10mV/s. The CV curves in this graph can be interpreted in four different potential regions. Starting from the left, are $H_{upd}$ potential region (0.06~0.4V), "double-layer" potential region, reversible $OH_{ad}$ region (0.6~1.0V) and irreversible "oxide" formation region (>1.0V). The result is consistent with previous research.[158] [132] Comparing the two figures in this graph, we see that the $H_{upd}$ (upd, under potential deposition) potential region is very similar, the only difference lies in the shift of the peak of proton desorption and adsorption. This indicates, at low potential region, the cation has little influence on ECSA. This also indicates that the available surface area in the two situations should be the same. However, at the high potential region, which is the

$OH_{ad}$ and oxide formation region in the graph, the OH adsorption and irreversible oxide formation is much enhanced in KOH solution relative to LiOH solution, and OH striping is also been delayed in the presence of $Li^+$ ions. Previous research from N.M.Markovic et al. suggest that ECSA cannot be influenced by cations, which agrees with results here. However, $Li^+$ can enhance OH adsorption but restrain reversible oxide formation on Pt (111).[85] In our case, for the nano size Pt particle, the $OH_{ad}$ and oxide formation region is well connected. The peak for OH adsorption shows up in KOH electrolyte but still cannot be distinguished from the oxide formation region. Therefore, we can only conclude that $Li^+$ will restrain the $OH_{ad}$ and oxide formation and delay the stripping of them.

For the other important aspect we are looking into, the concentration influence, we need to compare Fig 5.1, 5.2, 5.3 all together. From Fig 5.2 and 5.3, we can see the exact same trend of how $Li^+$ ions influence the chemisorptions on the Pt surface. And when comparing all three graphs together, we can see that the extent of how $Li^+$ ions change the CV compared to $K^+$ ions is directly proportional to the concentrations. Especially for Fig 5.3, since they are 1 magnitude lower alkaline concentration then the other two graphs, the CV in 0.1 M LiOH and 0.1 M KOH looks very identical. This leads us to the conclusion that the cations influence is increased with the alkaline concentration.

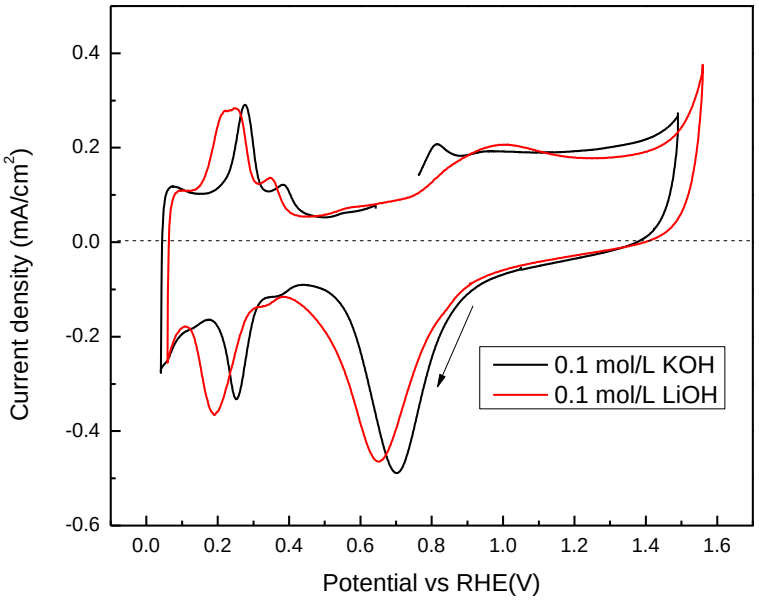


Figure 5.3 CV of Pt/Vulcan catalyst in 0.1 mol/L KOH and 0.1 mol/L LiOH electrolyte saturated with $N_2$ in a scan rate of 10mV/s

In order to see the influence of cations and alkaline concentration to the ORR, we use RDE to test the ORR performance. A polarization curve is obtained by subtracting CV of the nitrogen experiment from the CV of th eoxygen experiment at the same scan range with 10mv scan rate and 1000rpm. Figure 5.4 show the polarization curves of LiOH and KOH electrolyte, both at concentration of 0.1 M, 1M, and 2M.

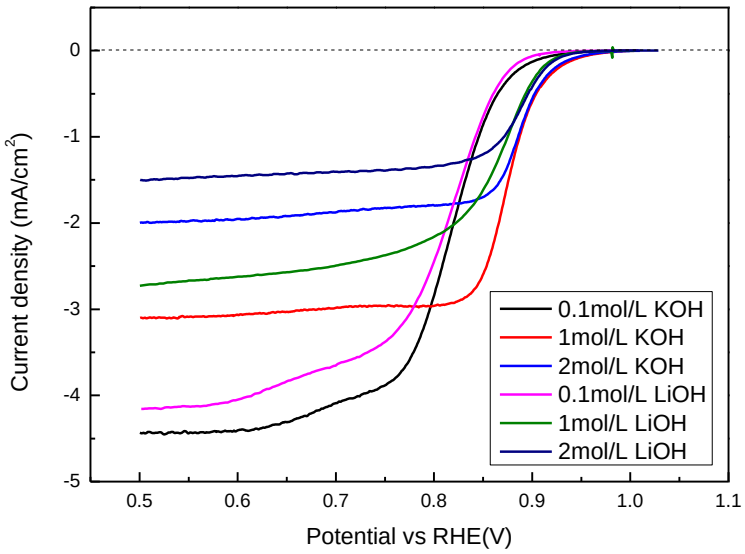


Figure 5.4 ORR polarization curves of Pt/C in saturated $O_2$ solution of 0.1M, 1M and 2M LiOH (scan rate:10mV, 1000 rpm)

The graph shows that the oxygen reduction current density of both KOH and LiOH electrolyte in 0.1mol/L LiOH is much larger than in 2 mol/L LiOH. This can be explained by the oxygen solubility and diffusivity difference in different alkaline concentrations and the Levich equation. As shown in equation 5.1, the current density($i_{ss}$) is a function of the number of electron(n) involved in mass transfer, oxygen solubility($C_{O2}$), diffusivity($D_{O2}$), kinematic viscosity( $v$ ) and rotation rate(ω). The oxygen solubility with LiOH concentration can be estimated by the "salting-out effect" and the Setchenow equation (eq 5.2). In the equation, C is the actual LiOH concentration, $C_{O2}$ is the solubility of $O_2$, $C^*_{O_2}$ is the solubility of $O_2$ in pure water, Setschenow constant($K^s$) of LiOH is positive(0.1605), KOH (0.1715) has a higher Setchenow constant than LiOH.[159] As the concentration of LiOH increases, the solubility of $O_2$ decreases. The diffusion coefficient of $O_2$ in LiOH

($D_{O2}$) can be estimated by the Stokes-Einstein equation (eq 5.3). In this equation, r is the effective hydrodynamic radius of the oxygen molecule (assumed spherical), k is Boltzmann constant, T is the absolute temperature. As the viscosity ($\eta$) of LiOH increases with the concentration[160], the diffusion coefficient($D_{O2}$) of oxygen decreases.

$$i_{ss} = 0.62nFAD_{O_2}^{2/3}\omega^{1/2}v^{-1/6}C_{O_2}^{*} \qquad (5.1)$$

$$\log\left(\frac{C_{O_2}}{C_{O_2}^{o}}\right) = K^{s}C \qquad (5.2)$$

$$D = kT/(6\pi r\eta) \qquad (5.3)$$

Apart from ORR current, we find that different concentration of electrolyte also has an influence on the reduction onset potential. The polarization curves of 1mol/L solution and 2 mol/L solution obviously have higher onset potential than 0.1 mol/L solution. This phenomenon is confirmed by repeated experiments with both KOH and LiOH solutions. We attribute this phenomenon to the thicker diffuse layer in 0.1m/L alkaline electrolyte. In modern surface electrochemistry, the Gouy-Chapman model with a diffuse layer of ions is generally more accepted than simple Helmholtz layer model. According to this model, dilute electrolyte systems with low density of charge carriers need a much thicker diffuse layer to counterbalance the excess charge on the electrode surface. This can also explains why the cation influence in 0.1m/L electrolyte is much weaker because those non-covalent interactions are also much weaker in dilute electrolyte. For the ORR case, lower charge carrier density on the electrode surface also means it ua harder for reactant and reaction intermediates to respond to the electrode potential change and begin reaction. The requires the electrode to have more overpotential to drive the reaction. This is why the onset

potential of the ORR in both 0.1m/L LiOH and KOH is slightly lower than for the other two concentrations. To understand the effect of concentration of cation on the reaction mechanism of ORR, we also compare the tafel slope extracted from Fig 5.4, as shown in Fig 5.5.

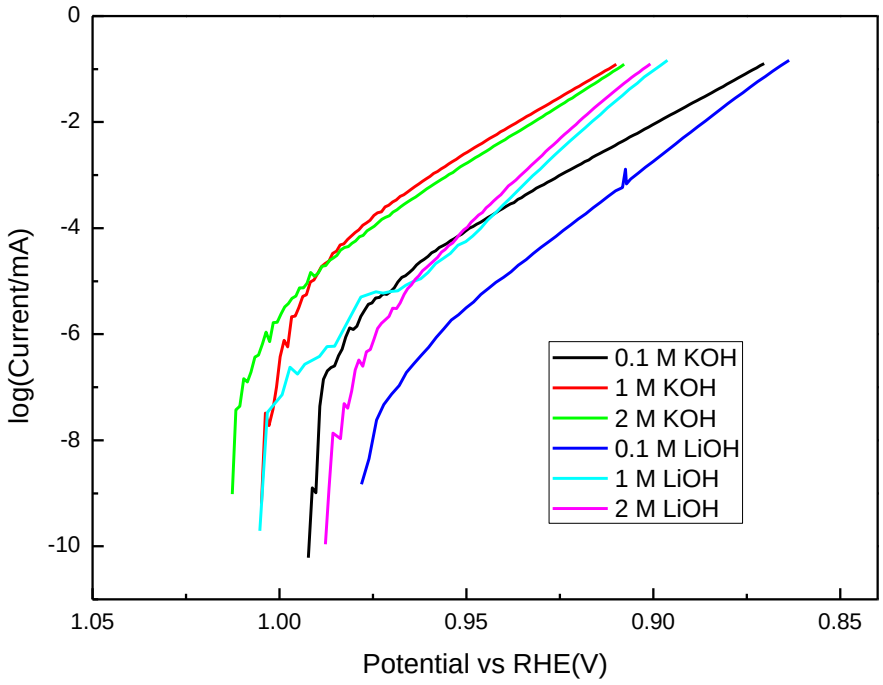


Figure 5.5 Tafel plot of kinetic region of polarization curves from figure 5.4

From Fig 5.5, we can see clearly that KOH solution has a larger tafel slope than LiOH solution in the potential region 0.88V to 0.97V. From the previous CVs (Fig 5.1, 5.2, 5.3), this is the region where OH- ions start to strip from the surface of the catalyst without significant difference in stripping rate. We suggest that the dominant factor here should be the higher OH- adsorption coverage in KOH solution rather than the faster OH stripping

speed in KOH. In the site-blocking of ORR, higher OH- ion coverage in KOH leads to less available sites on catalyst surface. Hence, when the OH- ions start to strip, there are more available sites in LiOH solution then in KOH solution, resulting a lower tafel slope in LiOH. This explanation also corresponds well with the N.M.Markovic's model in his previous paper.[85,86] Here, we also propose another explanation based on the direct interaction between cation and chemisorped oxygen. The formal explanation can be seen as the indirect influence model in which the cation influences the "spectator" chemisorbed species on catalyst surface, further influencing the catalyst performance. Since the ORR begins with the chemisorption of oxygen on the catalyst surface, we believe the direct interaction between the cations or cation based complexes is also very important for the ORR. When ORR happens, the cation complexes can also form non-covalent interaction with $O_2^{ad}$. If this interaction has the same trend with the hydration energy of cation ions, $K^+$ should have larger bonding energy. This should counterbalance the catalyst adsorption energy, which leads to a worse case. This can also explain why LiOH has a lower tafel slope. The experimental direct proof for the cation influence model will be very difficult to get, but a better understand of cation influence in the double layer structure needs be explored.

For further understanding the cation influence to the ORR on the noble metal catalyst, another Pt-group metal nano particles, Au nano particles, are also used for experiments. The diameter of Au nano particles and Pt nano particles are both 2nm, so they are very appropriate for comparison. The tafel slope of Au/C-b particles in the exact same experiment conditions with Fig 5.5 are shown in the Fig 5.6.

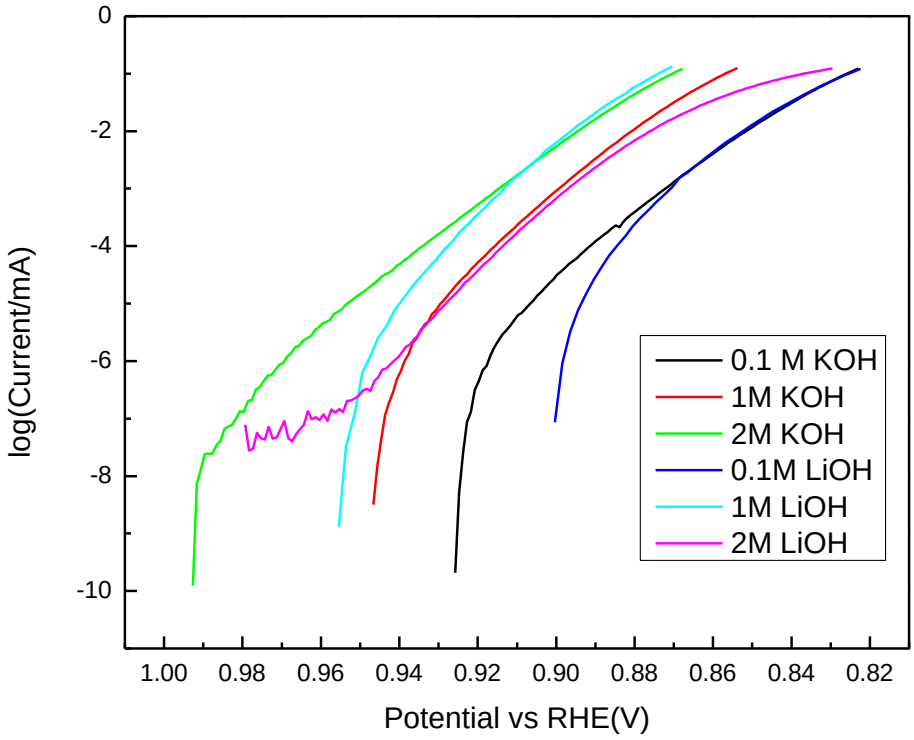


Figure 5.6 Tafel plots from ORR polarization curves of Pt/C in saturated O2 solution of 0.1M, 1M and 2M LiOH (scan rate:10mV, 1000 rpm)

As can be seen from Fig 5.6, the tafel slopes with the Au/C-b catalyst is not influenced by the cation or the concentration. This is because the coverage of $OH_{ad}$ on the Au catalyst is much smaller than on the Pt catalyst. Usually, we consider the coverage of $OH_{ad}$ on the Au catalyst is below 0.2ML (monolayer), and the coverage of $OH_{ad}$ on the Pt catalyst is above 0.6 ML. Thus, there are smaller influence of cation on the Au catalyst duo to the fewer oxygen containing spectators on the surface. And this supports the former interpretation which the cation influence is based on the non-covalent interactions between cation and spectator species.

# Chapter 6

# Application

## 6. 1 Electrochemical onsite production of hydrogen peroxide

Hydrogen peroxide is a heavily consumed "green" chemical and is widely used in several different industries, such as textile bleaching, paper bleaching, effluent treatment and chemical synthesis. Global hydrogen peroxide demand is increasing every year, and hopefully can reach 9 million metric ton per year by 2017. Around 50% of this demand is from the paper and pulp industry. However, although this is a booming industry with continuously increasing demand, the industrial scale production method is still dominated by anthraquinone oxidation (AO) process. The advantage of this process is that it has a high yield of hydrogen peroxide per cycle, but it needs very large scale factory space because it requires many extra procedures involving regeneration of solution and removal of the organic impurities from the hydrogen peroxide product, shown in Fig 6.1.

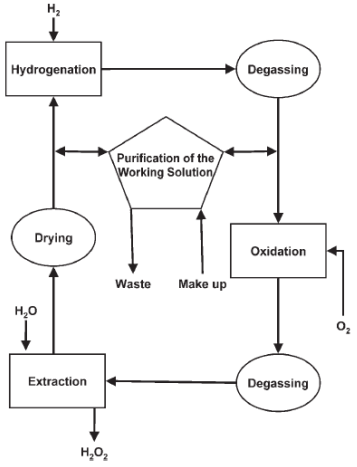


Figure 6.1 Block diagram of steps involved in the anthraquinone method[150]

The other drawbacks of this process includes: large consumption of organic solvent, extra procedures for high concentration solution; and transport, storage, and handling hazard of bulk hydrogen peroxide solution. Due to these drawbacks, the idea of onsite production of hydrogen peroxide has been proposed by many scientist and companies in recent years, and several different production methods have been explored to demonstrate a cleaner, smaller and safer $H_2O_2$ production approach. J. Zhou et al. show that $H_2O_2$ can be synthesized with high selectivity and productivity via the gas phase reaction of $H_2/O_2$ non-equilibrium plasma.[161,162] Although high selectivity has been achieved by this method and it is a green process, the experiment shows huge electric energy consumption, 80 kWh/kg $H_2O_2$. Supercritical $CO_2$ has also been proposed to replace aqueous or organic solvent to be a more efficient and greener reaction medium, but the $H_2O_2$ decomposition rate above 31.1$^oC$ is also been found to be too rapid for continuous production.[163,164] Among all the new proposed production methods, the most studied one is direct synthesis $H_2O_2$ in aqueous medium. [165,166] This is the most convenient way to make hydrogen peroxide solution and industry has been sponsoring efforts in R&D for this method for several decades. However, absolute safety has been found hard to achieve with enough production rate and selectivity due to the wide flammability limits for $H_2/O_2$ mixtures. A promising way to achieve safe operation is by using a membrane catalyst. The catalyst membrane is designed to feed hydrogen from inside the membrane towards the external part where oxygen saturated solution comes in contact with the catalyst.[167] Although the use of a membrane catalyst avoids the formation of explosive mixtures, the rate of $H_2/O_2$ formation, which is controlled by mass transport, is too low for industrial applications.

Summarizing the above elements for the best small scale onsite production method: (1) directly produce $H_2O_2$ in aqueous solution, (2) no direct contact for $H_2$ and $O_2$, (3) fast mass transport in the reaction medium with room temperature operation. A membrane hydrogen fuel cell seems a great fit for this onsite production idea.[148,168–175] The difference between the membrane fuel cell method and membrane catalyst method is that fuel cells have ions transfer though the membrane to finish the reaction and releasing electric energy while the catalyst membrane direct synthesis method needs the $H_2$ transfer though the membrane to finish the reaction. The nature of the electrochemical reaction means the ions transfer in fuel cell is under potential difference. And from the basic transport mechanism in membrane, gas transport through membrane is much slower than ions transport through membrane. Gas permeability is determined by the ability of the component to dissolve in and diffuse through the membrane material, and the rate is drived by the pressure difference between two sides of the film. For ion exchange membranes used in fuel cell, the ions are driven by not only concentration difference but also by potential difference. To our knowledge, the rate for ion transfer in this aspect is much faster than the hydrogen gas transfer, and thus, the electrochemical method for hydrogen peroxide production may be a more efficient way than the normal direct synthesis method and auxiliary power production can also further reduce the cost or help the plant to be more energy independent.

Apart from these advantages, electrochemical method of producing hydrogen peroxide is also the only method that can produce hydrogen peroxide without hydrogen supply. Electrochemical hydrogen peroxide production can run in two modes: electrolytic mode and fuel cell mode. For the fuel cell mode, oxygen (air) and hydrogen are input with products of electricity and hydrogen peroxide. The electrolytic mode input oxygen (air),

electricity and water (or alkaline) to produce hydrogen peroxide. The reactions for fuel cell mode and electrolytic mode in alkaline environment are as followed:

Electrolytic mode:

$$\text{Anode:} \quad 4OH^- \rightarrow 4e^- + 2H_2O + O_2$$

$$\text{Cathode:} \quad O_2 + 2H_2O + 2e^- \rightarrow 2OH^- + H_2O_2$$

Fuel cell mode:

$$\text{Anode:} \quad H_2 + 2OH^- \rightarrow 2H_2O + 2e^-$$

$$\text{Cathode:} \quad O_2 + 2H_2O + 2e^- \rightarrow 2OH^- + H_2O_2$$

An illustration figure of a peroxide producing cell operated under electrolytic mode is shown in Fig 6.2.

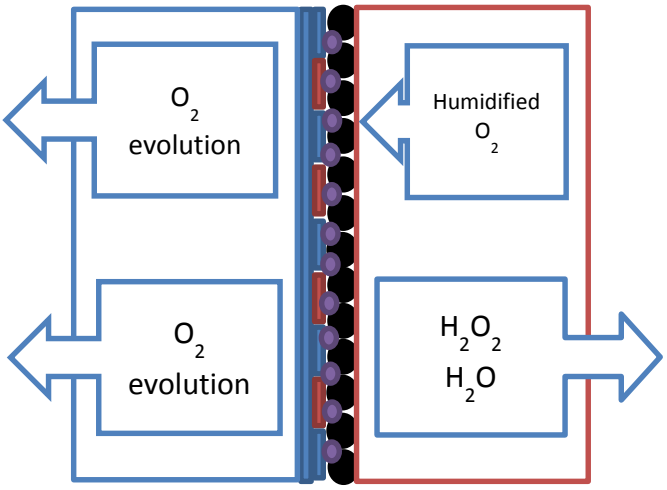


Figure 6.2 Illustration graph of electrolytic mode producing hydrogen peroxide

For small-scale onsite production in remote places, producing hydrogen peroxide without requiring hydrogen is very attractive. It makes hydrogen peroxide use in remote sites much easier. For certain industries, which need an auxiliary power supply, the fuel cell mode may be more attractive. The tradeoff between two modes also relies on the availability of hydrogen, and the price of hydrogen.

The next question is why our catalyst is suitable for this application. According to the previous conclusion, the main property of this catalyst is the reversible ORR and OER reaction that can greatly benefit the air battery technology. On the other hand, for the single direction reaction, the catalytic activity for both ORR and OER is also very attractive. We will primarily discuss the ORR direction here. As we discussed before, the reaction product from two-electron oxygen reduction is peroxide. Based on the electrolyte environment, the direct product will be hydrogen peroxide in acid condition and hydroperoxide ions in alkaline condition. Since we show that this catalyst is a pure two electron oxygen reduction catalyst, it surely can be used to produce peroxide in an electrochemical cell.

The next step is to see whether this catalyst is suitable for this application by comparing with conventional catalyst. Two electron ORR catalyst has not been widely studied compared with the four-electron ORR catalyst, fuel cell catalyst. Most commonly used two electron ORR catalyst includes carbon, gold, mercury, oxide covered metal and most transition metal oxide.[58] The search for nonprecious metal catalyst for fuel cell application also provides many near two electron ORR catalysts. However, a very high efficiency, selective 2 electron ORR has not been found yet. [176–180] The requirements for a good 2 electron ORR catalyst are: high kinetic performance (high onset potential, high reaction

rate) and high selectivity. However, for all existing two electron ORR catalyst, the catalytic performance is either high kinetic performance with low selectivity or high selectivity with low kinetic performance. The reason for this is that the peroxide reduction catalytic mechanism is very similar to the oxygen reduction catalytic mechanism. It is very hard to find a catalyst which can have very good oxygen chemisorption but no peroxide chemisorption at all. Considering the cost, most research and industry work used carbon as a peroxide producing catalyst.[148,168,169,181–190] Carbon has good catalytic selectivity but relatively large energy consumption. The major commercial trial from Dow Chemical and H-D tech use particulate carbon beds for peroxide production.[182] The operating voltage for electrolytic mode producing peroxide is estimated to be over 2.2V, which turns out to be too high for carbon material. Also a better catalyst is needed to make this process economically viable. Several efforts have been made to improve the carbon catalyst by surface modification.

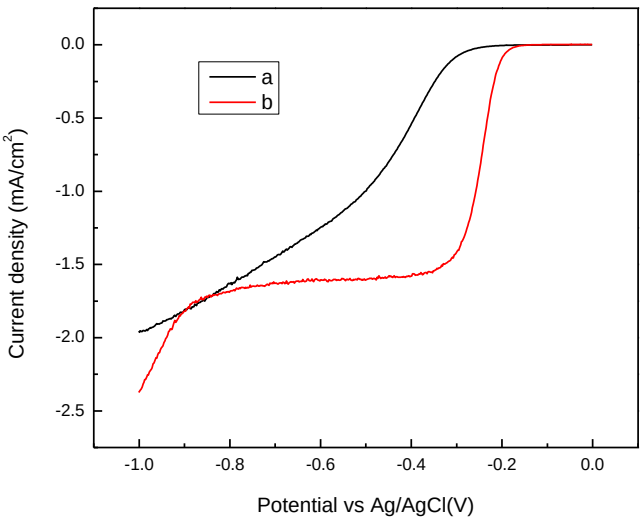


Figure 6.3 Polarization curves comparison of (a. XC-72 vulcan carbon b. cobalt salen modified poly Au) in 1 M KOH electrolyte saturated with oxygen. Scan rate: 50mV/s, 1000 rpm

## 6. 2 Aqueous flowing air cathode structure

### 6.2.1 Flowing electrolyte air cathode structure for Li-air battery

As discussed in the introduction chapter, the use of an aprotic air electrode for lithium air battery has many challenging problems, including discharge product clogging, irreversible side reactions and easy contamination from ambient operation. Due to the fact that no good solution has been found to have the potential to solve the above challenges, we generally consider the aprotic lithium air battery is not a realistic battery system in the near future. However, for the aqueous or mixed electrolyte lithium air battery, having an aqueous air electrode couple with a lithium metal anode also creates some new challenges for the rechargeable battery. In this section, we will discuss a new aqueous air electrode structure which is specifically designed for aqueous lithium air battery and can potentially solve several challenges for this system.

For the aqueous rechargeable air battery, a great deal of research has been done on the regenerative fuel cell and zinc air battery. Many features from the air electrode design of these two electrochemical systems can be borrowed to benefit the lithium air battery structure. Several differences caused by lithium metal electrode, however, make it a complex situation to transform these designs from fuel cells or conventional air battery. One of the most obvious differences is the discharge product for aqueous lithium air battery is LiOH (basic electrolyte) or lithium salt (acid electrolyte). This is a big difference and can greatly influence how to preserve the reaction product in an air cathode. For a regenerative fuel cell, the discharge product is water, and water is usually preserved in liquid form. Water management is a critical issue for discharge performance in fuel cell.

For convenient consideration, water is usually preserved within the cell; and for better performance consideration, water can be transferred out of the cell easily. For a zinc air battery, the discharge product is called zincate, which is a solid complex formed by zinc oxide and alkaline. This situation is more like aprotic lithium air battery discussed previously. For the classic three phase zone concept for aqueous air electrode, production of solid near the air electrode is very undesirable. The potential clogging problem can not only disfunctionize the air electrode, but also harm the air electrode structural stability. One good solution can be derived from how zinc air battery solves similar problems. The zinc air battery system solves the clogging problem by using alkaline membrane as a separator and preserving the zincate along with the porous zinc electrode. In this case, the discharge product is preserved on the surface of the porous zinc metal surface and replaces the zinc metal electrode. Within reasonable discharge rate, the discharge product can be preserved compactly. For the case of an aqueous lithium air battery, the situation is completely new, because the discharge product is soluble, but the solubility varies substantially with different electrolyte systems and is usually very small. Since the reaction product is dissolved in the electrolyte, this gives us two choices to store them. One is just let them dissolve in the electrolyte, the other is let them precipitate out on purpose so that we can store them in a solid compact way. If we want to store the product in the electrolyte, the solubility of the reaction product becomes crucially important for specific energy density and volumetric energy density. J.P.Zheng and his colleague did a detail calculation of real energy density with different kinds of electrolyte, as shown below. [191](Table A.1.1) From this table, we can conclude that the theoretical specific energy density drops due to the low solubility of lithium salt in the water.  This conflicts with the goal of building a

high energy density battery system. It also demands a lot of space within the cell to contain the reaction product. For the other method, the precipitated product actually has exactly the same problem as an aprotic electrolyte air electrode does. Since the lithium metal electrode must use solid electrolyte in the middle to form the water barrier, there is no possibility to preserve the product in the anode side as in a zinc air battery. Therefore, this method is generally considered not realistic. For solving the dilemma about preserving the product for an aqueous lithium air battery, we borrow the concept of circulating electrolyte from redox flow battery systems and propose a new flowing electrolyte air electrode structure specially for aqueous lithium air system, as shown in Fig 6.4.

Table 6.1 Summery of specific capacities and energy densities for aqueous Li-air batteries using different electrolytes[176]

**Table II. Summary of specific capacities and energy densities for Li-air batteries using different electrolytes, and weight ratios of active materials in batteries.**

| Salt in electrolyte | Minimum amount $H_2O$ for 1 mol of product (mol) | Additional $H_2O$ for 1 mol of product (mol) | Specific capacity (mAh/g) | Energy density at OCV = 3.69 V (Wh/kg) | Mass ratio (Li/Salt/Water) |
|---|---|---|---|---|---|
| Diluted LiOH | 11.14 | 11.14 | 129.19 | 476.70 | 3.35/0/96.65 |
| Acetic acid ($CH_3COOH$) | 8.15 | 7.65 | 130.97 | 483.28 | 3.39/29.35/67.26 |
| Chloric Acid ($HClO_3$) | 1.09 | 0.59 | 262.51 | 968.68 | 6.80/82.73/10.47 |
| Perchloric acid ($HClO_4$) | 10.07 | 9.57 | 95.83 | 353.63 | 2.48/35.92/61.60 |
| Formic acid (HCOOH) | 7.35 | 6.85 | 152.10 | 561.24 | 3.94/26.12/69.94 |
| Nitric acid ($HNO_3$) | 3.76 | 3.26 | 208.49 | 769.33 | 5.40/49.02/45.58 |
| Salicylic acid ($C_6H_4(OH)COOH$) | 6.00 | 5.50 | 109.78 | 405.10 | 2.84/56.58/40.58 |
| Sulfuric acid ($H_2SO_4$) | 17.86 | 17.36 | 72.73 | 268.37 | 1.88/13.31/84.81 |
| Hydrobromic acid (HBr) | 2.67 | 2.17 | 211.31 | 779.74 | 5.47/63.79/30.74 |
| Hydrochloric acid (HCl) | 2.79 | 2.29 | 316.88 | 1169.29 | 8.20/43.11/48.69 |
| Thiocyanic acid (HSCN) | 3.01 | 2.51 | 240.97 | 889.19 | 6.24/53.13/40.63 |

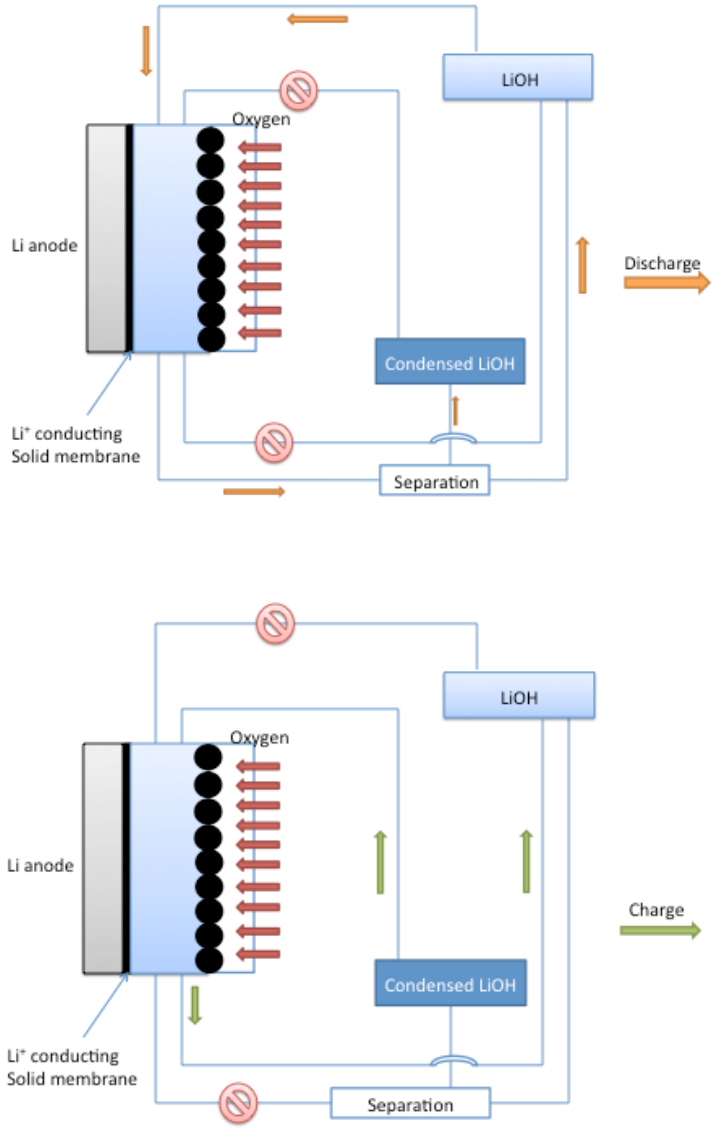


Figure 6.4 A brief illustration of flowing electrolyte air cathode structure and product separation

Figure 6.4 is a brief illustration of how a flowing electrolyte goes through a cell and how the discharge product is preserved in this situation. In the discharge process, a LiOH solution is pumped into the cell and acts as electrolyte and also takes the newly produced LiOH with it. Then the electrolyte goes through a separation process and separates the

excess solid LiOH in the solution. The excess LiOH is supposed to be preserved in a solid or slurry phase. When recharging, the concentrated LiOH is dissolved back into the solution phase and circulated back to the cell. There are two concepts for storing the reaction product. One is store the reaction product outside the cell rather than inside the cell; the air cathode is only a site for reaction. The other concept is to not only store the reaction product outside the cell, but also let the product go through a separation process to be stored in a concentrated compact way to increase the specific energy density. The general concept here is use redox flow battery concept and separate energy density with power density, and also separate the solid phase discharge product storage with air electrode performance. However, for fulfilling these concepts, several technical details need to be discussed. First, we need to develop a method of flowing the electrolyte though the air electrode; and this method should not jeopardize the three phase zone of the catalyst layer but still retain the function of providing transport pathway for the metal ions and dissolving the reaction product. (Figure 6.5)

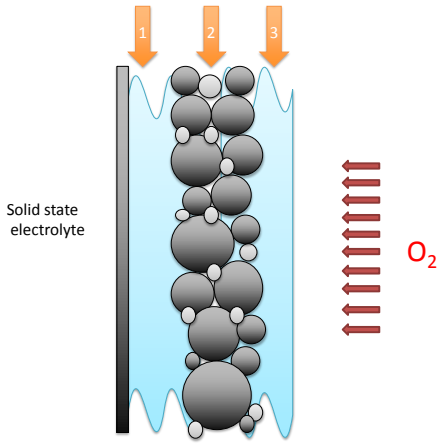


Figure 6.5 Three different possibilities of flowing electrolyte around catalyst layer

We want to discuss the flowing electrolyte possibility from the basics. There are three different situations for flowing electrolyte, as shown in the graph above. The first place is between solid electrolyte and catalyst layer, the second kind is just having electrolyte flowing through the catalyst layer, and the third is having electrolyte flowing between GDL and catalyst layer. Figure 6.6 shows a picture of three different situations.

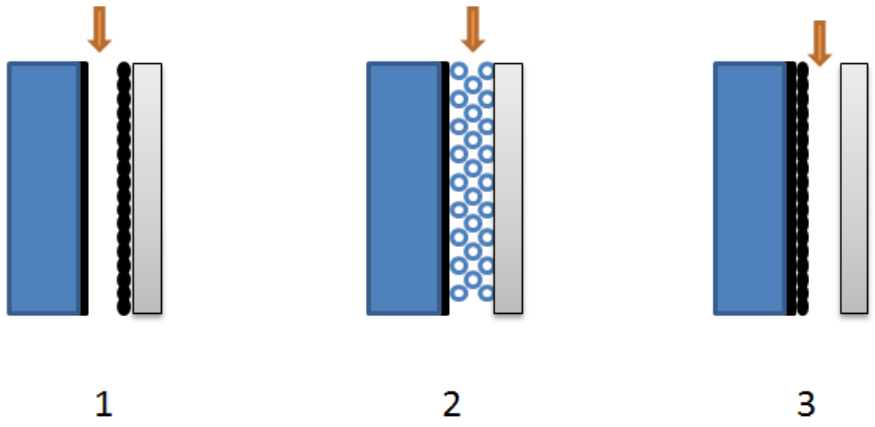


Figure 6.6 Three situation of flowing electrolyte with overall cell structure

The first flowing electrolyte case is the most commonly used structure, used in some systems like alkaline fuel cell and regenerative fuel cell.[57,192–195] However, in this new system, the liquid flowing electrolyte is not the only electrolyte in the middle, the flowing electrolyte in the middle will increase the resistance greatly while the solid electrolyte's high ionic resistance is already a big challenge. The flowing electrolyte in this case must be in microfluidic scale. The second choice is the most ideal situation if can be achieved in reality, it can provide the perfect tri-phase zone without extra resistance for ions and oxygen transfer. The intentional flowing of liquid electrolyte though the catalyst layer will

be very hard to manage. Because the speed of the movement across the porous layer depends on the surface properties of the catalyst layer, it needs very detailed calculation and fine manufacture of catalyst. The third choice is flowing electrolyte between GDL and catalyst layer, this method will not increase the resistance for ion transport and still can take away the reaction product rapidly. The problem here is we do not want the electrolyte to block the transport of oxygen. We need the flow of the electrolyte be a very thin and in non-laminar flow state. The flow also needs very precise calculation to control the surface property and the flow field. The other draw back about this method is that it has a risk of not being able to take away the product efficiently. Summarizing all the discussion above, we think the most realistic structure for aqueous lithium air battery should be the first graph in Fig 6.6. For better understanding of how to apply this flowing electrolyte structure, a detailed whole cell structure of mixed electrolyte lithium air battery using the first flowing electrolyte structure for the alkaline electrolyte situation is shown in the following graph. (Figure 6.7)

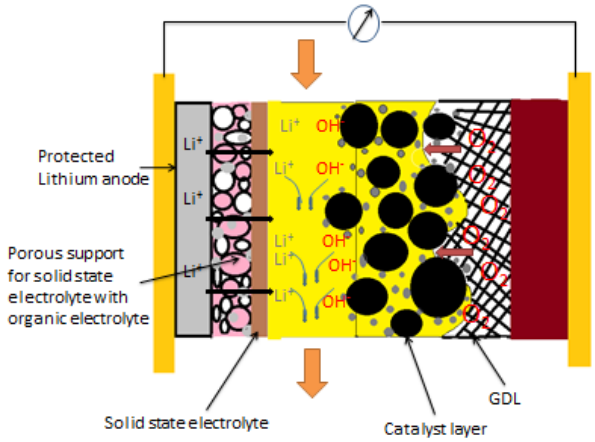


Figure 6.7 A detailed graph about how an aqueous lithium air battery works with a flowing air cathode structure.

As shown in the structure above, on the anode side, lithium metal becomes Li ions and travel through the organic electrolyte in the porous structure which is about 200 μm thick, in the middle, 3~5 μm thick solid state electrolyte is deposited on the porous structure; on the cathode side, oxygen is reduced to the hydroxide in alkaline environment, then diffuse to the flowing electrolyte, neutralized with lithium ion from anode side and lithium hydroxide exits the cell as a product.

Another important technical detail for using flowing electrolytes is how to separate the product from liquid phase and keep it compact as solid phase. This problem is a critical problem for all kinds of high energy density flow batteries. This is also related to what battery chemistry is used because the battery chemistry determines what the discharge product will be. The separation process is different for different materials. Since we previously discussed the benefits of using two electron reversible redox couples for aqueous air battery chemistry, we will discuss the separation process related to lithium peroxide in aqueous solution.

Unlike the peroxide compounds of sodium, potassium and cesium which form $M_2O_2$ and $M_2O_4$ or $MO_2$, respectively, lithium peroxide only forms the single peroxide compound of $Li_2O_2$.[196] It can form differently hydrated compounds. High purity lithium peroxide is not commercial available, mostly because the manufacturing process is too expensive. This can give us a general impression that the separation process of lithium peroxide is not easy. Based on the several patents related to lithium peroxide production, the normal extraction strategies all indicate that the best extraction is by solubility difference between aqueous and organic solutions.[197,198] One major problem of the extraction process is that some

impurities can be separated out together with the desired preserved chemical. An extra procedure may be needed to remove these impurities, because impurities from the extraction procedure will be harmful to the original battery system. However, the more complicated procedure of the separation process, the more irreversible the storage process will be. This will jeopardize the recharging of the battery. No simple and effective separation process has been found fitted to couple with this special battery chemistry. On the other hand, for a high performance battery system in which the operation rate can vary substantially, the rate of the separation process is very difficult to match up with the rate of the battery operation. This is a general challenge for developing high energy density redox flow batteries.

Thus, in this section, a possible flowing electrolyte air cathode structure for aqueous lithium air battery is discussed, which can potentially benefit power density, energy density and structure stability. The flowing electrolyte structure is considered to be realistic, but no proper discharge product separation and storage method has been found to fully apply the concept.

### 6.2.2 Flowing electrolyte management

The flowing electrolyte structure increases the system complexity relative to the static system because it needs extra material and pumps. However, on the other hand, it can also provide flexibility in several aspects. Here, we summarize several aspects that flowing electrolyte can contribute to the system, for a general concept of flowing electrolyte management.

1. Thermal control

Flowing electrolyte allows the electrolyte to carry heat from outside into the middle part of the cell or release the extra heat effectively from cell. This can decrease the temperature gradient within the cell effectively and simplify the cell thermal management. Not only can flowing electrolyte replace coolant, but in special situation, like freezing point start-up, external heat can easily reach the middle of the cell and effectively ‘wake up’ the cell from frozen state.

2. Energy density control

As described before, using the reaction product precipitation and storage method, we can have more flexibility on how to preserve the reaction product in the most compact way. This will greatly increase both the gravimetric and volumetric energy density because of less water needed in the system.

3. Conductivity control

For the same kind of electrolyte, the conductivity depends on the concentration and temperature. The conductivity of electrolyte usually increases first and then decreases with the increase of electrolyte concentration. When discharging, the electrolyte concentration within the cell is increased by the dissolved reaction product all the time. When charging, we can avoid the conductivity loss when the electrolyte is fully saturated. With the aid of reaction precipitation and storage system as mentioned earlier, we can manage the concentration of electrolyte which goes into cell. Thus, we can also manage the conductivity within the cell always at the highest level.

4. Contaminant control

The main contaminant from the air for the liquid alkaline electrolyte lithium air battery is carbon dioxide. This is the same with liquid alkaline fuel cell. The method used by the commercialized liquid alkaline fuel cell is just the method of flowing electrolyte. A carbon dioxide scrubber can easily eliminate 80%~90% of carbon dioxide from the air, but 100% block is impossible, you have to accept some carbon dioxide will get into the cell and decrease the conductivity to some level. Using flowing electrolyte provides a choice of changing the electrolyte once in a while. In an automobile application, requesting that the customer change electrolyte every half a year is very reasonable.

5. Reaction control

We all know that the half reaction at each electrode in an electrochemical system is determined by catalyst, reactant and electrolyte. In a static system, the reaction is almost fixed because nothing should be significantly changed for a well-designed cell. However, with a flowing electrolyte structure, you can actually gain the possibility of controlling the reaction as you need by changing the electrolyte. For example, in an aqueous air battery system, we can reduce the amount of water needed to dissolve the reaction product. This is a premium energy density reduction plan based on the reaction product precipitation and storage plan. The details are illustrated as in figure 6.8.

The ORR reaction in aqueous electrolyte has two types of half reaction. One is in acid electrolyte, the other is in alkaline electrolyte. When discharging, in acid environment, oxygen reacts with proton and electron to produce water, the pH value increases to 7 with discharging. In alkaline environment, oxygen reacts with water and electron to produce

hydroxyl. The pH value increases and water is consumed. When charging, everything is reversed. In this situation, if we start with cycling acid electrolyte, we will first consume acid and produce water. Then, in the electrolyte tank outside the cell, we can store the water and lithium salt in separate tank. When the pH value increases to the desired point, we now combine the water and alkaline together to start flowing alkaline electrolyte in the cell. This time, we are consuming water and increasing the pH. When charging, everything is reversed. In general, the pH value increases when discharging and decrease when charging. A cycle is complete here, and water has first been generated and then been consumed in the cell. Higher energy density will be achieved with less water inside. A brief illustration graph is shown in Fig 6.8.

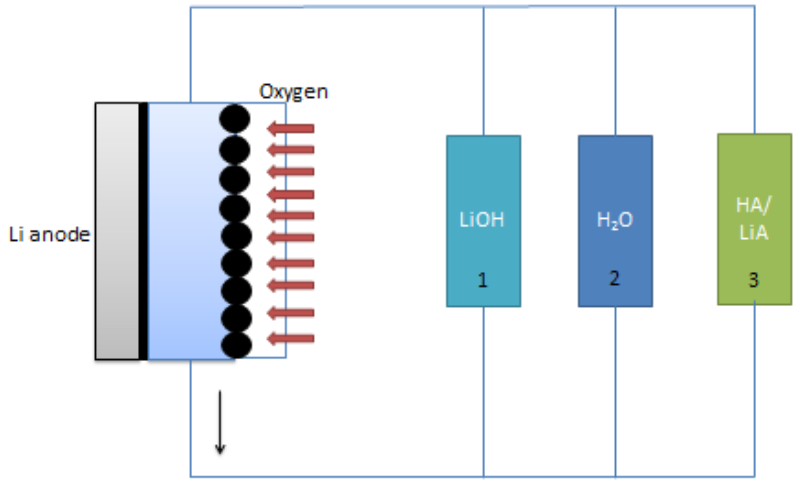


Figure 6.8 A brief illustration about how to use reaction control to decrease the energy density of lithium air battery

When discharging, tank 3 with HA acid initially circulates within the cell,;after reaction with oxygen, the remaining electrolyte goes through a separation process and water goes into tank 2 and salt LiA goes into tank 3. When the pH in tank 3 reach near 7, circulating tank 1 and tank 2 starts and change the reaction, after react with oxygen, condensed LiOH solution is generated and goes through a separation process, water is stored within tank 2 and LiOH is stored within tank 1.

Flowing electrolyte can also be used for the purpose of maintaining the stability of the catalyst. Changing reaction environments can be used to redeposit catalyst to the catalyst layer. Or, for the modified catalyst case, changing electrolyte environment can be used to conduct the modification to the catalyst layer again for long term stability.

## 6.3 Hydrogen peroxide preserving zinc air battery

As described in the first application, when coupled with an anion exchange membrane, we are able to produce hydrogen peroxide water solution. And from the discussion of the aqueous lithium air electrode structure, we also propose an out of cell discharge product separation and storage strategy. Here, we want to combine these two concepts together and propose a hydrogen peroxide storage rechargeable air battery structure.

From the physical property perspective, hydrogen peroxide solution is a very interesting product to preserve. In aqueous solutions, hydrogen peroxide is different from pure material, because of the hydrogen bonding between water and hydrogen peroxide molecules. Hydrogen peroxide and water forms a eutectic system. Both pure water and pure hydrogen peroxide melt and freeze at around 273K, but a 50% solution melts and

freezes at 221K. This actually provides a possibility of building a non-freezing aqueous flow battery system. On the other aspect, hydrogen peroxide and water are miscible together. This means hydrogen peroxide solution can also be preserved in high concentration, which is exactly what is needed for building a high energy density redox flow battery. Therefore, compared with the idea of preserve lithium peroxide, preserve hydrogen peroxide seems a much more realistic plan.

For building a device producing hydrogen peroxide solution, a special design also needs to be applied. The flowing electrolyte structure is not appropriate here because the electrolyte is either strong acid or alkaline that is not in the right pH range to preserve hydrogen peroxide. Thus, membrane technology is the best possibility to solve this problem. A membrane electrolyte can provide good ionic transport while it does not greatly influence production solution. For example, PEM fuel cell uses proton exchange membrane, but PEM fuel cell produces water as byproduct. Therefore, we can use AEM to provide alkaline reaction environment and expect an AEM based air electrode to produce hydrogen peroxide solution, which corresponds with previous hydrogen peroxide production discussion. The tradeoff of using membrane electrolyte structure producing hydrogen peroxide is that there is no easy pathway for the hydrogen peroxide solution to come out, which is very similar to the discussion related with Fig 6.5. The ideal way to transfer the product out of the cell is very similar with the second situation in Fig 6.6. A possible method here is that we can use water vapor to easily supply liquid electrolyte into the cell and collect peroxide at the same time. This is very different from the discussion in the last section, which LiOH solution is not realistic to pump through the catalyst layer. As far as

we understand, water vapor input seems to be the only possible way to realize the second flowing through situation in Fig 6.6.

On the other hand, for battery technology, we not only need to preserve the hydrogen peroxide, we also need to preserve the negative electrode material. For regenerative fuel cell, you can collect the hydrogen when the reaction is reversed. But collecting gradually generated hydrogen and put them back into a high-pressure hydrogen container is very difficult and is not realistic for portable device. Therefore, we need to seek other anode structure to match this hydrogen peroxide preserving air electrode.

A possible right anode structure is zinc anode. The conventional zinc air battery preserve the solid product zincate in the alkaline electrolyte. Some groups use alkaline membrane to separate the zincate storage with air cathode operation, which greatly improve the air electrode performance.[199] Similar idea can also been applied here. Together with previous discussion, hydrogen peroxide solution can be produced with the use of alkaline membrane in the air cathode. In this case, the combination of zinc anode, alkaline membrane and peroxide producing air electrode can actually become an attracting rechargeable battery system, as shown in Fig 6.9.

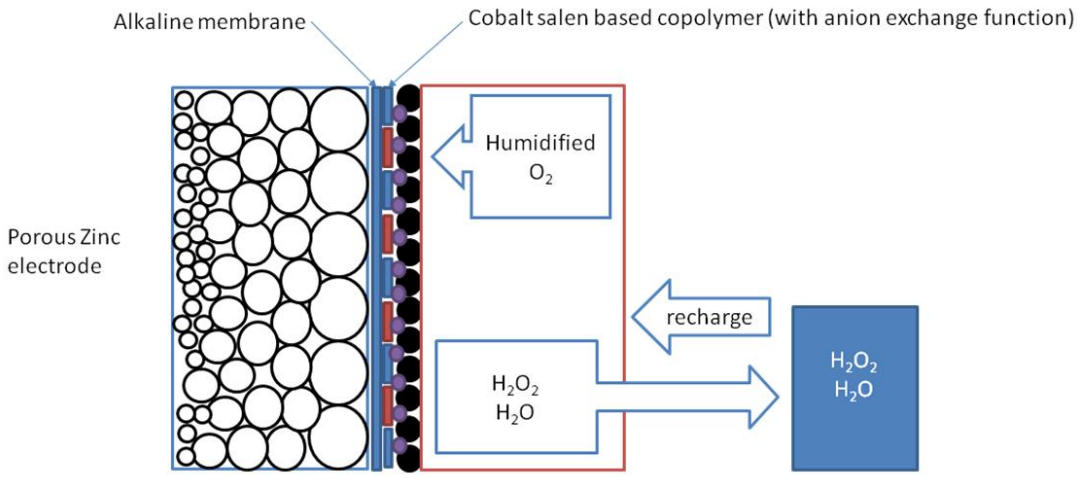


Figure 6.9 An illustration of zinc-air $H_2O_2$ preserving battery system

In this case, the battery chemistry is:

$$Zn + 4OH^- \rightarrow Zn(OH)_4^{2-} + 2e^-$$

$$O^2 + 2H_2O + 2e^- \rightarrow H_2O_2 + 2OH^-$$

In this system, the energy density depends on the preserved hydrogen peroxide concentration. For the convenience of calculation, we temporary assume that the concentration is 50%. In this case, the gravimetric energy capacity is:

$$C = \frac{F}{M_{Cu} + 2MH_2O + 1.88MH_2O} = \frac{96485\ C/mol\ \times 2}{65g/mol + 3.88 \times 18g/mol} = 1430\ C/g$$

From the normal operation experience of zinc air battery, the operation voltage is around 1V. Therefore, the gravimetric energy density of the proposed battery system is: 397

Wh/Kg. This is not a very attractive number compare to the energy density of lithium air battery, is a roughly around a normal zinc air battery energy density level. However, considering a huge improvement on system efficiency by adopting this new chemistry, this is still an interesting system to look into.

# Chapter 7

# Summary and Future directions

## 7.1 Summary

The combination of Au and cobalt salen has been found to be an innovative bifunctional air electrode catalyst, with the catalytic activity of two electron reversible ORR. Peroxide self-decomposition has been found as a follow up reaction after the electrochemical process. EDTA, as peroxide stabilizer, can greatly restrain this process when used as additive in electrolyte environment. The ORR reversible nature of this catalyst is explained by the theory of Au surface reconstruction induced by cobalt salen physisorption. The ORR kinetic improvement after the modification is explained by surface double layer theory with two different reaction mechanisms. The first reaction mechanism is cobalt salen promote oxygen chemisorption by first depolarize oxygen before ORR. The other theory is gold background increase the cobalt electron density, making cobalt a perfect ORR catalytic center. The catalyst reversibility is found to be greatly influenced by temperature and pH. High temperature can enhance the peroxide reduction activity and thus decrease the ORR reversibility. Low pH is found to be bad for peroxide oxidation when below 13. Electropolymerization is proved to be a reliable method to stabilize the catalyst composition without jeopardizing any catalytic activity. The modified catalyst based on Au nano particles is found to be less reversible duo the higher peroxide reduction activity on nano Au particles.

Cation influence to ORR is also been discussed using surface double layer theory. Our experiment results indicate that cation will not influence electrochemical surface area, but Li ions will greatly suppress the formation of $OH_{ad}^-$ and irreversible adsorption of oxygen-containing species by non-covalent interaction. RDE experiments show that both cation and alkaline concentration will greatly influence the oxygen solubility and diffusivity, and 0.1M alkaline solution shows lower onsite ORR potential than other high concentration alkaline solutions. The non-covalent interaction between cation and chemisorbed oxygen containing species is proved to have great influence to the ORR kinetic by Tafel plot comparison. The better Tafel plot of LiOH solution is explained with more available sites due to the weaker non-covalent interaction.

Three different electrochemical application using this new catalyst have been proposed. When using it as two electron ORR catalyst, a very energy efficient electrochemical peroxide producing process can be achieved. Depending on imputing electricity or hydrogen, either fuel cell mode or electrolytic mode can be used for this process. For using the catalyst as bifunctional air electrode catalyst, two different battery structures are proposed with the difference of using zinc anode or lithium anode. A flowing electrolyte air electrode structure is suggested to be used for lithium air battery application, but a perfect lithium peroxide storage method is not found to achieve the overall idea. Using similar concept, a zinc air battery structure is also proposed, hydrogen peroxide solution is suggested to be an ideal discharge product to be preserved out of cell. The feature of producing hydrogen peroxide solution and isolating zincate from anode department can be achieved by using alkaline membrane. The proposed zinc air peroxide preserving system is suggested as a high energy density, high system efficiency and high recharge speed

system, however, multiple challenges including developing anion exchange membrane and preserving high concentration peroxide solution needs to be overcome.

In conclusion, a new battery chemistry based on a new catalyst is explored in this work. The catalyst shows very good two electron reversible catalytic activity in low temperature and high pH alkaline electrolyte. A reaction mechanism model has been proposed to explain the catalyst activity. The influence of cobalt salen and cation has been discussed in the conventional surface double layer structure theory. Several important aspects for applying the catalyst into electrochemical system catalyst layer has been discussed including, catalyst stabilization, nano size effect and peroxide stabilization. Three electrochemical systems have been proposed to apply the new catalyst into both peroxide production and rechargeable batteries.

## 7.2 Summary for two electron reversible ORR reaction mechanism experimental evidence

In the previous section, we have shown that this catalyst can proceed a two electron reversible ORR in alkaline solutions. And we used many different analytic electrochemical methods to characterize the performance of the catalyst. The performance of the catalyst we are proposing is significant in the aspect of improving the performance of air battery. Several papers recently in nonaqueous air battery field have just been proved that the performance of the battery they characterize is not a result of battery chemistry they are claiming but side reaction within the cell. Therefore, we are very careful with what we are claiming and tried to have very strong evidence to prove that what we measured is purely about two-electron reversible oxygen reduction. One common drawback about analytic

electrochemistry is that it's very easy to tell how much and how good the reaction happened from the measurement but very hard to tell what is exactly happening. Strong argument in analytic electrochemistry needs very precise experiment design. Here, we give a summary of all the evidence about the reaction mechanism from previous sections. And we think these evidences together can prove that this is a pure two electron reversible ORR process.

1. It is a peroxide producing process in the cathodic scan direction

   The reaction mechanism can be divided into two parts, and the first part should be oxygen reduction producing peroxide. The most direct proof is from the RRDE experiment, the RRDE experiment proves that in around 600mV potential range, oxygen reduction follows two electron reduction mechanism. Although the RRDE experiment (Fig 3.20 A) is in the cobalt salen contained alkaline solution, the cobalt salen shouldn't contribute any to the reduction current. First, the first element in the cobalt salen is cobalt, and the valance of cobalt is $Co^{2+}$ in the compound is only active for been oxidized but not for been reduced. Second, the reduction current used in the calculation is background subtracted. That means the reduction current is only correspond with oxygen reduction.

   We also can prove this same result by proving there is peroxide in the solution after the oxygen reduction. A side evidence is that the electrochemical-chemical mechanism we obtained can explain very well with the theory of peroxide self-decomposation in the alkaline solution. The chemical process of peroxide decompose can explain very well the less current in the anodic scan. The other strong evidence is the influence of peroxide stabilizer. The addition of peroxide stabilizer makes the oxidation peak current as large as reduction peak current. This

directly indicates that oxygen reduction is producing peroxide and the stabilizer is very effective in preserve peroxide.

2. It is peroxide oxidizing process in the anodic scan direction

   The first direct experimental proof is from the "sample and hold" experiment. In the two cycles CV, when the potential holds at 0.2V in the first scan, the electrochemical process correlated should be producing oxygen and accumulate oxygen in the electrode surface. The second cycle following this potential hold proves this theory with a larger reduction peak current. If we are sure about the peroxide producing process in the cathodic scan direction, we can also sure with the peroxide oxidation process because more oxygen is been producing in the potential hold. The other evidence comes from the experiments with peroxide in the electrolyte. Put peroxide in the electrolyte can directly test the catalytic activity of peroxide oxidation. If the anodic reaction is not related with peroxide, then put several milimole peroxide in solution should not have any influence on the reaction. However, experiment result with 5mM peroxide solution in the alkaline has much higher oxidation and reduction current, this proves that peroxide oxidation is what happened in the anodic scan.

3. The redox potential of $Co^{2+}$/ $Co^{3+}$ does not shift positive in the presence of $O_2$

   The redox potential of $Co^{2+}$/ $Co^{3+}$ is around 400mV negative to $O_2$/ $O_2^{2-}$ potential, will it be any chance the redox couple we measured is actually because the $Co^{2+}$/ $Co^{3+}$ redox potential shift positively? The answer is no. The most direct evidence is from Fig 3.13, when the $O_2$/ $O_2^{2-}$ redox couple appears in the CV, the $Co^{2+}$/ $Co^{3+}$ redox couple appears at the same time and does not change their potential. Another

direct reason is the cobalt salen solution concentration influence to the catalytic activity. If the redox peaks we observed is because of the $Co^{2+}$/ $Co^{3+}$, the peak current density must be proportional to the cobalt salen concentration. However, the ORR redox peaks is not changed with cobalt salen concentration. Thus, the $Co^{2+}$/ $Co^{3+}$ does not shift positively to the ORR potential and don't have direct influence to the ORR activity.

4. The anodic peak is not because of Au surface reconstruction

   The potential range where peroxide oxidation happens is also possible for Au surface reconstruction to happen. However, the time scale for Au surface reconstruction to happen is much slower than a reversible redox process to happen. It's impossible for a surface reconstruction accelerate the process along with the increase of scan rate as a redox couple do. Therefore, surface reconstruction is not a part of the process we measured.

## 7.3 Future directions

The future direction of this work can be divided into scientific part and application part. For the scientific part, more effort needs to be put into further verification on the reaction mechanism proposed and deeper understanding about how to tune the catalyst activity by having desired molecule in the surface double layer structure. The first related and important experiment for the mechanism verification should be direct surface characterization to Au surface reconstruction. This is the base of the proposed mechanism. Although we proved that the cobalt salen induced Au surface reconstruction is a very reasonable interpretation, a direct experimental proof of this surface reconstruction is still

imperative. AFM or STM is preferred technics for this measurement, and special prepared single crystal Au electrode can also help verifying the theory if available. For better understanding the surface modification effect, the easiest approach is to use AFM to conduct a surface imagine of a cobalt salen electropolymerized Au surface. This can give us an instant insight on how cobalt salen is organized on the Au surface. For the influence of cobalt salen modification to the peroxide oxidation catalytic property, DFT calculation is needed for the proposed peroxide reversible bonding with cobalt salen. The cation influence research needs further experiment on other nano noble metal catalyst. Different metal surface has different oxygen related species coverage, this can give us more evidence to understand the influence of cation to ORR reaction available catalyst surface area.

On the application side, more efforts need to be put into developing a preparation method to transfer the desired catalytic property into electrochemical systems. Although electropolymerization method has been proved to be a good method to stabilize the catalyst composition, how to apply this method to the catalyst layer with nano Au particles is a challenge. The nature of how modified catalyst works varies a lot. For this catalyst, a direct modification on naon size Au particles without modifying carbon support is not realistic, an polymer layer on the surface of Au/C catalyst could be a solution but needs further experimental proof. Other methods also should be pursued, including immobilizing cobalt salen on the carbon surface or modifying cobalt salen compound to make it insoluble. The other important aspect to apply this catalyst is making customized structure for the three electrochemical systems proposed in chapter 6. The most viable system that should be built first is the electrolytic peroxide production system. Extra consideration should be put into the flow channel design for taking the peroxide solution out of the cell and an ideal alkaline

membrane that is relatively stable with peroxide radical. Then based on the work of peroxide production, a high concentration peroxide solution should be pursued to build the battery system with this catalyst, cause the peroxide oxidation is relatively easy reaction and a rechargeable battery system is very easy to be achieve if high concentration of peroxide solution can be preserved.

This work is more focused on understanding the catalyst properties rather than building new electrochemical systems around it. For future application with this catalyst, a lot more effort needs to be devoted in developing related system a potential high energy density, high performance and high stability battery system.

# List of References

(1) Song, M. K.; Park, S.; Alamgir, F. M.; Cho, J.; Liu, M. *Mater. Sci. Eng. R Reports* **2011**, *72*, 203–252.

(2) Park, M.; Zhang, X.; Chung, M.; Less, G. B.; Sastry, A. M. *J. Power Sources* **2010**, *195*, 7904–7929.

(3) Perry, M. L.; Fuller, T. F. *J. Electrochem. Soc.* **2002**, *149*, S59.

(4) J.OM. Bockris, A. J. Appleby *Energy* **1986**, *11*, 95.

(5) Bidault, F.; Brett, D. J. L.; Middleton, P. H.; Brandon, N. P. *J. Power Sources* **2009**, *187*, 39–48.

(6) Giilzow, E. *J. Power Sources* **1996**, *61*, 99–104.

(7) Neburchilov, V.; Wang, H.; Martin, J. J.; Qu, W. *J. Power Sources* **2010**, *195*, 1271–1291.

(8) Mulder, G.; Coenen, P.; Martens, A; Spaepen, J. *Int. J. Hydrogen Energy* **2008**, *33*, 3220–3224.

(9) Gouérec, P.; Poletto, L.; Denizot, J.; Sanchez-Cortezon, E.; Miners, J. H. *J. Power Sources* **2004**, *129*, 193–204.

(10) Brushett, F. R.; Naughton, M. S.; Yin, L.; Kenis, P. J. A. *Int. J. Hydrogen Energy* **2011**, *37*, 2559–2570.

(11) Brushett, F. R.; Zhou, W.P.; Jayashree, R. S.; Kenis, P. J. A. *J. Electrochem. Soc.* **2009**, *156*, B565.

(12) Anderson, A. B. *Electrocatal* **2012**, *3*, 176–182.

(13) Stephens, I. E. L.; Bondarenko, A. S.; Perez-Alonso, F. J.; Calle-Vallejo, F.; Bech, L.; Johansson, T. P.; Jepsen, A. K.; Frydendal, R.; Knudsen, B. P.; Rossmeisl, J.; Chorkendorff, I. *J. Am. Chem. Soc.* **2011**, *133*, 5485–91.

(14) Viswanathan, V.; Hansen, H. A.; Rossmeisl, J.; Nørskov, J. K. *ACS catal* **2012**, 1654–1660.

(15) Viswanathan, V.; Hansen, H. A.; Rossmeisl, J.; Nørskov, J. K. *J. Phys. Chem. Lett.* **2012**, *3*, 2948–2951.

(16) Ramaswamy, N.; Mukerjee, S. *J. Phys. Chem. C* **2011**, *115*, 18015–18026.

(17) Girishkumar, G.; McCloskey, B.; Luntz, A. C.; Swanson, S.; Wilcke, W. *J. Phys. Chem. Lett.* **2010**, *1*, 2193–2203.

(18) Abraham, K. M.; Jiang, Z. *Electrochem. Sci. Technol.* **1996**, *143*, 1–5.

(19) Xu, K. *Chem. Rev.* **2004**, *104*, 4303–417.

(20) Laoire, C. O.; Mukerjee, S.; Abraham, K.; Plichta, E. J.; Hendrickson, M. A. *J. Phys. Chem. C* **2009**, *113*, 20127–20134.

(21) Laoire, C. O.; Mukerjee, S.; Plichta, E. J.; Hendrickson, M. A.; Abraham, K. M. *J. Electrochem. Soc.* **2011**, *158*, A302.

(22) Lu, Y. C.; Gasteiger, H. A.; Crumlin, E.; McGuire, R.; Shao-Horn, Y. *J. Electrochem. Soc.* **2010**, *157*, A1016.

(23) Lu, Y. C.; Xu, Z.; Gasteiger, H. A; Chen, S.; Hamad-Schifferli, K.; Shao-Horn, Y. *J. Am. Chem. Soc.* **2010**, *132*, 12170.

(24) Giordani, V.; Freunberger, S. A.; Bruce, P. G.; Tarascon, J. M.; Larcher, D. *Electrochem. Solid-State Lett.* **2010**, *13*, A180.

(25) Zhang, S. S.; Foster, D.; Read, J. *Electrochim. Acta* **2011**, *56*, 1283–1287.

(26) Veith, G. M.; Dudney, N. J. *J. Electrochem. Soc.* **2011**, *158*, A658.

(27) Batteries, L. O.; Mccloskey, B. D.; Speidel, A.; Scheffler, R.; Miller, D. C.; Viswanathan, V.; Hummelshøj, J. S.; Nørskov, J. K.; Luntz, A. C. **2012**, 2–6.

(28) McCloskey, B. D.; Scheffler, R.; Speidel, A.; Bethune, D. S.; Shelby, R. M.; Luntz, a C. *J. Am. Chem. Soc.* **2011**, *133*, 18038–41.

(29) Freunberger, S. A; Chen, Y.; Peng, Z.; Griffin, J. M.; Hardwick, L. J.; Bardé, F.; Novák, P.; Bruce, P. G. *J. Am. Chem. Soc.* **2011**, *133*, 8040–7.

(30) Xiao, J.; Hu, J.; Wang, D.; Hu, D.; Xu, W.; Graff, G. L.; Nie, Z.; Liu, J.; Zhang, J.G. *J. Power Sources* **2011**, *196*, 5674–5678.

(31) Peng, Z.; Freunberger, S. A; Chen, Y.; Bruce, P. G. *Science* **2012**, *563*.

(32) Read, J.; Mutolo, K.; Ervin, M.; Behl, W.; Wolfenstine, J.; Driedger, A.; Foster, D. *J. Electrochem. Soc.* **2003**, *150*, A1351.

(33) Zhang, S. S.; Read, J. *J. Power Sources* **2011**, *196*, 2867–2870.

(34) Williford, R. E.; Zhang, J.G. *J. Power Sources* **2009**, *194*, 1164–1170.

(35) Beattie, S. D.; Manolescu, D. M.; Blair, S. L. *J. Electrochem. Soc.* **2009**, *156*, A44.

(36) Zhang, S. S.; Foster, D.; Read, J. *J. Power Sources* **2010**, *195*, 1235–1240.

(37) Xu, W.; Xiao, J.; Wang, D.; Zhang, J.; Zhang, J.G. *J. Electrochem. Soc.* **2010**, *157*, A219–A224.

(38) Park, C. K.; Park, S. B.; Lee, S. Y.; Lee, H.; Jang, H.; Cho, W. I. *Bull. Korean Chem. Soc.* **2010**, *31*, 3221–3224.

(39) Zhang, G. Q.; Zheng, J. P.; Liang, R.; Zhang, C.; Wang, B.; Hendrickson, M.; Plichta, E. J. *J. Electrochem. Soc.* **2010**, *157*, A953.

(40) Zhang, J.; Xu, W.; Li, X.; Liu, W. *J. Electrochem. Soc.* **2010**, *157*, A940.

(41) Zhang, J.; Xu, W.; Liu, W. *J. Power Sources* **2010**, *195*, 7438–7444.

(42) Andrei, P.; Zheng, J. P.; Hendrickson, M.; Plichta, E. J. *J. Electrochem. Soc.* **2010**, *157*, A1287.

(43) Tran, C.; Kafle, J.; Yang, X.Q.; Qu, D. *Carbon N. Y.* **2011**, *49*, 1266–1271.

(44) Visco, S. J.; Nimon, E.; Katz, B.; Chu, M.; Jonghe, L. De; *Scalable energy storage: Beyond Li-ion* **2009**.

(45) Kanno, R.; Murayama, M. *J. Electrochem. Soc.* **2001**, *148*, A742.

(46) Kamaya, N.; Homma, K.; Yamakawa, Y.; Hirayama, M.; Kanno, R.; Yonemura, M.; Kamiyama, T.; Kato, Y.; Hama, S.; Kawamoto, K.; Mitsui, A. *Nat. Mater.* **2011**, *10*, 682–686.

(47) Seo, I.; Martin, S. W. *Acta Mater.* **2011**, *59*, 1839–1846.

(48) Zhang, M.; Takahashi, K.; Uechi, I.; Takeda, Y.; Yamamoto, O.; Im, D.; Lee, D.-J.; Chi, B.; Pu, J.; Li, J.; Imanishi, N. *J. Power Sources* **2013**, *235*, 117–121.

(49) Zhang, T.; Imanishi, N.; Hasegawa, S.; Hirano, A.; Xie, J.; Takeda, Y.; Yamamoto, O.; Sammes, N. *J. Electrochem. Soc.* **2008**, *155*, A965.

(50) Wang, Y.; Zhou, H. *Chem. Commun. (Camb).* **2010**, 6305–6307.

(51) Wang, Y.; Zhou, H. *J. Power Sources* **2010**, *195*, 358–361.

(52) Zhang, T.; Imanishi, N.; Shimonishi, Y.; Hirano, A.; Takeda, Y.; Yamamoto, O.; Sammes, N. *Chem. Commun. (Camb).* **2010**, *46*, 1661–3.

(53) Shimonishi, Y.; Zhang, T.; Imanishi, N.; Im, D.; Lee, D. J.; Hirano, A.; Takeda, Y.; Yamamoto, O.; Sammes, N. *J. Power Sources* **2011**, *196*, 5128–5132.

(54) Ohkuma, H.; Uechi, I.; Imanishi, N.; Hirano, A.; Takeda, Y.; Yamamoto, O. *J. Power Sources* **2013**, *223*, 319–324.

(55) Nikolova, V.; Iliev, P.; Petrov, K.; Vitanov, T.; Zhecheva, E.; Stoyanova, R.; Valov, I.; Stoychev, D. *J. Power Sources* **2008**, *185*, 727–733.

(56) Garsuch, A.; Panchenko, A.; Querner, C.; Karpov, A.; Huber, S.; Oesten, R. *Electrochem. commun.* **2010**, *12*, 1642–1645.

(57) Huang, S.Y.; Ganesan, P.; Jung, H.Y.; Popov, B. N. *J. Power Sources* **2012**, *198*, 23–29.

(58) Jörissen, L. *J. Power Sources* **2006**, *155*, 23–32.

(59) Karlson, G. *J. Mol. Catal.* **1986**, *38*, 41–48.

(60) Kong, F. D.; Zhang, S.; Yin, G. P.; Zhang, N.; Wang, Z. B.; Du, C. Y. *J. Power Sources* **2012**, *210*, 321–326.

(61) Wu, X.; Scott, K. *J. Power Sources* **2012**, *206*, 14–19.

(62) Li, Y.; Gong, M.; Liang, Y.; Feng, J.; Kim, J. E.; Wang, H.; Hong, G.; Zhang, B.; Dai, H. *Nat. Commun.* **2013**, *4*, 1805.

(63) Prakash, J.; Tryk, D. A.; Yeager, E. B. *J. Electrochem. Soc.* **1999**, *146*, 4145–4151.

(64) Li, Y.; Hasin, P.; Wu, Y. *Adv. Mater.* **2010**, *22*, 1926–9.

(65) Li, Y.; Gong, M.; Liang, Y.; Feng, J.; Kim, J. E.; Wang, H.; Hong, G.; Zhang, B.; Dai, H. *Nat. Commun.* **2013**, *4*, 1805.

(66) KUBOKI, T.; OKUYAMA, T.; OHSAKI, T.; TAKAMI, N. *J. Power Sources* **2005**, *146*, 766–769.

(67) Cui, Z. H.; Fan, W. G.; Guo, X. X. *J. Power Sources* **2013**, *235*, 251–255.

(68) Inada, T.; Kobayashi, T.; Sonoyama, N.; Yamada, A.; Kondo, S.; Nagao, M.; Kanno, R. *J. Power Sources* **2009**, *194*, 1085–1088.

(69) Kumar, B.; Kumar, J.; Leese, R.; Fellner, J. P.; Rodrigues, S. J.; Abraham, K. M. *J. Electrochem. Soc.* **2010**, *157*, A50.

(70) Yeo, B. S.; Bell, A. T. *J. Am. Chem. Soc.* **2011**, *133*, 5587–93.

(71) Sadiek, I. M.; Mohammad, A. M.; El-shakre, M. E.; Awad, M. I. **2012**, *7*, 3350–3361.

(72) Palmas, S.; Ferrara, F.; Vacca, A.; Mascia, M.; Polcaro, A. M. *Electrochim. Acta* **2007**, *53*, 400–406.

(73) Brossard, L.; Lessard, M. *Int. J. Hydrogen Energy* **1993**, *18*, 807–816.

(74) Tatsuhiro Okada, Satoshi Gotou, Masaya Yoshida, M. Y.; Takuji Hirose, and I. S. *J. Inorg. Organomet. Polym.* **1999**, *9*, 199.

(75) Kingsborough, R. P.; Swager, T. M. *Chem. Mater.* **2000**, *12*, 872–874.

(76) Greeley, J.; Stephens, I. E. L.; Bondarenko, a S.; Johansson, T. P.; Hansen, H. a; Jaramillo, T. F.; Rossmeisl, J.; Chorkendorff, I.; Nørskov, J. K. *Nat. Chem.* **2009**, *1*, 552–6.

(77) Srivastava, R.; Mani, P.; Hahn, N.; Strasser, P. *Angew. Chem. Int. Ed. Engl.* **2007**, *46*, 8988–91.

(78) Nilekar, A. U.; Xu, Y.; Zhang, J.; Vukmirovic, M. B.; Sasaki, K.; Adzic, R. R.; Mavrikakis, M. *Top. Catal.* **2007**, *46*, 276–284.

(79) Van der Vliet, D.; Wang, C.; Debe, M.; Atanasoski, R.; Markovic, N. M.; Stamenkovic, V. R. *Electrochim. Acta* **2011**, *56*, 8695–8699.

(80) Strasser, P.; Koh, S.; Anniyev, T.; Greeley, J.; More, K.; Yu, C.; Liu, Z.; Kaya, S.; Nordlund, D.; Ogasawara, H.; Toney, M. F.; Nilsson, A. *Nat. Chem.* **2010**, *2*, 454–60.

(81) Stamenkovic, V. R.; Fowler, B.; Mun, B. S.; Wang, G.; Ross, P. N.; Lucas, C. A; Marković, N. M. *Science* **2007**, *315*, 493–7.

(82) Gasteiger, H. A; Marković, N. M. *Science* **2009**, *324*, 48–9.

(83) Vaz-dom, C.; Pita, M.; Lacey, A. L. De; Shleev, S.; Cuesta, A. *J. Phys. Chem. c* **2012**, *116*, 16532.

(84) Lucas, C. A.; Thompson, P.; Gründer, Y.; Markovic, N. M. *Electrochem. commun.* **2011**, *13*, 1205–1208.

(85) Strmcnik, D.; Kodama, K.; van der Vliet, D.; Greeley, J.; Stamenkovic, V. R.; Marković, N. M. *Nat. Chem.* **2009**, *1*, 466–72.

(86) Strmcnik, D.; Escudero-Escribano, M.; Kodama, K.; Stamenkovic, V. R.; Cuesta, A.; Marković, N. M. *Nat. Chem.* **2010**, *2*, 880–5.

(87) D.V.Tripkovic; D.Strmcnik; Vliet, D. va. der; V.Stamenkovic; N.M.Markovic *Faraday Discuss.* **2009**, *140*, 9.

(88) Angelucci, C. A.; Varela, H.; Tremiliosi-Filho, G.; Gomes, J. F. *Electrochem. commun.* **2013**, *33*, 10–13.

(89) Katsounaros, I.; Mayrhofer, K. J. J. *Chem. Commun. (Camb).* **2012**, *48*, 6660–2.

(90) Nesselberger, M.; Ashton, S.; Meier, J. C.; Katsounaros, I.; Mayrhofer, K. J. J.; Arenz, M. *J. Am. Chem. Soc.* **2011**, *133*, 17428–33.

(91) Kimling, J.; Maier, M.; Okenve, B.; Kotaidis, V.; Ballot, H.; Plech, A *J. Phys. Chem. B* **2006**, *110*, 15700–7.

(92) Markovic, N.; Adzic, R.; VešoviC, V. *J. Electroanal. Chem.* **1984**, *165*, 121–133.

(93) El-Deab, M. S.; Arihara, K.; Ohsaka, T. *J. Electrochem. Soc.* **2004**, *151*, E213.

(94) Strbac, S.; Adzic, R. R. *J. Electroanal. Chem.* **1996**, *403*, 7–9.

(95) Markovic, N. M.; Lucas, A.; Ross, N. *Phys. Rev.* **1993**, *47*, 542–553.

(96) Kolb, D. M.; Schneider.J *Electrochim. Acta* **1986**, 929.

(97) Ca, Y. S.; Mbvr, D. V. C. I.; Ocko, B. M.; Helgesen, G.; Schardt, B.; Hamelin, A. *Phys. Rev. Lett.* **1992**, *1*, 3350–3354.

(98) Weaver, M. J.; Gao, X.; Hamelin, A. *Phys. Rev. B* **1992**, *46*, 7096.

(99) Kolb, D. M. *Prog. Surf. Sci.* **1996**, *51*, 109–173.

(100) Zhao, X.; Yan, H.; Zhao, R. G.; Yang, W. S. *Langmuir* **2002**, *18*, 3910–3915.

(101) Smith, C. I.; Bowfield, A.; Almond, N. J.; Mansley, C. P.; Convery, J. H.; Weightman, P. *J. Phys. Condens. Matter* **2010**, *392001*, 3–8.

(102) Polewska, W.; Vitus, C.; Ocko, B. ; Adzic, R.R. *J. Electroanal. Chem.* **1994**, *364*, 265–269.

(103) Dakkouri, A. *Solid State Ionics* **1997**, *94*, 99–114.

(104) Lipkowski, J.; Ross, P. N. *Structure of electrified interfaces*; 1999.

(105) Othman, S. H.; El-deab, M. S.; Ohsaka, T. *Water* **2011**, *6*, 6209–6219.

(106) Eldeab, M.; Ohsaka, T. *Electrochim. Acta* **2007**, *52*, 2166–2174.

(107) Awad, M. I.; Ohsaka, T. *J. Power Sources* **2013**, *226*, 306–312.

(108) Miah, M.; Ohsaka, T. *Electrochim. Acta* **2009**, *54*, 1570–1577.

(109) Miah, M.; Ohsaka, T. *Electrochim. Acta* **2007**, *52*, 6378–6385.

(110) Miah, M. R.; Ohsaka, T. *J. Electrochem. Soc.* **2007**, *154*, F186.

(111) Miah, M. R.; Ohsaka, T. *J. Electrochem. Soc.* **2009**, *156*, B429.

(112) Miah, M. R.; Ohsaka, T. *Electrochim. Acta* **2009**, *54*, 5871–5876.

(113) Mominul Islam, M.; Ohsaka, T. *J. Electroanal. Chem.* **2008**, *623*, 147–154.

(114) El-Deab, M.; Ohsaka, T. *Electrochem. commun.* **2003**, *5*, 214–219.

(115) El-Deab, M. *Electrochem. commun.* **2003**, *5*, 214–219.

(116) Miah, M. R.; Ohsaka, T. *J. Electroanal. Chem.* **2009**, *633*, 71–77.

(117) Miah, M. R.; Ohsaka, T. *J. Electrochem. Soc.* **2006**, *153*, E195.

(118) Ortiz, B.; Park, S. *Bull. Korean Chem. Soc* **2000**, *21*, 405–411.

(119) Pletcher, D.; Thompson, H. *J. Chem. Soc. Trans.* **1997**, *93*, 3669–3675.

(120) Okada, T.; Katou, K.; Hirose, T.; Yuasa, M.; Sekine, I. *Chem. Lett.* **1998**, 841.

(121) Nielsen, M.; Larsen, N. B.; Gothelf, K. V *Langmuir* **2002**, 2795–2799.

(122) Kingsborough, B. R. P.; Swager, T. M. *Adv. Mater.* **1998**, 1100–1104.

(123) Zhang, R.; Ma, J.; Wang, W.; Wang, B.; Li, R. *J. Electroanal. Chem.* **2010**, *643*, 31–38.

(124) Zhang, G.; Yang, F. *Electrochim. Acta* **2007**, *52*, 6595–6603.

(125) Okada, T.; Katou, K.; Hirose, T.; Yuasa, M.; Sekine, I.; Soc, J. E. *J. Electrochem. Soc.* **1999**, *146*, 2562–2568.

(126) Zurilla, R. W. *J. Electrochem. Soc.* **1978**, *125*, 1103.

(127) Sarapuu, A.; Nurmik, M.; Mändar, H.; Rosental, A.; Laaksonen, T.; Kontturi, K.; Schiffrin, D. J.; Tammeveski, K. *J. Electroanal. Chem.* **2008**, *612*, 78–86.

(128) Erikson, H.; Jürmann, G.; Sarapuu, A.; Potter, R. J.; Tammeveski, K. *Electrochim. Acta* **2009**, *54*, 7483–7489.

(129) Xu, Y.; Mavrikakis, M. *J. Phys. Chem. B* **2003**, *107*, 9298–9307.

(130) Panchenko, A.; Koper, M. T. M.; Shubina, T. E.; Mitchell, S. J.; Roduner, E. *J. Electrochem. Soc.* **2004**, *151*, A2016.

(131) Lima, F. H. B.; Zhang, J.; Shao, M. H.; Sasaki, K.; Vukmirovic, M. B.; Ticianelli, E. A.; Adzic, R. R. *J. Phys. Chem. C* **2007**, *111*, 404–410.

(132) Schmidt, T.; Marković, N. M.; Ross, P. N. *Electrochim. Acta* **2002**, *47*, 3765–3776.

(133) Tripachev, O. V.; Tarasevich, M. R. *Russ. J. Phys. Chem. A* **2013**, *87*, 820–825.

(134) Davis, R. E.; Horvath, G. L. *Electrochimica.Acta* **1967**, *12*, 287.

(135) Hicholson, R. S. *Anal. Chem.* **1965**, *11*, 1351–1355.

(136) Antoine, O.; Bultel, Y.; Durand, R.; Ozil, P. *Electrochim.Acta* **1998**, *43*.

(137) Genièès, L.; Faure, R.; Durand, R. *Electrochim. Acta* **1998**, *44*, 1317–1327.

(138) Tang, W.; Lin, H.; Kleiman-Shwarsctein, A.; Stucky, G. D.; McFarland, E. W. *J. Phys. Chem. C* **2008**, *112*, 10515–10519.

(139) Guerin, S.; Hayden, B. E.; Pletcher, D.; Rendall, M. E.; Suchsland, J. P. *J. Comb. Chem.* **2006**, *8*, 679–86.

(140) Lee, Y.; Loew, A.; Sun, S. *Chem. Mater.* **2010**, *22*, 755–761.

(141) A.Hamelin *J. Electroanal. Chem.* **1996**, *407*, 1–11.

(142) A.Hamelin; A.M.Martins *J. Electroanal. Chem.* **1996**, *407*, 13–21.

(143) Herna, J.; Herrero, E.; Aldaz, A.; Feliu, J. M. *J.Phys.Chem.C* **2007**, *111*, 14078–14083.

(144) Inasaki, T.; Kobayashi, S. *Electrochim. Acta* **2009**, *54*, 4893–4897.

(145) Jena, B. K.; Raj, C. R. *J.Phys.Chem.C* **2007**, *111*, 15146–15153.

(146) M.S.Chen; D.W.Goodman *Catalysis Today.* **2006**, *111*, 22-33.

(147) Shao, M. H.; Adzic, R. R. *J. Chem. B Lett.* **2005**, *109*, 16563–16566.

(148) Asokan, K.; Subramanian, K. *Proc. world Congr. Eng. Comput. Sci.* **2009**, *I*, 20–23.

(149) Pletcher, D. *Electrosynthesis* **1999**, *4*.

(150) Campos-Martin, J. M.; Blanco-Brieva, G.; Fierro, J. L. G. *Angew. Chem. Int. Ed. Engl.* **2006**, *45*, 6962–84.

(151) Hämäläinen, H.; Aksela, R.; Rautiainen, J.; Sankari, M.; Renvall, I.; Paquet, R. *Conf. report, Kemira Gr.*

(152) Watts, R. J.; Finn, D. D.; Cutler, L. M.; Schmidt, J. T.; Teel, A. L. *J. Contam. Hydrol.* **2007**, *91*, 312–26.

(153) Schmidt, J. T.; Ahmad, M.; Teel, A. L.; Watts, R. J. *J. Contam. Hydrol.* **2011**, *126*, 1–7.

(154) Croft, S.; Gilbert, B. C.; Smith, J. R. L.; Stell, J. K.; Sandersonb, W. R.; *J.CHEM.SOC.PERKIN TRANS* **1992**, *2*, 153–160.

(155) D.V.Tripkovic; N.M.Markovic; D.strmcnik *Faraday Discuss.* **2009**, *140*, 9.

(156) Markovi, N. M.; D.Strmcnik; Vliet, D. F. van der *Phys. Chemsitry Lett.* **2011**, 2733–2736.

(157) Zhang, C.; Fan, F. R. F.; Bard, A. J. *J. Am. Chem. Soc.* **2009**, *131*, 177–81.

(158) Schmidt, T. J.; Ross, P. N.; Markovic, N. M. *J. Phys. Chem. B* **2001**, *105*, 12082–12086.

(159) Sechenov, T.; Schumpe, R.; Hoftijzer, K. *Chem. Enoineering Sci.* **1995**, *50*, 1673–1675.

(160) Sipos, P. M.; Hefter, G.; May, P. M. *J. Chem. Eng. Data* **2000**, *45*, 613–617.

(161) Zhou, J.; Guo, H.; Wang, X.; Guo, M.; Zhao, J.; Chen, L.; Gong, W. *Chem. Commun. (Camb).* **2005**, 1631–3.

(162) Locke, B. R.; Shih, K. Y. *Plasma Sources Sci. Technol.* **2011**, *20*, 034006.

(163) Landon, P.; Collier, P. J.; Papworth, A. J.; Kiely, C. J.; Hutchings, G. J. *Chem. Commun. (Camb).* **2002**, 2058–9.

(164) Landon, P.; Collier, P. J.; Carley, A. F.; Chadwick, D.; Papworth, A. J.; Burrows, A.; Kiely, C. J.; Hutchings, G. J. *Phys. Chem. Chem. Phys.* **2003**, *5*, 1917–1923.

(165) Li, G.; Edwards, J.; Carley, A. F.; Hutchings, G. J. *Catal. Commun.* **2007**, *8*, 247–250.

(166) Samanta, C. *Appl. Catal. A Gen.* **2008**, *350*, 133–149.

(167) Vulpescu, G.; Ruitenbeek, M.; Vanlieshout, L.; Correia, L.; Meyer, D.; Pex, P. *Catal. Commun.* **2004**, *5*, 347–351.

(168) Brillas, E.; Alcaide, F.; Cabot, P. L. *Electrochim. Acta* **2002**, *48*, 331–340.

(169) Alcaide, F.; Brillas, E.; Cabor, P.; Investiqacidn, D. De **1998**, *145*, 3444–3449.

(170) Fukuzumi, S.; Yamada, Y.; Karlin, K. D. *Electrochim. Acta* **2012**, *82*, 493–511.

(171) Giomo, M.; Buso, A.; Fier, P.; Sandonà, G.; Boye, B.; Farnia, G. *Electrochim. Acta* **2008**, *54*, 808–815.

(172) Yamanaka, I. *Catal. Surv. from Asia* **2008**, *12*, 78–87.

(173) Yamanaka, I.; Onizawa, T.; Takenaka, S.; Otsuka, K. *Angew. Chem. Int. Ed. Engl.* **2003**, *42*, 3653–5.

(174) Yamanaka, I.; Tazawa, S.; Murayama, T.; Iwasaki, T.; Takenaka, S. *ChemSusChem* **2010**, *3*, 59–62.

(175) You, S. J.; Wang, J. Y.; Ren, N. Q.; Wang, X. H.; Zhang, J. N. *ChemSusChem* **2010**, *3*, 334–8.

(176) El-Deab, M. S.; Okajima, T.; Ohsaka, T. *J. Electrochem. Soc.* **2003**, *150*, A851.

(177) Gyenge, E. L.; Oloman, C. W. *J. Applied Electrochemistry* **2001**, *31*, 233–243.

(178) Kolyagin, G. A.; Vasil'eva, I. S.; Kornienko, V. L. *Russ. J. Appl. Chem.* **2008**, *81*, 983–987.

(179) Lobyntseva, E.; Kallio, T.; Alexeyeva, N.; Tammeveski, K.; Kontturi, K. *Electrochim. Acta* **2007**, *52*, 7262–7269.

(180) Wang, A.; Bonakdarpour, A.; Wilkinson, D. P.; Gyenge, E. *Electrochim. Acta* **2012**, *66*, 222–229.

(181) Agladze, G. R.; Tsurtsumia, G. S.; Jung, B. I.; Kim, J. S.; Gorelishvili, G. *J. Appl. Electrochem.* **2007**, *37*, 375–383.

(182) Foller, P. C.; Bobard, R. T. *J. Appl. Electrochem.* **1995**, *25*, 613–627.

(183) Yamanaka, I.; Hashimoto, T.; Ichihashi, R.; Otsuka, K. *Electrochim. Acta* **2008**, *53*, 4824–4832.

(184) Alcaide, F.; Brillas, E.; Cabot, P. L. *J. Electrochem. Soc.* **2002**, *149*, E64.

(185) Balej, J.; Balogh, K.; Špalek, O. *Chem.zvesti* **1976**, *30*, 384.

(186) Choi, J.; Hwang, S. H.; Jang, J.; Yoon, J. *Electrochem. commun.* **2013**, *30*, 95–98.

(187) Gupta, N.; Oloman, C. W. *J. Appl. Electrochem.* **2005**, *36*, 255–264.

(188) Murayama, T.; Tazawa, S.; Takenaka, S.; Yamanaka, I. *Catal. Today* **2011**, *164*, 163–168.

(189) Pozzo, A. Da; Palma, L. Di; Merli, C.; Petrucci, E. *J. Appl. Electrochem.* **2005**, *35*, 413–419.

(190) Yamanaka, I.; Onisawa, T.; Hashimoto, T.; Murayama, T. *ChemSusChem* **2011**, *4*, 494–501.

(191) Zheng, J. P.; Andrei, P.; Hendrickson, M.; Plichta, E. J. *J. Electrochem. Soc.* **2011**, *158*, A43.

(192) Xuan, J.; Leung, D. Y. C.; Leung, M. K. H.; Ni, M.; Wang, H. *Int. J. Hydrogen Energy* **2011**, *36*, 9231–9241.

(193) Chen, G.; Zhang, H.; Cheng, J.; Ma, Y.; Zhong, H. *Electrochem. commun.* **2008**, *10*, 1373–1376.

(194) Millet, P.; Dragoe, D.; Grigoriev, S.; Fateev, V.; Etievant, C. *Int. J. Hydrogen Energy* **2009**, *34*, 4974–4982.

(195) Markgraf, S.; Hörenz, M.; Schmiel, T.; Jehle, W.; Lucas, J.; Henn, N. *J. Power Sources* **2012**, *201*, 236–242.

(196) S.Z.Makarov; T.A.Dobrynina *Bull. Acad. Sci. USSR* **1955**, 365.

(197) D.J.Salmon **1988**, US Patent 473275122.

(198) W.N.Smith **1969**, US Patent 344658827.

(199) Lee, J. S.; Tai Kim, S.; Cao, R.; Choi, N. S.; Liu, M.; Lee, K. T.; Cho, J. *Adv. Energy Mater.* **2011**, *1*, 34–50.

# Vita

Ming Qi was born in Liaoyang, Liaoning province, China. He is the only child in his family. He received his early education, including elementary school and high school education, at his hometown. Later, he went to the city, Dalian, and finished a Chemical Engineering Bachelor Degree at Dalian University of Technology. In the meantime, he developed an interest in the technology development and decided to build a career around it. In 2009, he accepted the scholarship from the Chemical and Biomolecular Engineering department of the University of Tennessee, Knoxville. He finally found a chance to study the battery technology with professor, Dr. Thomas A. Zawodzinski. He wrote a thesis about an innovative catalyst and new battery systems based on it. He graduated at the end of 2013, but his work on his battery research continued.